The Scientific World Journal

# Emerging Water Quality Problems in Developing Countries

Guest Editors: Manish Kumar, Gurmeet Singh, Tushara Chaminda, Pham Van Quan, and Keisuke Kuroda

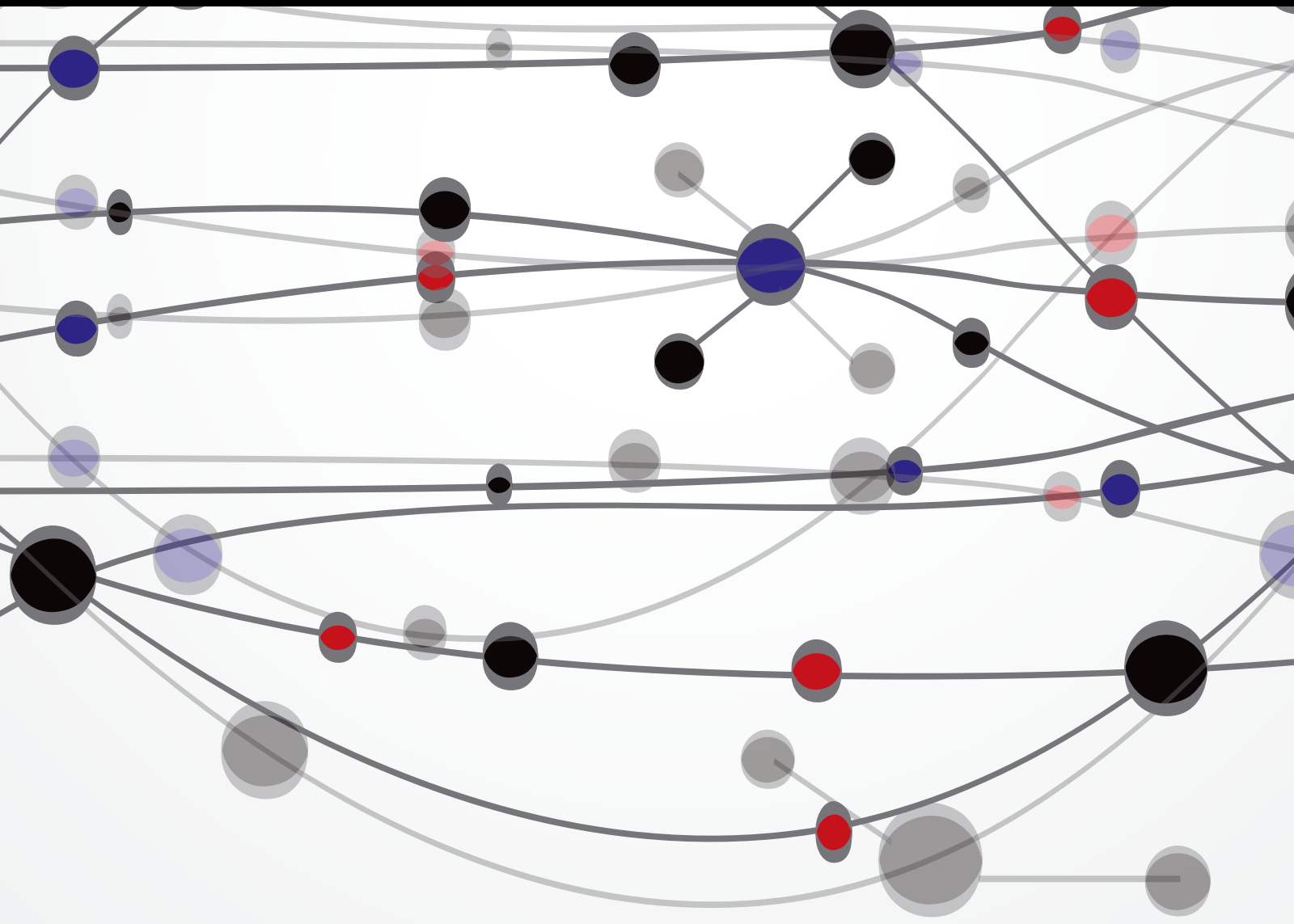

# Emerging Water Quality Problems in Developing Countries

The Scientific World Journal

# Emerging Water Quality Problems in Developing Countries

Guest Editors: Manish Kumar, Gurmeet Singh, Tushara Chaminda, Pham Van Quan, and Keisuke Kuroda

# Contents

Hindawi Publishing Corporation
The Scientific World Journal
Volume 2014, Article ID 215848, 2 pages
http://dx.doi.org/10.1155/2014/215848

*Editorial*

# Emerging Water Quality Problems in Developing Countries

**Manish Kumar,[1] Gurmeet Singh,[2] Tushara Chaminda,[3] Pham Van Quan,[4] and Keisuke Kuroda[5]**

[1] *Department of Environmental Science, Tezpur University, Tezpur, Assam 784028, India*
[2] *Jawaharlal Nehru University, New Delhi, India*
[3] *Department of Civil and Environmental Engineering, Faculty of Engineering, University of Ruhuna, Galle, Sri Lanka*
[4] *Hanoi Architectural University, Vietnam*
[5] *Center for Environmental Risk Research, National Institute for Environmental Studies (NIES), 16-2 Onogawa, Tsukuba, Ibaraki 305-8506, Japan*

Correspondence should be addressed to Manish Kumar; manish.env@gmail.com

Received 29 April 2014; Accepted 29 April 2014; Published 12 May 2014



It has been an interesting endeavor for us to contribute as the guest editors for this special issue. At the same time, it was a daunting task for us editors to go through each of the papers thoroughly and select only the ones which we thought were unique and matched the scope of this special edition of the journal.

According to Nobel Laureate Richard Smalley (1996 Noble in Chemistry), water is the second, next to energy, among the humanity's top ten problems in the next 50 years. Water, one of the most important factors required for life to sustain on planet Earth, requires proper attention in terms of uses as well as treatments. The challenge for scientists and engineers working in the field of water is that they encounter new problems with every passing day, where the effective use of new techniques, such as tracers and modelling simulation, is becoming inevitable. The purpose of this special issue is to define the emerging water problems and possible technical solutions to the arising problems. We were interested in articles that explore various water research domains with relevant techniques and integrate in a single text the subject matter that deals with the concurrent "Emerging Water Quality Issues." We, in principle, wanted to emphasize on topics like (i) emerging water problems in developing countries, (ii) emerging pollutants in water environment, (iii) health-related issues of water environment, (iv) water analysis tools and techniques, (v) flood-related issues, (vi) public involvement and participation, and so forth.

This special issue is comprised of topics dealing with the subject mentioned above and intended for the students, professionals, and researchers working on various aspects of water quality issues. The issue seeks its impact from its diverse topic coverage revealing situations of different contemporary issues, such as drinking water treatment, microbial contamination in fresh water system as well as in sewage water, metal contamination in sediment using isotope tracers, using low cost adsorbent like rice husk, and projections of climate change in Tibetan Plateau. Various case studies have been discussed to present a cutting edge scenario of the problem, perspective, and challenges of emerging water quality issues in the present context of climate change and significant human interventions.

To mention a few highlights of the findings reported in the issues are as follows: H. Sakai et al. have conducted a survey of the quality of the source water and drinking water in urban areas of Myanmar; for this study two urban areas were selected and the drinking water samples were collected from a variety of sources like public pots, nonpiped taps, piped taps, and bottled waters. The overall water quality of the samples was found to be good while As and $F^-$ were present at relatively higher levels and should be remediated. The microbial levels were found to be least in the bottled

water and highest in pots. This study could be used to devise better solutions for treatment and supply of drinking water in the urban areas of Myanmar.

H. Sakai et al. also conducted a study on the occurrence and distribution of microcystins in Lake Taihu, China. Microcystin is an emerging pollutant and very toxic in nature; it is reported to be carcinogenic in animals including humans. Microcystin levels correlated with COD, chlorophyll-a, and turbidity. This study is important because, unlike traditional pollutants like As or $F^-$ in the water, research in the field of microcystin is limited and its effects were not properly understood. Moreover, the study has been carried out in the third largest lake of China, Lake Taihu, which is a unique opportunity to study the effects of this pollutant in a lake ecosystem.

Z. Hao et al. have checked the effectiveness of 22 different global climate models (GCMs) provided by the IPCC to predict the climate change pattern in the Tibetan Plateau. Tibetan Plateau is a very large area and almost all the models which were reviewed for their climate predicting abilities had limitations in predicting the precipitation (which was overestimated) and temperature (which was underestimated). It has been suggested that both the temperature as well as the precipitation levels in the Tibetan Plateau will increase in the next 90 years. Barring a few models, resolution of most of the climate predicting models were low and further work needs to be done in order to improve the accuracy of these models. Based on the studied models, the authors have predicted three possible scenarios of future climate in the Tibetan Plateau, A1B, A2, and B1. In A2 scenario, the greatest increase in precipitation was observed while in the least increase in precipitation was observed in the A1B scenario. This study is important, because it tests the effectiveness of different established GCMs to predict the changes in the climate of a large geographical area. The inputs from this study can be used for further improvement and development of the climate predicting models.

Vedat et al. tested the effectiveness of a hybrid membrane system in removing natural organic matter (NOM); ultrafiltration membranes fortified with powdered activated carbon (PAC) were found to remove NOM more effectively than unfortified UF and microfiltration (MF) membranes. This technique also required less amount of energy as the pressure required for separation of NOM in PAC-UF was lesser than that required in MF and UF membranes. However, the problem with using PAC activated filters was the clogging of the filter pores by the deposited PAC, called membrane fouling.

S. Rungrodnimitchai reported a cost effective method of heavy metal remediation using raw materials widely available in their geographical locality using bagasse and rice husk to effectively sequester $Pb^{2+}$, $Cd^{2+}$, and $Cr^{2+}$ ions in sorption experiments. The bagasse and rice husk were phosphorylated after pretreatment with NaOH to increase their sorption capacity; it was found that these two waste materials could remove the heavy metals more effectively than commercially available ion exchange resins like Dowax. Modified rice husk took lesser time (about 20 minutes) to reach 92% removal of $Pb^{2+}$, while Dowax took 90 minutes to reach the same efficiency. This study is important because it highlights the effectiveness of easily available crop waste like bagasse and rice husk in removal of heavy metals.

A study to determine the effects of nutrient inputs on strophic state and environmental quality of coastal ecosystem has been also included. Both TRIX (Trophic Index) and the AZCI (Arid Zone Coastal Water Quality Index) systems were used to assess the seasonal change in the trophic levels of the Gulf of California. In summer, an oligotrophic condition prevailed due to absence of sewage disposal into the Gulf of Mexico, while in winter there was an increase in the nutrient load of the water in the Gulf, which leads to a mesotrophic condition. Temperature variation between summer and winter in the region is high and water temperature itself varies by ~12°C between summer and winter. This difference would play an important role in the growth of phytoplanktons in the Gulf of California which also affects the overall quality and DO of the water.

It is evident but worth mentioning that all the papers have been prepared by individuals who are experts in their field. Honest effort has been made to check the scientific validity, depth of study, and justification of each chapter through several iterations. We, the editor, publisher, and hard-working water professionals, have put together a comprehensive reference work with a belief that this issue will be of immense use for present and future colleagues who teach, study, research, and/or practice in this particular field.

*Manish Kumar*
*Gurmeet Singh*
*Tushara Chaminda*
*Pham Van Quan*
*Keisuke Kuroda*

Hindawi Publishing Corporation
The Scientific World Journal
Volume 2014, Article ID 158796, 6 pages
http://dx.doi.org/10.1155/2014/158796

*Research Article*

# Heavy Metals Pollution and Pb Isotopic Signatures in Surface Sediments Collected from Bohai Bay, North China

**Bo Gao,[1,2] Jin Lu,[1] Hong Hao,[1] Shuhua Yin,[1] Xiao Yu,[1] Qiwen Wang,[1] and Ke Sun[3]**

[1] *State Key Laboratory of Simulation and Regulation of Water Cycle in River Basin, China Institute of Water Resources and Hydropower Research, Beijing 100038, China*
[2] *Department of Water Environment, China Institute of Water Resources and Hydropower Research, Beijing 100038, China*
[3] *State Key Laboratory of Water Environment Simulation, School of Environment, Beijing Normal University, Beijing 100875, China*

Correspondence should be addressed to Ke Sun; sunke@bnu.edu.cn

Received 27 October 2013; Accepted 5 March 2014; Published 10 April 2014

Academic Editors: T. Chaminda, K. Kuroda, and G. Singh



To investigate the characteristics and potential sources of heavy metals pollution, surface sediments collected from Bohai Bay, North China, were analyzed for the selected metals (Cd, Cr, Cu, Ni, Pb, and Zn). The Geoaccumulation Index was used to assess the level of heavy metal pollution. Pb isotopic compositions in sediments were also measured to effectively identify the potential Pb sources. The results showed that the average concentrations of Cd, Cr, Cu, Ni, Pb, and Zn were 0.15, 79.73, 28.70, 36.56, 25.63, and 72.83 mg/kg, respectively. The mean concentrations of the studied metals were slightly higher than the background values. However, the heavy metals concentrations in surface sediments in Bohai Bay were below the other important bays or estuaries in China. The assessment by Geoaccumulation Index indicated that Cr, Zn, and Cd were classified as "the unpolluted" level, while Ni, Cu, and Pb were ranked as "unpolluted to moderately polluted" level. The order of pollution level of heavy metals was: Pb > Ni > Cu > Cr > Zn > Cd. The Pb isotopic ratios in surface sediments varied from 1.159 to 1.185 for $^{206}Pb/^{207}Pb$ and from 2.456 to 2.482 for $^{208}Pb/^{207}Pb$. Compared with Pb isotopic radios in other sources, Pb contaminations in the surface sediments of Bohai Bay may be controlled by the mix process of coal combustion, aerosol particles deposition, and natural sources.

## 1. Introduction

Bohai Bay is a semienclosed bay located in the western region of the Bohai Sea and is one of the four major compositions in Bohai Sea, North China. It covers an area of $1.60 \times 104\,km^2$ with a population of about 70 million. The average depth is 12.5 m with the maximum of 32 m. Bohai Bay is important harbor and marine lines of economic development in North China. With the rapid development of urban economy and industry around sea, Bohai Bay receives both industrial and domestic wastewater discharges from Beijing, Tianjin, and Hebei province. All the wastewater through rivers and channels drains into the near-shore waters of Bohai Bay directly. This process produced a certain degree of heavy metal pollution for ocean environment [1]. In fact, sediments can receive and absorb metal pollutants from natural weathering, erosion, and anthropogenic activities. Heavy metal concentrations in ocean sediments are important indicators which can reflect the heavy metal pollution of ocean environment [2]. Moreover, heavy metals may be recycled via chemical and biological processes within these sedimentary compartment and back to the water column [3]. The accumulation of metal contaminants in sediments can pose serious environmental problems to the ocean environment. Therefore, identifying the sources of heavy metals is of key importance for making decisions concerning site remediation. Up till now, most researchers have identified the metal sources in sediments by using variations of metal concentrations and enrichment factors relative to natural inputs. However, recent studies have proved that the Pb stable isotopic signatures were a useful tool to effectively identify various sources of Pb pollution in water environment [4–6].

In the recent years, the researches of heavy metals in Bohai Bay had mainly focused on the estuarine and the intertidal zone [7–9]. The scale of whole Bay consisting of the estuarine, the intertidal zone, and centre of the Bay was

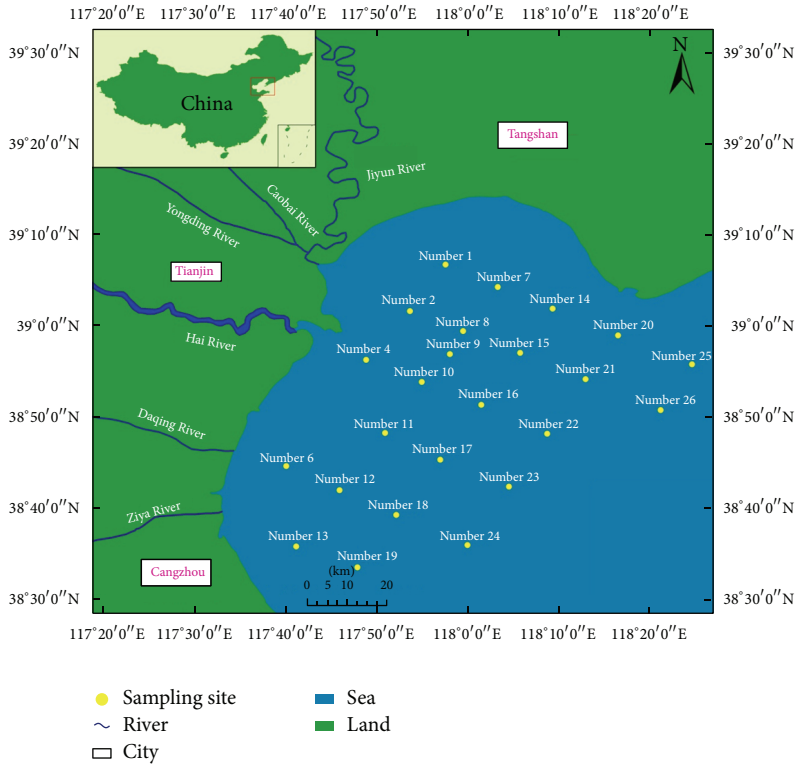


Figure 1: Sampling sites in Bohai Bay.

not fully researched for the characteristics of heavy metals pollution. The objectives of this present study were (1) to determine concentrations and distribution characteristics of heavy metals in surface sediments collected from the Bohai Bay, (2) to evaluate the degree of heavy metal contamination, and (3) to identify the metal pollution sources using Pb isotopic signature. We hope our research on heavy metals contamination and Pb isotopic signatures will be useful to assess the environmental impact of urbanization and economic development on ocean water environment, while providing scientific information for environmental management and restoration in this region.

## 2. Materials and Methods

*2.1. Sampling Sites.* Eighteen surface sediments (0–10 cm) were collected from Bohai Bay, North China. A map of the sampling sites is shown in Figure 1. After sampling, the sediment samples were taken back to indoor laboratory and dried at a temperature below −40°C, crushed, and sieved to less than 200 $\mu$m before the chemical measurements were taken as described below.

*2.2. Analytical Methods.* All chemical treatments were in the ultraclean laboratory, and all reagents were of high purity grade. A strong acid digestion method ($HNO_3$ + $H_2O_2$ + HF) was used to dissolve heavy metals in solution [10]. The digested solutions were measured using inductively coupled plasma-mass spectrometry (ICP-MS, Perkin Elmer Elan DRC-e) for the concentrations of Cd, Cr, Cu, Ni, Pb, and Zn. The accuracy of the analytical procedures employed for the analysis of the metals in sediments was checked using the certified reference material of China stream sediment (GSD-12, GBW07312), obtaining good agreement with certified values.

*2.3. Pb Isotopic Measurement.* Pb isotopic analyses was separated using microexchange columns of anion resin of Dowex-I (200–400 mesh) and HBr and HCl as eluants [11]. Measurements of Pb isotopic compositions were carried out using an ICP-MS (Perkin Elmer Elan DRC-e). The average measured values of the standard NIST SRM-981 are $^{206}Pb/^{207}Pb$ = 1.0937 ± 0.0012 and $^{208}Pb/^{207}Pb$ = 2.3695 ± 0.032 ($n$ = 20), respectively, which were in close agreement with the certified standard values (1.0933 and 2.3704, resp.). Analytical uncertainties in 2s (2s, 2 standard deviation, $n$ = 20) for Pb isotopic ratios ($^{206}Pb/^{207}Pb$) were generally <0.5%.

## 3. Results and Discussion

*3.1. Heavy Metal Concentrations in Surface Sediments.* The heavy metal concentrations and statistics results of all investigated sediments in Bohai Bay are summarized in Table 1. For the comparison purpose, the background values of heavy metals and heavy metals concentrations in sediments from the other Bays and Estuaries were also shown. As can be seen, the concentration ranges of heavy metals of Cr, Ni, Cu, Zn, Cd, and Pb in Bohai Bay sediments were 51.32~

Table 1: Heavy metal concentrations in surface sediments of Bohai Bay and other Bays in China (mg/kg).

| Station | Cr | Ni | Cu | Zn | Cd | Pb | References |
|---|---|---|---|---|---|---|---|
| Minimum | 51.32 | 21.88 | 16.84 | 45.31 | 0.11 | 20.69 | This study |
| Maximum | 94.33 | 47.04 | 34.99 | 84.19 | 0.18 | 28.33 | |
| Mean | 79.73 | 36.56 | 28.70 | 72.83 | 0.15 | 25.63 | |
| Variable coefficient (%) | 11.39 | 13.84 | 12.71 | 12.04 | 10.29 | 7.25 | |
| Intertidal Bohai Bay, China | 68.6 | 28.0 | 24.0 | 73.0 | 0.12 | 25.6 | [5] |
| Southern Bohai Bay, China | 33.5 | 30.5 | 22.7 | 71.7 | 0.14 | 21.7 | [9] |
| Western Bohai Bay, China | 53.1 | 31.4 | 27.9 | 83.6 | 0.13 | 20.5 | [8] |
| Upper continental crust | 35 | 20 | 25 | 71 | 0.098 | 16.6 | [12] |
| Yangtze Estuary, China | 78.9 | 31.8 | 30.7 | 94.3 | 0.26 | 27.3 | [18] |
| Pearl River Estuary, China | 89.0 | 41.7 | 46.2 | 150 | n.d. | 59.3 | [19] |
| Marine sediment quality I | 80 | n.d. | 35 | 150 | 0.5 | 60 | [20] |
| Marine sediment quality II | 150 | n.d. | 100 | 350 | 1.5 | 130 | [20] |
| Target* | 25 | 20 | 20 | 75 | 0.4 | 35 | [13] |
| Trigger* | 50 | 35 | 55 | 150 | 1.0 | 65 | [13] |
| Action* | 80 | 40 | 65 | 200 | 1.5 | 75 | [13] |

*Target indicates the desired quality for fairly clean sediment that is close to background levels.
Trigger indicates that the sediment is moderately contaminated.
Action indicates heavily polluted sediments.

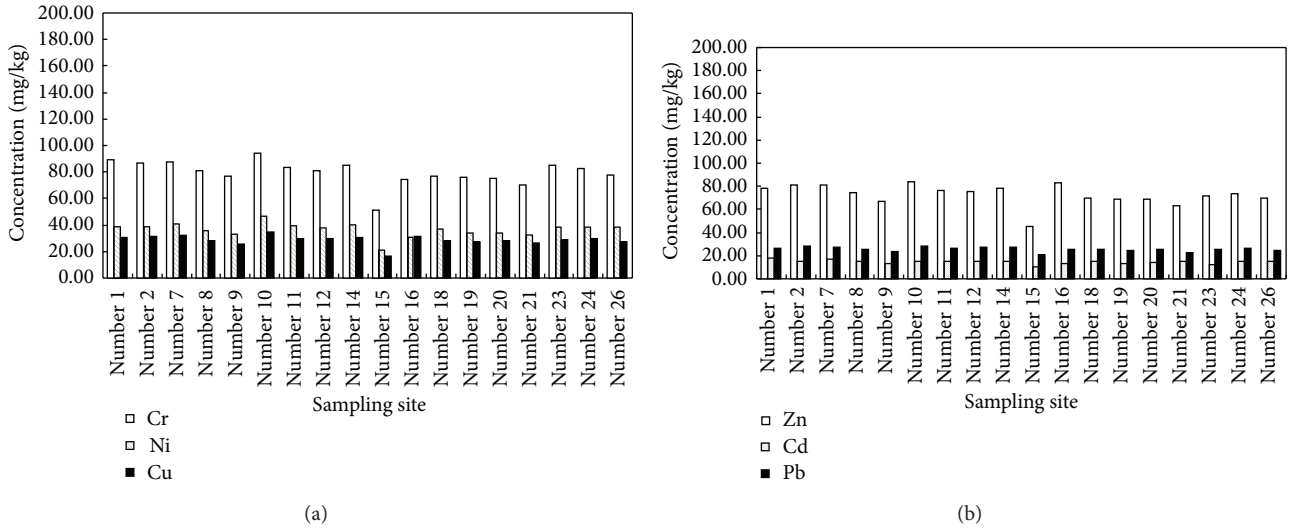


Figure 2: Spatial distribution of heavy metals in surface sediments of Bohai Bay.

94.33, 21.88~47.04, 16.86~34.99, 45.31~84.19, 0.11~0.18, and 20.69~28.33 mg/kg, respectively; and the mean concentrations of these metals were 79.73, 36.56, 28.70, 72.83, 0.15, and 25.63 mg/kg, respectively. The order of mean concentrations in surface sediments was Cr > Zn > Ni > Cu > Pb > Cd. In the sediments from the Bohai Bay, the mean concentrations of the studied metals were slightly higher than the background values [12]. In addition, low variable coefficient (<15%) of these metals showed that the heavy metals were evenly distributed in the Bohai Bay. In fact, the heavy metals concentrations in surface sediments of Bohai Bay were above those in the intertidal Bohai Bay, Southern Bohai Bay, and Western Bohai Bay, indicating that possible anthropogenic input was in the central part of Bohai Bay. However, heavy metals concentrations in surface sediments in Bohai Bay were below those in the other estuaries in China, such as Yangtze Estuary and Pearl River Estuary. In addition, the spatial distribution of heavy metals in sediments collected from Bohai Bay is shown in Figure 2 (Cd concentration is 100 times more than the actual concentration). From Figure 2, it can be seen that heavy metal concentrations in sediments close to center of Bay (number 10) were the highest among all sediments in the whole Bay (Figure 1).

Marine sediment quality (GB 18668-2002), established by China State Bureau of Quality and Technical Supervision (CSBTS, 2002), contains three standard criteria for marine sediments. The marine sediment quality I is applied to protect the habitats for marine life including natural, rare, and endangered species as well as the areas for human recreation and sports, while the marine sediment quality II is applied to

Table 2: $I_{geo}$ values of heavy metals in surface sediments of Bohai Bay.

| Sampling sites | Cr | Ni | Cu | Zn | Cd | Pb |
|---|---|---|---|---|---|---|
| 1# | −0.01/0 | 0.36/1 | 0.23/1 | −0.08/0 | −0.24/0 | 0.66/1 |
| 2# | −0.05/0 | 0.39/1 | 0.24/1 | −0.03/0 | −0.47/0 | 0.73/1 |
| 7# | −0.03/0 | 0.46/1 | 0.31/1 | −0.04/0 | −0.34/0 | 0.70/1 |
| 8# | −0.15/0 | 0.27/1 | 0.11/1 | −0.16/0 | −0.49/0 | 0.57/1 |
| 9# | −0.23/0 | 0.13/1 | −0.03/0 | −0.30/0 | −0.62/0 | 0.50/1 |
| 10# | 0.07/1 | 0.65/1 | 0.41/1 | 0.02/1 | −0.50/0 | 0.74/1 |
| 11# | −0.11/0 | 0.39/1 | 0.17/1 | −0.12/0 | −0.44/0 | 0.62/1 |
| 12# | −0.15/0 | 0.35/1 | 0.16/1 | −0.14/0 | −0.44/0 | 0.67/1 |
| 14# | −0.09/0 | 0.42/1 | 0.20/1 | −0.08/0 | −0.46/0 | 0.68/1 |
| 15# | −0.81/0 | −0.46/0 | −0.64/0 | −0.87/0 | −0.98/0 | 0.29/1 |
| 16# | −0.28/0 | 0.04/1 | 0.27/1 | 0.00/0 | −0.64/0 | 0.61/1 |
| 18# | −0.22/0 | 0.26/1 | 0.09/1 | −0.25/0 | −0.46/0 | 0.58/1 |
| 19# | −0.25/0 | 0.22/1 | 0.04/1 | −0.27/0 | −0.67/0 | 0.54/1 |
| 20# | −0.25/0 | 0.21/1 | 0.08/1 | −0.27/0 | −0.54/0 | 0.60/1 |
| 21# | −0.35/0 | 0.11/1 | −0.01/0 | −0.39/0 | −0.49/0 | 0.41/1 |
| 23# | −0.08/0 | 0.37/1 | 0.15/1 | −0.20/0 | −0.72/0 | 0.61/1 |
| 24# | −0.12/0 | 0.35/1 | 0.16/1 | −0.17/0 | −0.49/0 | 0.62/1 |
| 26# | −0.22/0 | 0.31/1 | 0.07/1 | −0.25/0 | −0.46/0 | 0.55/1 |
| Average | −0.19/0 | 0.27/1 | 0.11/1 | −0.20/0 | −0.53/0 | 0.59/1 |

regulating general industrial use and coastal tourism. Based on marine sediment quality (GB 18668-2002), the overall mean concentrations of all selected heavy metals in Bohai Bay are below those value of the marine sediment quality I, indicating that the overall sediments quality in the Bohai Bay has not been obviously impacted by these six heavy metals. However, the mean concentration of Cr was close to the marine sediment quality I and Cr concentrations in some sampling sites have higher values than the value of marine sediment quality I, especially for the number 10 (Figure 2).

Sediment quality guidelines (SQGs) have been developed to deal with environmental concerns, and a stricter criterion in Hong Kong was also chosen to assess the contamination level of individual metals in sediments of the Bohai Bay (Table 1) [13]. The concentrations of Cu, Pb Zn, and Cd in sediments from 94.4%, 100%, 44.4%, and 100% of stations, respectively, were lower than "target" values and showed no signs of contamination. The contents of Cr at 100% of stations and Ni at 66.7% of stations were higher than the "trigger" values which are regarded as the upper limit of the desired quality for fairly clean sediments, indicating Bohai Bay sediments were moderately contaminated for Cr and Ni. In fact, there were 55.6% and 16.7% sediments heavily polluted by Cr and Ni (Figure 2 and Table 1).

*3.2. Pollution Assessment.* The Geoaccumulation Index ($I_{geo}$) introduced by Müller (1979) was used to assess metal pollution in sediments of Bohai Bay [14]. Geoaccumulation Index is expressed as follows:

$$I_{geo} = \log_2\left(\frac{C_n}{1.5B_n}\right), \quad (1)$$

where $C_n$ is the measured concentration of heavy metal ($n$) in the sediment, $B_n$ is the geochemical background value of heavy metal ($n$), and 1.5 is the background matrix correction factor due to lithogenic effects. In the present study, $B_n$ was selected from the literature [15]. Geoaccumulation Index includes seven grades from Class 0 ($I_{geo} \leq 0$) to Class 6 ($I_{geo} \geq 5$). The $I_{geo}$ is associated with a qualitative scale of pollution intensity; samples may be classified as unpolluted ($I_{geo} \leq 0$), unpolluted to moderately polluted ($0 \leq I_{geo} \leq 1$), moderately polluted ($1 \leq I_{geo} \leq 2$), moderate to strongly polluted ($2 \leq I_{geo} \leq 3$), strongly polluted ($3 \leq I_{geo} \leq 4$), strongly to extremely polluted ($4 \leq I_{geo} \leq 5$), and extremely polluted ($I_{geo} \geq 5$).

Based on the $I_{geo}$ data and the Geoaccumulation Index, the results of the $I_{geo}$ values and pollution level of heavy metals of surface sediment in Bohai Bay are shown in Table 2. In general, the average $I_{geo}$ values are −0.91 for Cr, 0.27 for Ni, 0.11 for Cu, −0.20 for Zn, −0.53 for Cd, and 0.59 for Pb. The order of average $I_{geo}$ values was Pb > Ni > Cu > Cr > Zn > Cd. Among the average $I_{geo}$ of Cr, Zn and Cd were less than zero ($I_{geo} \leq 0$), which were classified as "unpolluted" level. However, the $I_{geo}$ value of Cr and Zn in sampling site number 10 was more than zero, which were ranked as "unpolluted to moderately polluted" level. In addition, the average $I_{geo}$ values of Ni, Cu, and Pb were ranked as "unpolluted to moderately polluted" level ($0 \leq I_{geo} \leq 1$). However, the $I_{geo}$ value of Ni and Cu in sampling site number 15 was less than zero. In general, the worst pollution of heavy metals occurred in sampling site number 10 and the lightest pollution of heavy metals was in sampling site number 15.

*3.3. Pb Isotopic Compositions in Surface Sediments.* The results of Pb isotope ratios of sediment samples in Bohai Bay and other environmental samples (natural sources, ores in

Table 3: Comparison of Pb isotope ratios of surface sediments in Bohai and other sources in environment.

| Sample | $^{206}Pb/^{207}Pb$ | $^{208}Pb/^{207}Pb$ | Reference |
|---|---|---|---|
| Sediments in Bohai Bay | 1.159–1.185 (average 1.176) | 2.456–2.482 (average 2.473) | In this study |
| Natural sources | 1.178–1.202 | 2.462–2.526 | In this study |
| Ores in this region | 1.143–1.205 | 2.446–2.494 | [21] |
| Vehicle exhaust (leaded) | 1.099 | 2.4349 | [22] |
| Vehicle exhaust (unleaded) | 1.1468 | 2.4358 | [22] |
| Unburned coal | 1.1628 | 2.4548 | [22] |
| Air deposition | 1.150–1.194 | 2.428–2.485 | [16] |

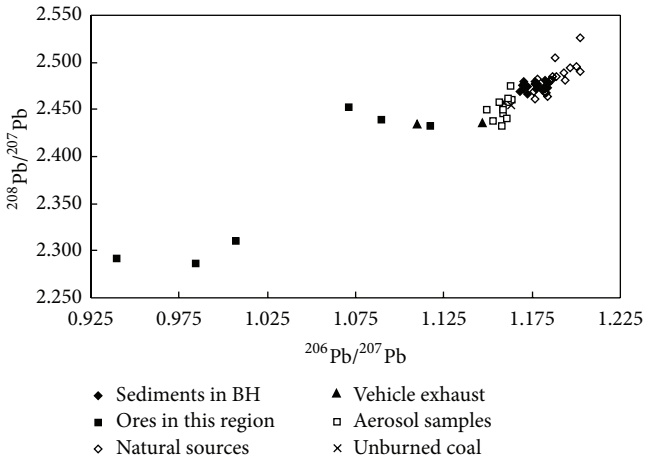


Figure 3: Comparison of the Pb isotopic ratios in sediments of Bohai Bay and other sources.

this region, vehicle exhaust, aerosol samples, and unburned coal) are shown in Table 3. Lead isotopic ratios ranged from 1.159 to 1.185 for $^{206}Pb/^{207}Pb$ and 2.456 to 2.482 for $^{208}Pb/^{207}Pb$. From Table 3, it can be seen that sediments from all sampling sites have relative lower values of $^{206}Pb/^{207}Pb$ ratios close to those values in pollution sources, suggesting the influence of anthropogenic inputs in Bohai Bay. In order to assess Pb contamination and identify potential Pb sources of sediments, the correlation between 1/Pb concentrations and $^{206}Pb/^{207}Pb$ ratios were analyzed. The analytic results showed that the relationship was not obviously correlated ($R^2 = 0.2772$), indicating that Pb sources of sediments were relatively complicated and cannot be simply attributed to binary mixing process of two sources [6].

Source apportionment can also be accomplished by analyzing the Pb isotopic radios ($^{206}Pb/^{207}Pb$ and $^{208}Pb/^{207}Pb$) in the environmental samples and major pollution sources with a lines mixing model [6]. The comparison between $^{206}Pb/^{207}Pb$ and $^{208}Pb/^{207}Pb$ ratios in sediments and other environmental samples showed that the $^{206}Pb/^{207}Pb$ ratios in surface sediments collected from Bohai Bay were obviously higher than those from the emission of vehicle exhaust and Pb ores mining, indicating that these two anthropogenic inputs were not important factors for Pb pollution in sediments (Figure 3). Wang et al. also have confirmed that lead concentrations of atmospheric aerosols in Tianjin were decreased significantly after the leaded gasoline ban [16]. In fact, the $^{206}Pb/^{207}Pb$ and $^{208}Pb/^{207}Pb$ ratios in sediments were significantly similar to those in natural sources, unburned coal, and aerosol samples in the city of Tianjin. In the northern part of China, coal became one of most important energy resources in urban economical and industrial development. The leaded particular matter from coal combustion and coupled with the urban dusts (contain a mass of cement material) can be transported to the Bohai Bay by atmospheric deposition and surface river runoff. Previous study has shown that a large amount of Pb was supplied by the precipitation of aerosols in coastal environments and coal burning from power generation plants and other industrial activities may be the major source of Pb in its sediments [17]. Therefore, Pb contamination in the sediments of Bohai Bay may be controlled by the mix process of coal combustion, aerosol particles deposition, and natural sources.

## 4. Conclusion

Our investigation of heavy metals (Cr, Ni, Cu, Zn, Cd, and Pb) in surface sediments collected from Bohai Bay showed that the mean concentrations of the studied metals were slightly higher than the background values. However, the heavy metals concentrations in surface sediments in Bohai Bay were below the other important bays or estuaries in China. The assessment by Geoaccumulation Index indicated that Cr, Zn, and Cd were at the "unpolluted" level, while Ni, Cu, and Pb were ranked as "unpolluted to moderately polluted" level. The pollution level of the heavy mental was Pb > Ni > Cu > Cr > Zn > Cd. The Pb isotopic ratios in surface sediments varied from 1.159 to 1.185 for $^{206}Pb/^{207}Pb$ and from 2.456 to 2.482 for $^{208}Pb/^{207}Pb$. Pb sources in sediments from Bohai Bay were more complicated (more than two sources), and there may exist various pollution sources. Compared with the Pb isotopic radios in other sources, coal combustion, aerosol particles deposition, and natural sources may be the major sources for Pb pollution in surface sediments of Bohai Bay.

## Conflict of Interests

The authors declare that there is no conflict of interests regarding the publication of this paper.

## Acknowledgment

This work was supported by the National Instrumentation Program (Grant no. 2011YQ14015009).

## References


[1] J. H. Tao, "Numerical simulation of aquatic eco-environment of Bohai Bay," in *Proceedings of the Conference of Global Chinese Scholars on Hydrodynamics*, Shanghai, China, 2006.

[2] L. G. Zheng, G. Wang, and G. Yao, "The study of heavy metal in offshore and environmental significance," *Marine Geology Letters*, vol. 18, no. 12, pp. 1–5, 2003 (Chinese).

[3] A. Tessier, P. G. C. Campbell, and M. Bisson, "Sequential extraction procedure for the speciation of particulate trace metals," *Analytical Chemistry*, vol. 51, no. 7, pp. 844–851, 1979.

[4] S. C. Wong, X. D. Li, G. Zhang, S. H. Qi, and Y. S. Min, "Heavy metals in agricultural soils of the Pearl River Delta, South China," *Environmental Pollution*, vol. 119, no. 1, pp. 33–44, 2002.

[5] B. Gao, X. R. Liang, H. D. Zhou, and X. L. Tu, "Lead isotopes as a tracer of Pb origin in the sediments from Beijiang River, South China," *Water Science and Technology*, vol. 66, no. 12, pp. 2613–2619, 2012.

[6] H. Cheng and Y. Hu, "Lead (Pb) isotopic fingerprinting and its applications in lead pollution studies in China: a review," *Environmental Pollution*, vol. 158, no. 5, pp. 1134–1146, 2010.

[7] Y. W. Qin, W. Meng, B. H. Zheng, L. Zhang, and Y. B. Su, "Contaminative features of heavy metals for tidal sediment cores in Tianjin Bohai Bay," *Environmental Science*, vol. 27, no. 2, pp. 268–273, 2006 (Chinese).

[8] H. Feng, H. Jiang, W. Gao et al., "Metal contamination in sediments of the western Bohai Bay and adjacent estuaries, China," *Journal of Environmental Management*, vol. 92, no. 4, pp. 1185–1197, 2011.

[9] B. Q. Hu, G. G. Li, J. Q. Bi, J. T. Zhao, and R. Y. Bu, "Spatial distribution and ecotoxicological risk assessment of heavy metals in surface sediments of the Southern Bohai Bay, China," *Environmental Science and Pollution Research*, vol. 20, pp. 4099–4110, 2013.

[10] Y. Liu, H. C. Liu, and X. H. Li, "Simultaneous and precise determination of 40 trace elements in rock samples using ICP-MS," *Geochimica*, vol. 25, no. 6, pp. 552–226, 1966 (Chinese).

[11] B.-Q. Zhu, Y.-W. Chen, and J.-H. Peng, "Lead isotope geochemistry of the urban environment in the pearl river delta," *Applied Geochemistry*, vol. 16, no. 4, pp. 409–417, 2001.

[12] S. R. Taylor and S. M. Mclenman, "The chemical composition evolution of the continental crust," *Reviews of Geophysics*, vol. 33, pp. 241–265, 1995.

[13] M. M. Lau, R. C. Rootham, and G. C. Bradley, "A strategy for the management of contaminated dredged sediment in Hong Kong," *Journal of Environmental Management*, vol. 38, no. 2, pp. 99–114, 1993.

[14] G. Müller, "Schwermetalle in den sedimenten des Rheins—veränderungen seitt 1971," *Umschan*, vol. 79, pp. 778–783, 1979.

[15] S. Y. Li, F. M. Miao, and G. X. Liu, "The distribution and environment background values of the heavy metals in sediment of Bohai Sea," *Chinese Environment Science*, vol. 14, no. 5, pp. 370–376, 1994 (Chinese).

[16] W. Wang, X. Liu, L. Zhao, D. Guo, X. Tian, and F. Adams, "Effectiveness of leaded petrol phase-out in Tianjin, China based on the aerosol lead concentration and isotope abundance ratio," *Science of the Total Environment*, vol. 364, no. 1–3, pp. 175–187, 2006.

[17] X. Li, O. W. H. Wai, Y. S. Li, B. J. Coles, M. H. Ramsey, and I. Thornton, "Heavy metal distribution in sediment profiles of the Pearl River estuary, South China," *Applied Geochemistry*, vol. 15, no. 5, pp. 567–581, 2000.

[18] W. Zhang, H. Feng, J. Chang, J. Qu, H. Xie, and L. Yu, "Heavy metal contamination in surface sediments of Yangtze River intertidal zone: an assessment from different indexes," *Environmental Pollution*, vol. 157, no. 5, pp. 1533–1543, 2009.

[19] H.-Y. Zhou, X.-T. Peng, and J.-M. Pan, "Distribution, source and enrichment of some chemical elements in sediments of the Pearl River Estuary, China," *Continental Shelf Research*, vol. 24, no. 16, pp. 1857–1875, 2004.

[20] CSBTS, *Marine Sediment Quality*, Standards Press of China, Beijing, China, 2002.

[21] B. Zhu, "The mapping of geochemical provinces in China based on Pb isotopes," *Journal of Geochemical Exploration*, vol. 55, no. 1–3, pp. 171–181, 1995.

[22] J. Chen, M. Tan, Y. Li et al., "A lead isotope record of shanghai atmospheric lead emissions in total suspended particles during the period of phasing out of leaded gasoline," *Atmospheric Environment*, vol. 39, no. 7, pp. 1245–1253, 2005.

Hindawi Publishing Corporation
The Scientific World Journal
Volume 2014, Article ID 618054, 7 pages
http://dx.doi.org/10.1155/2014/618054

*Research Article*

# Effects of Sewage Discharge on Trophic State and Water Quality in a Coastal Ecosystem of the Gulf of California

**Héctor Hugo Vargas-González,[1] José Alfredo Arreola-Lizárraga,[1] Renato Arturo Mendoza-Salgado,[2] Lía Celina Méndez-Rodríguez,[2] Carlos Hernando Lechuga-Deveze,[2] Gustavo Padilla-Arredondo,[1] and Miguel Cordoba-Matson[2]**

[1] *Centro de Investigaciones Biológicas del Noroeste, S. C. (CIBNOR, S.C.), 85454 Guaymas, SON, Mexico*
[2] *Centro de Investigaciones Biológicas del Noroeste, S. C. (CIBNOR, S.C.), 23090 La Paz, BCS, Mexico*

Correspondence should be addressed to José Alfredo Arreola-Lizárraga; aarreola04@cibnor.mx

Received 2 November 2013; Accepted 25 November 2013; Published 24 February 2014

Academic Editors: M. Kumar and K. Kuroda



This paper provides evidence of the effects of urban wastewater discharges on the trophic state and environmental quality of a coastal water body in a semiarid subtropical region in the Gulf of California. The concentrations of dissolved inorganic nutrients and organic matter from urban wastewater primary treatment were estimated. La Salada Cove was the receiving water body and parameters measured during an annual cycle were temperature, salinity, dissolved oxygen, nitrite, nitrate, ammonia, orthophosphate, and chlorophyll *a*. The effects of sewage inputs were determined by using Trophic State Index (TRIX) and the Arid Zone Coastal Water Quality Index (AZCI). It was observed that urban wastewater of the city of Guaymas provided 1,237 ton N $yr^{-1}$ and 811 ton P $yr^{-1}$ and TRIX indicated that the receiving water body showed symptoms of eutrophication from an oligotrophic state to a mesotrophic state; AZCI also indicated that the environmental quality of the water body was poor. The effects of urban wastewater supply with insufficient treatment resulted in symptoms of eutrophication and loss of ecological functions and services of the coastal ecosystem in La Salada Cove.

## 1. Introduction

Mexico has 110 million inhabitants, of which ~15% live in the coastal zone [1] in 156 coastal municipalities located along ~11,000 km of coastline [2], and one of the main environmental problems on the national level is that most coastal cities are characterized by the insufficient treatment of municipal wastewater [3]. It is estimated that 58% of the wastewater from urban centers and 81% of industrial wastes are discharged directly into water bodies with no or inadequate treatment resulting in ~73% of the water bodies being contaminated [4]. Industrial or municipal sewage is fast emerging as an environmental problem whereby untreated or poorly treated water is discharged directly into coastal water bodies making them highly susceptible to eutrophication.

In general, it has been observed that tropical coastal ecosystems of developing countries have limited treatment processes of wastewater, causing possibly eutrophication problems of adjacent coastal systems due to nutrient inputs from anthropogenic sources, as well as the increased intensity and duration of solar radiation [5, 6].

The current state of knowledge of coastal eutrophication paradigm is changing and evolving from the traditional limited definition: an increase in the rate of supply of organic matter to an ecosystem [7]. Coastal eutrophication should now also include a macroscopic component where it takes into account the impacts of the drivers of global change and the increases in world population on the coasts with up to 50% of the earth's surface having been converted to agricultural and livestock production [8]. For this reason, it is imperative to increase the studies providing evidence of change in coastal ecosystems in order to evaluate the responses to nutrient stimulation [9].

Eutrophication is a process that involves an increase in the trophic status of a water body [7] and therefore the understanding of changes in the trophic status has been an important issue that has motivated the design of indexes and models. An example of this is the TRIX index (Trrophic Index) [10] and AZCI (Arid Zone Coastal Water Quality Index) [11]. The TRIX has been applied mainly in-coastal water bodies of Europe [12–17]. The AZCI has been applied in coastal water bodies in arid regions of Northwest Mexico [11, 18].

This study was conducted at La Salada Cove, a coastal subtropical water body in an arid region that receives urban sewage from the city of Guaymas (~120,000 inhab.) located on the east coast of the Gulf of California. The objective is to determine the effects of nutrient inputs on trophic state and environmental quality of the ecosystem.

## 2. Materials and Methods

*2.1. Study Area.* La Salada Cove is located on the Gulf of California in the State of Sonora, Mexico (27°52′N, 110°55′W). This cove has an area of ~11 ha and a mean depth of 3 m, it receives ~80% of the total sewage from the city of Guaymas (~120,000 inhab.), and receives a primary treatment (Figure 1). La Salada Cove has a seasonal pattern of water temperature with maximum of 32°C in August and minimum of 15°C in January; salinity varies from 35 to 37 [19]. The tide is mixed-semidiurnal with a range of 1 m [19]. This region has a dry desert climate with evaporation of ~3000 mm $yr^{-1}$ which exceeds rainfall of <300 mm $yr^{-1}$ [20]. The seasonal pattern of winds is southeastern in summer at 5 m $s^{-1}$ and northwestern in winter at 8–12 m $s^{-1}$, and this pattern also influences coastal circulation [21].

An important consideration is that during the study period, in summer, there was an extreme event of rain due to Tropical Storm Jimena in September 3, 2009. This event collapsed drainage system of the city and urban wastewater was discharged directly to Guaymas Bay; hence, La Salada Cove did not receive wastewater in the summer season and it served as a control period.

*2.2. Sampling and Measurements.* Nutrients and organic matter loading was estimated by its concentrations observed in the discharge site, and the wastewater flow (18600 $m^3$ $d^{-1}$) to La Salada Cove. In the discharge site, integrated water samples were collected in each season for the determination of nitrite, nitrate, ammonium, orthophosphate, biochemical oxygen demand, and chemical oxygen demand. Its concentrations were determined by chemical methods [22].

In La Salada Cove, water quality was sampled at 12 sampling stations each week three times in a representative month of each season: winter (February), spring (April), summer (September), and fall (November). Water samples were taken between 7:00 and 13:00 h. At each sampling station, water was collected both near the surface and near the bottom in 1 L plastic bottles; these samples were used to measure nutrients (nitrite, nitrate, ammonium, and orthophosphate) and chlorophyll *a*. Measurements of temperature, salinity, and dissolved oxygen were made at each station using a Hydrolab DS5X multisensor, Hach, Loveland, CO, USA. Water samples were transported on ice to the laboratory for analysis. Nutrient concentration was determined by chemical methods [22]. Samples for analysis of chlorophyll a were collected by filtration through Whatman GF/C glass fiber filters, extracted with 90% *v*/*v* acetone, and measured by spectrophotometry according to [23].

*2.3. Indexes and Statistical Data Analysis.* A multivariate, multidimensional scaling on nonparametric transformed data ($\log_{x+1}$) was applied and standardized to determine whether seasons had an effect in terms of water quality, the statistical software PRIMER 6 (Primer-E, Ivybridge, UK) was used to perform the analysis.

The Trophic Index (TRIX) based on the pooled effect of oxygen saturation, nitrite, nitrate, ammonium, orthophosphate, and chlorophyll *a* was used to assess water body trophic state according to [10]. The index is given by

$$\mathrm{TRIX} = \frac{\left[\log 10\left(\mathrm{Chl}\ a \cdot \mathrm{D\%O} \cdot \mathrm{N} \cdot \mathrm{P}\right) + 1.5\right]}{1.2}, \quad (1)$$

where Chl *a* is chlorophyll *a* ($\mu$g L-1), D%O is oxygen as an absolute deviation (%) from saturation, N is dissolved inorganic nitrogen N – $NO_3$ + $NO_2$ + $NH_4$ ($\mu$M), and P is the total phosphorus P-$PO_4$ ($\mu$M). TRIX was scaled from 0 to 10, covering a range of four trophic states (0–4 high quality and low trophic level; 4-5 good quality and moderate trophic level; 5-6 moderate quality and high trophic level; 6–10 degraded and very high trophic level).

Also, the Arid Zone Coastal Water Quality Index (AZCI) which is based on the combined effects of dissolved oxygen, nitrite, nitrate, ammonium, and orthophosphate was used to assess water quality [11]. The index is given by

$$\mathrm{AZCI} = \frac{\sum_{i=1}^{n} I_i \zeta_i}{\sum_{i=1}^{n} \zeta_i}, \quad (2)$$

where $I_i\zeta_i$ is the specific environmental index for variable *i*, *n* is the number of variables, and the range of AZCI is from 0 to 1, where a threshold level of 0.1172 (≈0.12) is used to define the overall environmental quality index. Above this level is considered to be of good environmental quality while below this level is of poor quality.

The TRIX and AZCI data grouped by transect for each season were analyzed by comparison of means with one-way ANOVA analysis of variance and box and whisker plot results were obtained. For the statistical analysis of the data, Statgraphics Plus 4.1 was used.

## 3. Results

*3.1. Nutrients and Organic Matter Loads.* La Salada Cove receives 1,237 ton N $yr^{-1}$ and 811 ton P $yr^{-1}$ from sewage. In addition, values of BOD and COD were 3422 and 2503 kg $d^{-1}$, respectively (Table 1).

*3.2. Seasonal Hydrologic Patterns.* The hydrological behavior data based on temperature, salinity, dissolved oxygen, nitrite,

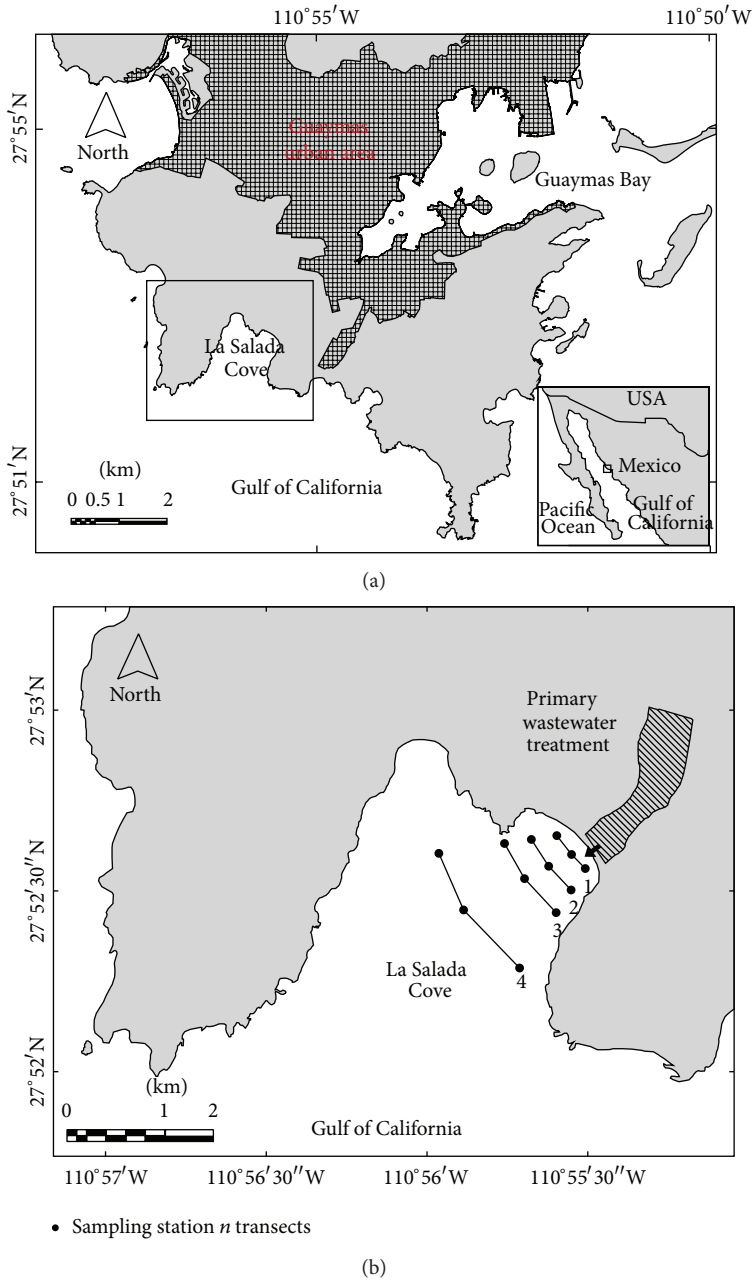


Figure 1: La Salada Cove, including urban area from Guaymas city and showing sampling stations and transects.

nitrate, ammonia, orthophosphate, and chlorophyll *a* showed that between winter and summer environmental conditions were significantly different, while in spring and autumn, there were particular hydrological conditions but with greater similarity to each other (Figure 2). The values of these variables are shown in Table 2.

*3.3. Environmental Indexes.* TRIX results indicated that the summer prevailing state was oligotrophic, while in autumn and winter the state mesotrophic was observed. In spring transects 1 and 2 closer to the discharge, a mesotrophic state was found, while in transects 3 and 4 farther away from the discharge, water quality was oligotrophic (Figure 3(a)).

AZCI results indicated better environmental quality in the summer and worse conditions in the autumn and winter. A loss of environmental quality, that is, poor water quality, was observed in spring transects 1 and 2 closer to the discharge, while transects 3 and 4 farther from the discharge had better water quality (Figure 3(b)).

## 4. Discussion

The La Salada Cove urban wastewater receiving primary treatment is insufficient to reduce inputs of N and P. The evidence of the results in this study suggests that these nutrient inputs are associated with increasing trophic state

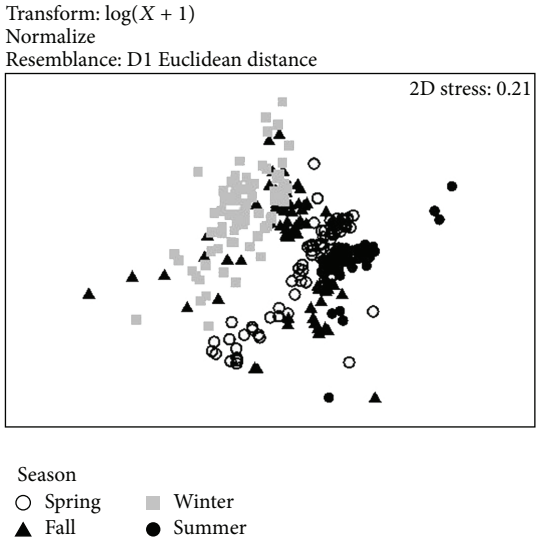


Figure 2: nMDS ordination of water quality parameters for the study area. Temperature, dissolved oxygen, nitrite, nitrate, ammonium, ortophosphate, and chlorophyll *a*, were included in the multivariate analysis.

in the coastal ecosystem and where AZCI and TRIX indexes were consistent in indicating symptoms of eutrophication.

Multivariate analysis (nMDS) showed particular hydrological conditions in each season. The marked differences between summer and winter are attributed on the one hand to the water temperature and phytoplankton biomass and on the other hand to La Salada Cove summer conditions where it did not receive nutrient inputs from sewage, while in winter it received input nutrients from sewage and specifically phosphorus concentrations on this season were higher. Also, the water temperature was different by ~12°C between summer and winter and this is a feature typically observed in this region of the Gulf of California. The temperature differences is attributed to the influence of the air temperature in this arid region that has annual oscillations >14°C [17], as well as water bodies of the Gulf region characterized by values of surface temperature of 26°C in summer and 17°C in winter [24].

The effects of urban wastewater discharges to La Salada Cove were observed in two key variables, in addition to being indicated by the TRIX and AZCI. The responses of the body of water to sewage inputs were more evident by the fact that the summer condition in this study served as the reference. In relation to key variables, (1) it was observed in summer that the average chlorophyll *a* concentration was ~6 mg $m^{-3}$, but the maximum values occurred with blooms that were observed exclusively in the other seasons which received loads by sewage, and (2) dissolved oxygen concentrations in summer had average values of ~5 mg $L^{-1}$ and ~5.5 mg $L^{-1}$ in winter, which is substantially lower from that observed in winter (~8 mg $L^{-1}$) in this area of the Gulf of California without sewage influence [24]. The lower values of dissolved oxygen concentration are attributed to the organic load contributed by sewage and indicated by values of BOD and COD. Dissolved oxygen concentrations

Table 1: Inputs of organic matter and inorganic dissolved nutrients of La Salada Cove.

| Variable | Load kg $d^{-1}$ |
|---|---|
| Biochemical oxygen demand (5 days) | 3422 |
| Chemical oxygen demand | 12503 |
| Soluble phosphorus | 307 |
| Nitrite | <1 |
| Nitrate | 4 |
| Ammonium | 375 |
| Total dissolved inorganic nitrogen | 417 |

of water ≥4 mg $L^{-1}$ observed throughout the year both in the medians and the means suggest that the system has sufficient capacity to assimilate the organic load received but does not imply the absence of adverse effects. Concentrations of dissolved oxygen <3 mg $L^{-1}$ were observed in autumn and winter indicating hypoxic events and this represents an impact to the environment and aquatic life.

The TRIX indicated that in summer, when there were no sewage inputs, the system was oligotrophic, while in the other seasons mesotrophic conditions were observed, and this is attributed to nutrient inputs from sewage increasing the rate of supply organic material causing eutrophication symptoms. The TRIX, in general, has been well accepted for application in environmental management actions [25], even established in the Italian environmental legislation [26]; the results of this study suggest that the TRIX can be applicable for monitoring and trophic state evaluation in coastal water bodies of the Gulf of California. In this study, it was notable that, in autumn and winter, the spatial influence of wastewater discharges covered all the system, but in spring the influence was in the first two sampling transects nearest to discharges, which had significant differences to transects that are more distant. This variability is associated with the load of nutrients and organic matter and coastal hydrodynamic conditions prevailing in each season [19–21], considering that La Salada Cove is an open system influenced by seasonal wind patterns that occurs in the Gulf and induces waves [21], coastal circulation as well as tidal mixing [19] which are processes that favor the dilution and assimilation of nutrients and organic matter and generally contribute to this body of water which is less susceptible to eutrophication. This is consistent with observations [27, 28] in the sense that the magnitude of the adverse effects of sewage sources and depends on the magnitude of the discharges of nitrogen and phosphorus, as well as potential dilution and assimilative capacity of each coastal water body.

The AZCI indicated the same pattern as the TRIX on the effects of wastewater discharges in La Salada Cove, showing a poor environmental quality as the median of the data sampling transects is below the alert threshold (0.15) in seasons that the body of water sewage inputs was received, and it was also notable that the first two transects closest to the discharge area had the worst environmental quality. Previous studies showed that AZCI also worked to characterize seasonal changes by environmental effects (rain and coastal

Table 2: Values of temperature, salinity, dissolved oxygen, nitrite, nitrate, ammonium, orthophosphate, and chlorophyll *a* around year in La Salada Cove.

| | Spring | | | Summer | | | Fall | | | Winter | | |
|---|---|---|---|---|---|---|---|---|---|---|---|---|
| | Mean ± SD | Median | Min. – Max. | Mean ± SD | Median | Min. – Max. | Mean ± SD | Median | Min. – Max. | Mean ± SD | Median | Min. – Max. |
| Temperature (°C) | 27.4 ± 0.5 | 28.1 | 27.2 – 29.7 | 29.3 ± 0.8 | 29.6 | 28.0 – 30.2 | 22.4 ± 2.8 | 21.2 | 17.9 – 26.9 | 16.9 ± 1.1 | 16.9 | 14.4 – 18.9 |
| DO ($mg\,L^{-1}$) | 4.3 ± 0.7 | 4.2 | 3.4 – 6.7 | 5.6 ± 0.3 | 5.6 | 4.7 – 6.1 | 5.8 ± 1.7 | 5.6 | 2.5 – 8 | 5.5 ± 1.6 | 5.8 | 1.7 – 8.1 |
| $N\text{-}NO_2^-$ ($\mu$M) | 0.218 ± 0.47 | 0.131 | 0 – 3.87 | 1.798 ± 1.63 | 1.277 | 0.35 – 9.11 | 0.511 ± 0.38 | 0.378 | 0.03 – 1.46 | 0.661 ± 0.37 | 0.521 | 0.01 – 1.32 |
| $N\text{-}NO_3$ ($\mu$M) | 0.145 ± 0.17 | 0.074 | 0.01 – 0.96 | 0.09 ± 0.08 | 0.064 | 0.02 – 0.46 | 0.359 ± 0.25 | 0.377 | 0.03 – 0.82 | 0.517 ± 0.23 | 0.456 | 0.06 – 0.94 |
| $N\text{-}NH_4$ ($\mu$M) | 5.82 ± 6.83 | 19.79 | 0.23 – 19.31 | 1.733 ± 2.6 | 0.806 | 0.05 – 16.22 | 4.371 ± 6.13 | 1.197 | 0.01 – 19.09 | 1.609 ± 1.21 | 1.238 | 0.09 – 3.99 |
| $PO_4$ ($\mu$M) | 4.291 ± 6.38 | 1.231 | 0.34 – 21.98 | 1.495 ± 0.55 | 1.26 | 1.07 – 5.1 | 2.439 ± 3.4 | 13.54 | 0.32 – 16.42 | 5.014 ± 3.03 | 2.184 | 1.38 – 21.98 |
| Chl a ($mg\,m^{-3}$) | 0.9 ± 1.8 | 0.4 | 0 – 13.7 | 5.7 ± 0.7 | 5.6 | 3.4 – 6.7 | 2.5 ± 5.6 | 0.8 | 0 – 37.2 | 2.2 ± 2.9 | 1 | 0 – 16.9 |

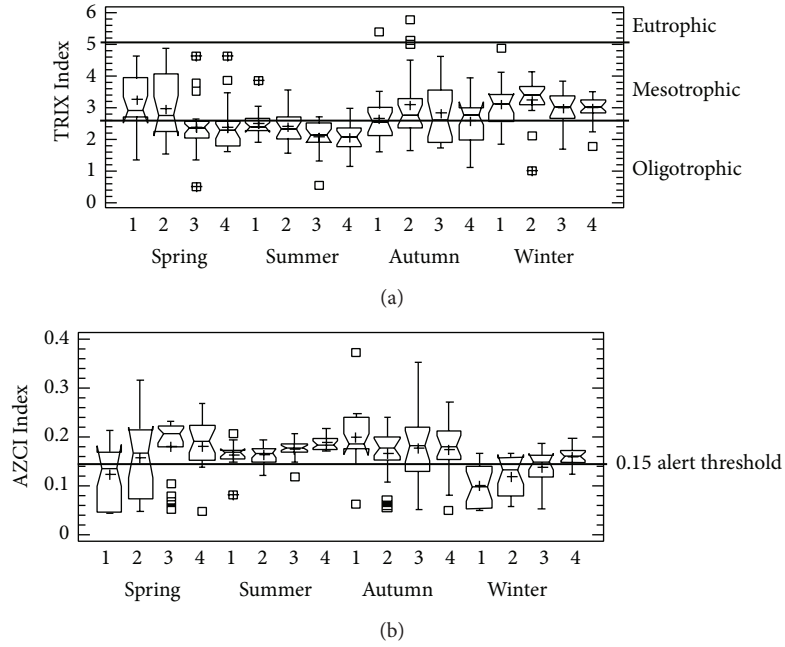


Figure 3: Box and whisker plot of the (a) TRIX, and (b) AZCI for La Salada Cove during seasons. Numbers 1 to 4 represent the transects. Median, quartiles, ranges, and outliers of data are shown for each event. It shows levels of trophic state and water quality influences from urban sewage inputs.

processes) [11] and anthropogenic influences [18] in coastal lagoons from the Gulf of California.

AZCI and TRIX indices differ primarily in that (1) the first incorporates chlorophyll *a*, a biological variable expressing phytoplankton biomass, and (2) the second used algebraic function involving different scale and interpretation, in addition to the fact that AZCI applicates standardization process of the inverses values of the variables and the lowest concentration is the weight value which is more important. In particular, the average chlorophyll *a* value was <2.5 relatively low for seasons, where there were sewage inputs, but eventually had extreme values that might make a difference between TRIX and AZCI. In practical terms, the two water indices provided similar results and were consistent with the environmental condition of La Salada Cove. Taking this into consideration, priority should be given to the development of reliable indicators of trophic levels of coastal ecosystems; also it would be useful to identify policies aimed at establishing environmental legislation in order to help abate the causes of the process of eutrophication [29].

This study provides evidence of the process of eutrophication in the coastal ecosystem of La Salada Cove; this information is useful since it is necessary to increase the amount of data of many coastal water bodies in Mexico [30], in order to compare coastal scenarios in other parts of the world in order to achieve a better understanding of the eutrophication processes [31]. The challenge is to establish a strategy to reduce nutrient inputs from urban wastewater in order to maintain and prevent the loss of ecosystem services provided by coastal ecosystems. In particular, to explore cases where the cost benefit of control measures of excessive nutrient loading is considered and evaluated, there are limited case studies; a good example is the recent work done in the Gulf of Finland [32].

## Conflict of Interests

The authors declare that there is no conflict of interests regarding the publication of this paper.

## Acknowledgments

Refugio López and Andrés Hernández of CIBNOR provided technical support during sampling and provided water analysis. David Urías prepared the map. Comision Nacional del Agua (CONAGUA) and Consejo Nacional de Ciencia y Tecnología (CONACYT) provided funding to this study by research project CONAGUA-CONACYT-2007-01-66573. Héctor Hugo Vargas-González would also like to thank CONACYT for the grant that has allowed him to pursue his master studies.

## References

[1] INEGI, "*Aspectos Geográficos*," Instituto Nacional de Geografía, Estadística e Informática, México, 2010.

[2] CIMARES, "Política Nacional de Mares y Costas de México, Gestión Integral de las Regiones más Dinámicas del Territorio Nacional," Comisión Intersecretarial para el Manejo Sustentable de Mares y Costas, Secretaría de Medio Ambiente y Recursos Naturales, México, 2012.

[3] CONABIO, "Capital Natural y bienestar social," Comisión Nacional para el Conocimiento y Uso de la Biodiversidad, México, 2006.

[4] CONAGUA, "Estadísticas del Agua en México, edición 2011," Comisión Nacional del Agua, SEMARNAT-CONAGUA, México, 2011.

[5] J. E. Corredor, R. W. Howarth, R. R. Twilley, and J. M. Morell, "Nitrogen cycling and anthropogenic impact in the tropical interamerican seas," *Biogeochemistry*, vol. 46, no. 1–3, pp. 163–178, 1999.

[6] J. A. Downing, M. McClain, R. Twilley et al., "The impact of accelerating land-use change on the N-cycle of tropical aquatic ecosystems: current conditions and projected changes," *Biogeochemistry*, vol. 46, no. 1–3, pp. 109–148, 1999.

[7] S. W. Nixon, "Coastal marine eutrophication: a definition, social causes, and future concerns," *Ophelia*, vol. 41, pp. 199–229, 1995.

[8] S. W. Nixon, "Eutrophication and the macroscope," *Hydrobiologia*, vol. 629, no. 1, pp. 5–19, 2009.

[9] J. E. Cloern, "Our evolving conceptual model of the coastal eutrophication problem," *Marine Ecology Progress Series*, vol. 210, pp. 223–253, 2001.

[10] R. A. Vollenweider, F. Giovanardi, G. Montanari, and A. Rinaldi, "Characterization of the trophic conditions of marine coastal waters with special reference to the NW Adriatic Sea: proposal for a Trophic Scale, Turbidity and generalized Water Quality Index," *Environmetrics*, vol. 9, pp. 329–357, 1998.

[11] R. A. Mendoza-Salgado, C. H. Lechuga-Devéze, and A. Ortega-Rubio, "First approach of a method to assess water quality for arid climate bay in the Gulf of California," *Science of the Total Environment*, vol. 347, no. 1–3, pp. 208–216, 2005.

[12] S. Moncheva, V. Dontcheva, G. Shtereva, L. Kamburska, A. Malej, and S. Gorinstein, "Application of eutrophication indices for assessment of the Bulgarian Black Sea coastal ecosystem ecological quality," *Water Science and Technology*, vol. 46, no. 8, pp. 19–28, 2002.

[13] F. Giovanardi and R. A. Vollenweider, "Trophic conditions of marine coastal waters: experience in applying the Trophic Index TRIX to two areas of the Adriatic and Tyrrhenian seas," *Journal of Limnology*, vol. 63, no. 2, pp. 199–218, 2004.

[14] M. Pettine, B. Casentini, S. Fazi, F. Giovanardi, and R. Pagnotta, "A revisitation of TRIX for trophic status assessment in the light of the European Water Framework Directive: application to Italian coastal waters," *Marine Pollution Bulletin*, vol. 54, no. 9, pp. 1413–1426, 2007.

[15] F. Salas, H. Teixeira, C. Marcos, J. C. Marques, and A. Pérez-Ruzafa, "Applicability of the trophic index TRIX in two transitional ecosystems. The Mar Menor lagoon (Spain) and the Mondego estuary (Portugal)," *ICES Journal of Marine Science*, vol. 65, no. 8, pp. 1442–1448, 2008.

[16] I. Primpas and M. Karydis, "Scaling the trophic index (TRIX) in oligotrophic marine environments," *Environmental Monitoring and Assessment*, vol. 178, no. 1–4, pp. 257–269, 2011.

[17] N. Balkis, B. Toklu-Alici, and M. Balci, "Evaluation of Ecological quality Status with the Trophic Index (TRIX), values in the coastal waters of the Gulfs of Erdek and Bandirma In the Marmara Sea," in *Ecological Water Quality Water Treatment and Reuse*, K. Voudouris, Ed., pp. 1–22, InTech, 2012.

[18] L. Morquecho, R. Alonso-Rodríguez, J. A. Arreola-Lizárraga, and A. Reyes-Salinas, "Factors associated with moderate blooms of Pyrodinium bahamense in shallow and restricted subtropical lagoons in the Gulf of California," *Botanica Marina*, vol. 55, pp. 611–623, 2012.

[19] M. F. Lavin and S. G. Marinone, "An overview of the physical oceanography of the Gulf of California," in *Nonlinear Processes in Geophysical Fluid Dynamics*, O. U. Velasco-Fuentes, J. Sheinbaum, and J. Ochoa, Eds., pp. 173–204, Kluwer Academic Publishers, 2003.

[20] E. García, *Modificaciones al sistema de clasificación climática de Koppen (para adaptarlo a las condiciones climáticas de México)*, Instituto de Geografía UNAM, México DF, 5th edition, 2004.

[21] A. Parés-Sierra, A. Mascarenhas, S. G. Marinone, and R. Castro, "Temporal and spatial variation of the surface winds in the Gulf of California," *Geophysical Research Letters*, vol. 30, no. 6, pp. 1–4, 2003.

[22] J. D. H. Strickland and T. R. Parsons, *A Practical Handbook of Seawater Analysis*, Fisheries Research Board of Canada Bulletin, 2nd edition, 1972.

[23] T. R. Parsons, Y. Maita, and C. M. Lalli, *A Manual Chemical and Biological Methods for Seawater Analysis*, Pergamon Press, New York, NY, USA, 1984.

[24] S. Álvarez-Borrego and J. R. Lara-Lara, "The physical environment and primary productivity of the Gulf of California," in *The Gulf of California and Peninsular Province of the Californias*, J. P. Dauphin and B. R. Simoneit, Eds., Memoir 47, pp. 555–567, American Association of Petroleum Geologists, Tulsa, Okla, USA, 1991.

[25] M. Vascetta, P. Kauppila, and E. Furman, "Aggregate indicators in coastal policy making: potentials of the trophic index TRIX for sustainable considerations of eutrophication," *Sustainable Development*, vol. 16, no. 4, pp. 282–289, 2008.

[26] G. Casazza, C. Silvestri, and E. Spada, "Classification of coastal waters according to the new Italian water legislation and comparison with the European Water Directive," *Journal of Coastal Conservation*, vol. 9, no. 1, pp. 65–72, 2003.

[27] S. J. Painting, M. J. Devlin, S. J. Malcolm et al., "Assessing the impact of nutrient enrichment in estuaries: susceptibility to eutrophication," *Marine Pollution Bulletin*, vol. 55, no. 1–6, pp. 74–90, 2007.

[28] D. Scavia and Y. Liu, "Exploring estuarine nutrient susceptibility," *Environmental Science and Technology*, vol. 43, no. 10, pp. 3474–3479, 2009.

[29] C. M. Duarte, "Coastal eutrophication research: a new awareness," *Hydrobiologia*, vol. 629, no. 1, pp. 263–269, 2009.

[30] J. R. Lara-Lara, J. A. Arreola-Lizárraga, and L. E. Calderón-Aguilera, "Los ecosistemas costeros, insulares y epicontinentales," in *Capital Natural de México, vol 1: Conocimiento Actual de la Biodiversidad*, CONABIO, Ed., pp. 109–134, México, 2008.

[31] J. H. Andersen and D. J. Conley, "Eutrophication in coastal marine ecosystems: towards better understanding and management strategies," *Hydrobiologia*, vol. 629, no. 1, pp. 1–4, 2009.

[32] K. Hyytiäinen and A. Huhtala, "Combating eutrophication in coastal areas at risk for oil spills," *Annals of Operations Research*, vol. 191, pp. 63–274, 2011.

Hindawi Publishing Corporation
The Scientific World Journal
Volume 2014, Article ID 634837, 9 pages
http://dx.doi.org/10.1155/2014/634837

*Research Article*

# Rapid Preparation of Biosorbents with High Ion Exchange Capacity from Rice Straw and Bagasse for Removal of Heavy Metals

**Supitcha Rungrodnimitchai**

*Department of Chemical Engineering, Faculty of Engineering, Thammasat University, Khlong Luang, Pathum Thani 12120, Thailand*

Correspondence should be addressed to Supitcha Rungrodnimitchai; supitcha@engr.tu.ac.th

Received 2 November 2013; Accepted 8 December 2013; Published 21 January 2014

Academic Editors: M. Kumar, K. Kuroda, and G. Singh



This work describes the preparation of the cellulose phosphate with high ion exchange capacity from rice straw and bagasse for removal of heavy metals. In this study, rice straw and bagasse were modified by the reaction with phosphoric acid in the presence of urea. The introduced phosphoric group is an ion exchangeable site for heavy metal ions. The reaction by microwave heating yielded modified rice straw and modified bagasse with greater ion exchange capacities (~3.62 meq/g) and shorter reaction time (1.5–5.0 min) than the phosphorylation by oil bath heating. Adsorption experiments towards $Pb^{2+}$, $Cd^{2+}$, and $Cr^{3+}$ ions of the modified rice straw and the modified bagasse were performed at room temperature (heavy metal concentration 40 ppm, adsorbent 2.0 g/L). The kinetics of adsorption agreed with the pseudo-second-order model. It was shown that the modified rice straw and the modified bagasse could adsorb heavy metal ions faster than the commercial ion exchange resin (Dowax). As a result of $Pb^{2+}$ sorption test, the modified rice straw (RH-NaOH 450W) removed $Pb^{2+}$ much faster in the initial step and reached 92% removal after 20 min, while Dowax (commercial ion exchange resin) took 90 min for the same removal efficiency.

## 1. Introduction

Rice straw and sugarcane bagasse are abundant agroresidues in Thailand. The sugarcane bagasse is currently used as a biofuel and in the manufacture of pulp and building materials. On the other hand, open field burning of rice straw frequently causes serious air pollution [1]. Thus a new technology for utilization of these agroresidues to a more value added material should be developed. Many researchers proposed the use of lignocellulosic waste as biosorbents for the removal of heavy metal ions in waste water (i.e., [2–6]).

The advantage of biosorbents from lignocellulosic materials is that they are biobased and biodegradable so that the use and disposal of biosorbents contribute to the reduction of theenvironmental load. On the other hand, commercial ion exchange resins are petroleum based polymers so that the cost is relatively high. Since they are nonbiodegradable, then the environmental impact for disposal is larger than the use of biosorbents.

Although biosorbents are environmental friendly and low cost, most of raw biosorbents have low metal sorption capacity because they do not contain suitable functional group for effective adsorption.

The lignocellulosic biosorbent can be modified by chemical treatment. It was reported that the adsorption capacity of wood was increased by phosphorylation of wood [7]. The enhancement of cadmium sorption capacity of juniper wood by sulfonation mainly originated from the production of sulfonic acid groups, which are binding sites for heavy metals [8]. The phosphoric acid modified rice straw showed high ability for dyes removal from aqueous solution [9]. It was found that cellulose phosphate in modified rice straw prepared by conventional heating could remove almost 100% of $Cd^{2+}$ [10]. As shown in Table 1, rice straw and sugarcane bagasse contain approximately 30–35% and 32–43% cellulose, respectively [11].

Due to hydroxyl groups that exist in cellulose, a series of chemical reaction can easily happen. The phosphorylation

Table 1: Composition of rice straw and sugarcane bagasse (Sakdaronnarong and Jonglertjunya (2012)) [11].

| Composition | Rice straw | Bagasse |
|---|---|---|
| Cellulose | 30–35% | 32–43% |
| Hemicellulose | 25–30% | 19–24 |
| Lignin | 15–28% | 25–32 |
| Ashes | 4–7% | 2–6% |

of hydroxyl groups in bagasse by phosphoric acid in the presence of urea leads to the formation of cellulose phosphate:

$$H_3PO_4 + H\text{–}O\text{–cellulose} \longrightarrow \text{cellulose}\text{–}O\text{–}PO_3H_2 \quad (1)$$

But as the low degree of substitution of cellulose phosphate is described by Inagaki et al. [12], the phosphorylation of cellulose with phosphoric acid (150°C, 8 hr) gave low degree of substitution (0.33). Microwave heating was proposed to give a rapid reaction of cellulose phosphate [13–16].

In this work, the modified rice straw by phosphorylation was compared with the modified bagasse by phosphorylation. The effect of heating methods using oil bath and microwave was discussed. Furthermore, the pretreatment of both materials using dimethyl formamide (DMF) or NaOH solution was attempted to increase the phosphorus content of the modified biosorbents. The feasibility of the modified product as cationic sorbents for removing $Cd^{2+}$, $Cr^{3+}$, and $Pb^{2+}$ from aqueous solution was investigated.

## 2. Materials and Methods

*2.1. Materials.* Rice straw (*Oryza sativa*) was obtained from a local field in Ayutthaya Province, Thailand. It was washed with tap water to remove residual sugar and then dried overnight at 100°C. It was cut and ground with cooking mixer (RS). Some of rice straw was pretreated by being boiled in 16% NaOH solution for 1 hour (RS-NaOH) or immersed in DMF for 1 night (RS-DMF), washed and dried, sieved to 500 micron, and then used in chemical modification.

Sugarcane bagasse (*Saccharum* spp.) was collected from a sugarcane juice shop. Bagasse was washed with tap water to remove residual sugar and then dried overnight at 100°C. It was cut and ground with cooking mixer (Bagasse). Some of bagasse was pretreated by being boiled in 16% NaOH solution for 1 hour (Bagasse-NaOH) or immersed in DMF for 1 night (Bagasse-DMF), washed and dried, sieved to 500 micron, and then used in chemical of modification. All chemicals were reagent grade or analytical grade and used as received.

*2.1.1. Phosphorylation of Rice Straw and Bagasse.* Rice straw or bagasse (2.00 g), urea (22.4 g, 0.37 mol), and phosphoric acid (16.8 mL, 0.29 mol) were mixed and then preheated at 80°C for 15 min in 200 mL round bottom flask. Then it was heated by oil bath at 150°C for 2 hours or by microwave irradiation (Electrolux EMM 2005) at 300 W (5.0 min), 450 W (3.0 min), 600 W (2.0 min), or 800 W (1.5 min). After cooling to room temperature, the mixture was washed with tap water to neutral pH, rinsed with acetone, and dried at 80°C. After that, the modified bagasse was immersed in 100 mL of 1.0 M HCl solution for 1 night, then washed by deionized water, and dried before analysis and sorption tests.

*2.2. Fourier Transform Infrared (FTIR) Spectroscopy.* Treated rice straw and sugarcane bagasse samples were ground and then mixed with KBr to form a disc. FTIR spectroscopy of a KBr disc containing 1% finely ground sample was performed with absorbance mode in a range of 400 to 4.000 $cm^{-1}$.

*2.3. Determination of Total Phosphorus.* Ammonium vanadate-molybdate method was used for spectrophotometric determination of total phosphorus modified bagasse. Sample (0.02 g) and perchloric acid (2 mL) were mixed and digested at 165°C for 12 hours or until the mixtures tuned into colorless clear solution. Vanadate-molybdate acid solution (10 mL) was added to the sample (1 mL). The solution was made up to the mark (50 mL) and the absorbance was measured at 400 nm against blank sample. The total phosphorus content in samples was derived from calibration curve that was obtained using standard solution of $KH_2PO_4$ in the same spectrophotometric analytical condition.

*2.4. Ion Exchange Capacity.* Adsorbents (0.2 g) were immersed in 100 mL of 1.0 M NaCl for 12 hours. By the ion exchange reaction, parts of $H^+$ in the samples were substituted by $Na^+$ and give HCl solution. HCl solutions were collected and titrated with a standard NaOH solution (5 mM).

*2.5. Sorption Experiments.* Metal ion solutions for sorption experiment (40 ppm) were prepared from stock standard solution. The pH values of the solution for experiment were adjusted to $5 \pm 0.1$ by $HNO_3$ or NaOH. Sorbents (0.2 g) were added to 100 mL of 40 ppm metal solutions. This solution was taken every fixed time for 180 minutes. Concentrations of the samples were determined using AAnalyst 800 (Perkin Elmer Instrument). The experiments were conducted in duplicate.

## 3. Results and Discussions

Reaction conditions for preparations of modified rice straw, phosphorus content, degree of substitution, and ion exchange capacity of the modified rice straw are shown in Table 2. The data of the modified bagasse are shown in Table 3.

*3.1. Effect of Pretreatment Methods on Ion Exchange Capacity of Modified Rice Straw and Modified Bagasse.* The effect of pretreatment methods on ion exchange capacity of the sample was tested by using DMF or NaOH solution. For the modified rice straw, the samples which were pretreated by DMF (RS-DMF oil 2 hr, RS-DMF 300 W, RS-DMF 450 W, RS-DMF 600 W, RS-DMF 800 W) showed slightly lower ion exchange capacity than the no pretreatment samples (RS-oil 2 hr, RS 300 W, RS 450 W, RS 600 W, and RS 800 W). However, RS-DMF oil 3 hr showed almost 2.5 times of that of RS-DMF

Table 2: Reaction conditions for preparations of modified rice straw, phosphorus content, degree of substitution, and ion exchange capacity of the modified rice straw.

| Sample names | Heating methods | Conditions | % P | Degree of substitution | Ion exchange capacity (meq/g) |
|---|---|---|---|---|---|
| RS* | — | — | — | — | 0.12* |
| RS-oil 2 hr | Oil bath | 150°C 120 min | 2.85 | 0.16 | 1.29 |
| RS-oil 3 hr | Oil bath | 150°C 180 min | 2.11 | 0.12 | 0.99 |
| RS 300 W | Microwave | 300 W 5 min | 3.03 | 0.17 | 1.30 |
| RS 450 W | Microwave | 450 W 3 min | 3.75 | 0.22 | 1.73 |
| RS 600 W | Microwave | 600 W 2 min | 3.66 | 0.21 | 1.64 |
| RS 800 W | Microwave | 800 W 1.5 min | 3.49 | 0.20 | 1.51 |
| RS-DMF oil 2 hr | Oil bath | 150°C 120 min | 2.65 | 0.15 | 1.13 |
| RS-DMF oil 3 hr | Oil bath | 150°C 180 min | 5.74 | 0.35 | 2.46 |
| RS-DMF 300 W | Microwave | 300 W 5 min | 3.14 | 0.18 | 1.36 |
| RS-DMF 450 W | Microwave | 450 W 3 min | 3.27 | 0.19 | 1.34 |
| RS-DMF 600 W | Microwave | 600 W 2 min | 3.56 | 0.21 | 1.48 |
| RS-DMF 800 W | Microwave | 800 W 1.5 min | 3.14 | 0.18 | 1.24 |
| RS-NaOH oil 2 hr | Oil bath | 150°C 120 min | 6.23 | 0.39 | 2.98 |
| RS-NaOH oil 3 hr* | Oil bath | 150°C 180 min | 6.32 | 0.39 | 2.99* |
| RS-NaOH 300 W | Microwave | 300 W 5 min | 5.96 | 0.37 | 2.21 |
| RS-NaOH 450 W* | Microwave | 450 W 3 min | 7.07 | 0.45 | 2.61* |
| RS-NaOH 600 W | Microwave | 600 W 2 min | 6.99 | 0.45 | 2.50 |
| RS-NaOH 800 W | Microwave | 800 W 1.5 min | 7.04 | 0.45 | 2.58 |

*Samples for sorption test.

Table 3: Reaction conditions for preparations of modified rice straw, phosphorus content, degree of substitution, and ion exchange capacity of the modified rice straw.

| Sample names | Heating methods | Conditions | % P | Degree of substitution | Ion exchange capacity (meq/g) |
|---|---|---|---|---|---|
| Bagasse* | — | — | — | — | 0.11* |
| Bagasse oil 2 hr | Oil bath | 150°C 120 min | 2.90 | 0.16 | 0.86 |
| Bagasse 300 W | Microwave | 300 W 5 min | 4.04 | 0.24 | 1.51 |
| Bagasse 450 W | Microwave | 450 W 3 min | 4.70 | 0.28 | 2.17 |
| Bagasse 600 W | Microwave | 600 W 2 min | 3.82 | 0.22 | 1.36 |
| Bagasse 800 W | Microwave | 800 W 1.5 min | 2.63 | 0.15 | 0.85 |
| Bagasse DMF oil 2 hr | Oil bath | 150°C 120 min | 0.95 | 0.05 | 0.25 |
| Bagasse-DMF 300 W | Microwave | 300 W 5 min | 3.37 | 0.19 | 1.26 |
| Bagasse-DMF 450 W | Microwave | 450 W 3 min | 4.83 | 0.29 | 1.83 |
| Bagasse-DMF 600 W | Microwave | 600 W 2 min | 4.64 | 0.28 | 1.60 |
| Bagasse-DMF 800 W | Microwave | 800 W 1.5 min | 4.58 | 0.27 | 1.59 |
| Bagasse-NaOH oil 2 hr | Oil bath | 150°C 120 min | 2.61 | 0.32 | 1.23 |
| Bagasse-NaOH 300 W | Microwave | 300 W 5 min | 5.81 | 0.36 | 2.38 |
| Bagasse-NaOH 450 W | Microwave | 450 W 3 min | 7.19 | 0.46 | 3.50 |
| Bagasse-NaOH 600 W* | Microwave | 600 W 2 min | 7.76 | 0.51* | 3.62* |
| Bagasse-NaOH 800 W | Microwave | 800 W 1.5 min | 6.89 | 0.44 | 3.08 |

*Samples for sorption test.

oil 3 hr. On the other hand, for the modified bagasse, the samples which were pretreated by DMF (Bagasse-DMF oil 2 h, Bagasse-DMF 300 W, and Bagasse-DMF 450 W) showed slightly lower ion exchange capacity than the no pretreatment samples (RS-oil 2 hr, RS 300 W, and RS 450 W). But Bagasse-DMF 600 W and Bagasse-DMF 800 W showed higher ion exchange capacities than those of Bagasse 600 W and Bagasse 800 W. This may be explained by the temperature profile that DMF improved the ion exchange capacity at long reaction time or at high temperature. As seen in Tables 1 and 2, that the samples treated by NaOH solution (all RS-NaOH samples and all Bagasse-NaOH samples) gave the highest phosphorus content at every condition. It is shown that the treatment of lignocellulosic materials with NaOH solution leached out hemicellulose and lignin. It was reported that the pretreatment results in enlargement of the inner surface area

Table 4: Ion exchange capacity of each adsorbent in the sorption test.

| Adsorbents | Ion exchange capacities (meq/g) |
|---|---|
| RS | 0.12 |
| RS-NaOH oil 3 hr | 2.99 |
| RS-NaOH 450 W | 2.61 |
| Bagasse | 0.11 |
| Bagasse-NaOH 600 W | 3.62 |
| Dowax | 1.20 |

of substrate particles were accomplished by partial solubilization and/or degradation of hemicellulose and lignin [17]. For this reason, the ion exchange capacities of modified samples treated by NaOH solution were much higher than those of the other kinds of modified samples. In summary, RS-NaOH oil 3 h showed the highest ion exchange capacity among modified rice straws (2.99 meq/g). RS-NaOH 450 W showed the highest ion exchange capacity among modified rice straws prepared by microwave heating (2.61 meq/g). On the other hand, Bagasse-NaOH 600 W showed the highest ion exchange capacity among modified rice straws (3.62 meq/g). It should be noted that all the modified samples treated by NaOH solution except for Bagasse-NaOH oil 2 h showed higher degree of substitution than the previously reported value (150°C, 8 hr, degree of substitution 0.33) by Inagaki et al. [12].

*3.2. Effect of Heating Methods.* From Table 1, the modified rice straw prepared by oil bath heating (RS-NaOH-oil 3 hr, 2.99 meq/g) gave lower phosphorus content (6.32%) than those of the modified rice straws prepared by microwave heating (RS-NaOH 450 W (7.07%, 2.61 meq/g), RS-NaOH 600 W (6.99%, 2.50 meq/g), and RS-NaOH 800 W (7.04%, 2.58 meq/g)). However, the ion exchange capacity of RS-NaOH-oil 3 hr was higher than the modified rice straws from microwave heating.

The modified rice straws in this work exhibited higher phosphorus contents and ion capacities than the modified rice straw (no pretreatment), which was reported by Gong and coworker (2.1% P) and also those of our previous work (2.8% P). The difference between ion capacities of the modified rice straws from conventional heating and those from microwave heating may be explained by the temperature profile of the microwave reaction (Figure 1).

In case of oil bath heating, the temperatures of the reactions were kept constantly at 150°C. But in microwave reaction at 800 W, the temperature rose up to 220°C in 90 sec. In case of 600 W (120 sec), 450 W (180 sec), and 300 W (300 sec) the temperatures at the end of reaction were about 170–180°C. All of these temperatures exceeded the optimum temperature for phosphorylation at 150°C. This may cause the side reactions and generation of by-products that contains phosphorus in microwave reaction.

Temperature profile of phosphorylation of bagasse by microwave heating is shown in Figure 2. From the results in Table 2, microwave treatment was shown to be more

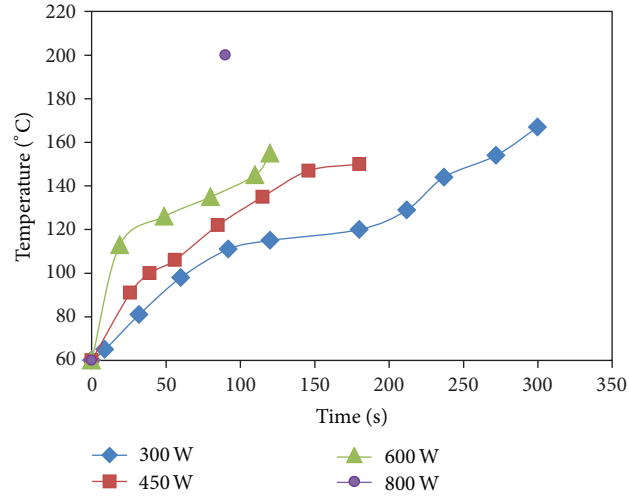


Figure 1: Temperature profile of phosphorylation of rice straw by microwave heating.

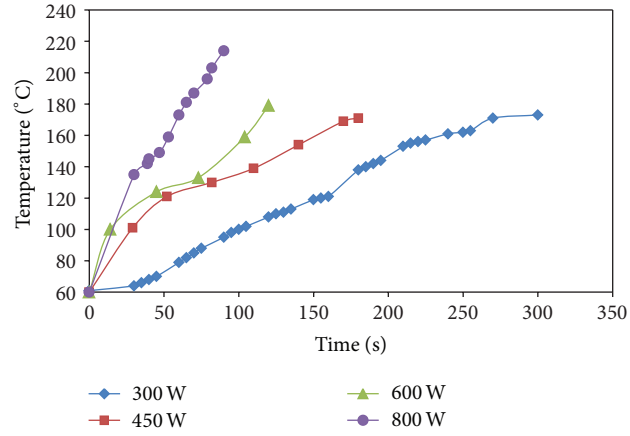


Figure 2: Temperature profile of phosphorylation of bagasse by microwave heating.

efficient than oil bath. As described by Shibata et al. (1996), that microwave irradiation might interact directly with the reactants to cause an enhancement of the reaction rate. This is in contrast to conventional heating where heat enters the sample through its surface and is transferred towards the centre of the sample mainly by thermal conduction [18]. As a result of more effective heating, the modified bagasse prepared by microwave heating gave higher phosphorus content and faster production rate leading to very short production times. From the temperature profile of microwave reaction (Figure 2), in case of 600 W (120 sec), 450 W (180 sec) the temperature at the end of reaction was about 150–160°C which is the optimum temperature for phosphorylation, while at 800 W it rose up to 200°C in 90 sec in which this temperature exceeded the optimum temperature (150°C). Likewise, at 300 W it rose up to 150°C in 240 sec, and then the temperature increased over the optimum temperature (150°C). As seen in Table 2, the modified bagasse which has

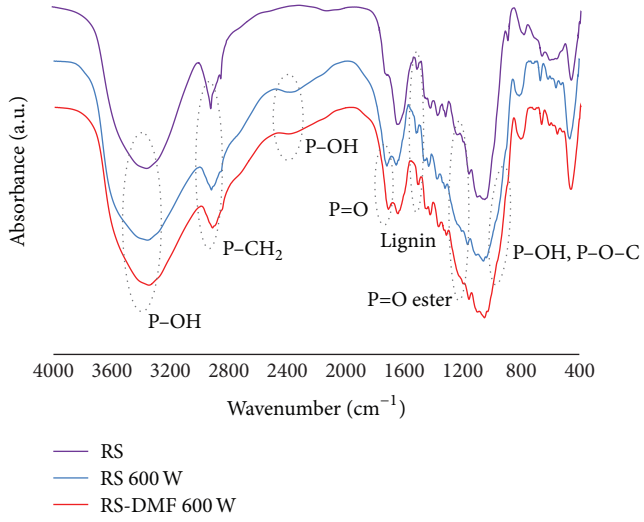


Figure 3: IR spectra of unmodified rice straw (RS), modified rice straw (RS 600 W), and RS-DMF 600 W.

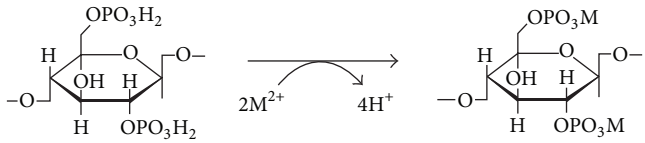


Scheme 1: Ion exchange mechanism of cellulose phosphate.

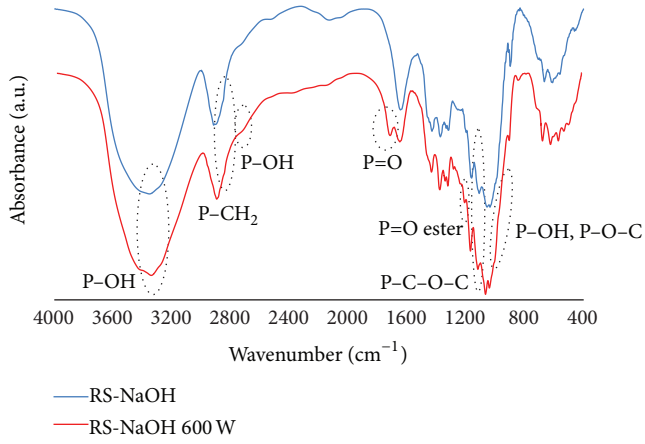


Figure 4: IR spectra of unmodified rice straw after treatment by NaOH solution (RS-NaOH) and modified rice straw (RS-NaOH 600 W).

the highest phosphorus content was prepared by microwave heating at 600 W and 450 W respectively.

*3.3. IR Spectra.* IR spectra of unmodified rice straw (RS) and modified rice straw (untreated (RS 600 W) treated with DMF (RS-DMF 600 W)) by microwave heating at 600 W are shown in Figure 3.

The unmodified rice straw (RS) showed strong broad adsorption at 3350 $cm^{-1}$ from vibration of –OH groups medium adsorption at 2900 $cm^{-1}$ from $–CH_2$ group, and adsorption at 1160 $cm^{-1}$ and 1110 $cm^{-1}$ from C–O–C bond of glycosidic or $\beta$-(1 → 4)-glycosidic bond. These absorption bands indicated the presence of cellulose unit in rice straw. Furthermore, absorption at 1510 $cm^{-1}$ can be attributed to the vibration of aromatic units in lignin of rice straw. In the spectra of the modified rice straw (RS 600 W), a new weak absorption from P–OH bond was found at 2400 $cm^{-1}$ and a shoulder at 2700 $cm^{-1}$. Another absorption at 1710–1720 $cm^{-1}$ was from the vibration of P=O bond; a shoulder at 1200–1300 $cm^{-1}$ was from the vibration of P=O of phosphate ester. At 900–1000 $cm^{-1}$ a shoulder from the vibration of P–OH bond and P–O–C bond was observed.

On the other hand, the spectrum of the modified rice straw treated by DMF (RS-DMF 600 W); showed almost the same absorption spectrum as that of RS 600 W. It implied that treatment by DMF led no significant change in the molecular structure of the modified rice straw.

IR spectra of the rice straw treated by NaOH solution (RS-NaOH), the modified rice straw (treated by NaOH solution) by 3-hour reaction in oil bath (RS-oil 3 hr), and the modified rice straw (treated by NaOH solution) by microwave heating at 600 W (RS-NaOH 600 W) are shown in Figure 4.

In Figure 4, the IR spectra of rice straw treated by NaOH before and after modification are similar to spectra of rice straw before modification (RS) and sample RS 600 W, respectively, except that the absorption at 1510 $cm^{-1}$, which indicates the presence of lignin, disappeared. Lignin in rice straw was removed by NaOH treatment. Thus the main component of the rice straw after NaOH treatment was cellulose. The IR spectrum of RS-oil 3 hr was not different from that of RS-NaOH 600 W. The result suggests that the reaction by microwave heating gave the same product as that from the reaction in oil bath. From IR spectra, it could be concluded that the phosphoric acid group was successfully introduced into the modified rice straws.

IR spectra of the modified bagasse are shown in Figures 5 and 6. They could be explained in similar manners as those of the modified rice straw but with stronger absorption at 1710–1720 $cm^{-1}$ from the vibration of P=O bond.

*3.4. Kinetics Study on Adsorption of Heavy Metal Ions.* The adsorption abilities of modified rice straws (RS-NaOH oil 3 hr and RS-NaOH 450 W) and modified bagasse (Bagasse-NaOH 600 W) were compared with the unmodified rice straw (RS), the unmodified bagasse (Bagasse), and a commercial ion exchange resin (Dowax). The ion exchange reaction is shown in Scheme 1. The ion exchange capacity of each adsorbent is listed in Table 4. The ion exchange capacities of the modified rice straw from oil bath reaction (RS-NaOH oil 3 hr), the modified rice straw from microwave reaction (RS-NaOH-450 W), the unmodified rice straw (RS), the modified bagasse from microwave reaction (Bagasse-NaOH 600 W), and Dowax were 2.99 meq/g, 2.61 meq/g, 0.12 meq/g, 3.62 meq/g, and 1.20 meq/g, respectively.

In the sorption test of 40 ppm $Cd^{2+}$ with 2.0 g/L of the modified rice straw, the modified rice straw prepared by

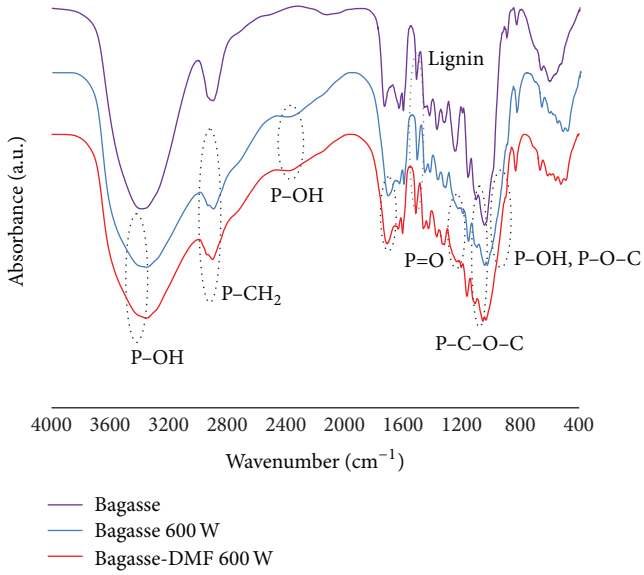


Figure 5: IR spectra of unmodified bagasse (Bagasse), modified bagasse (Bagasse 600 W), and Bagasse-DMF 600 W.

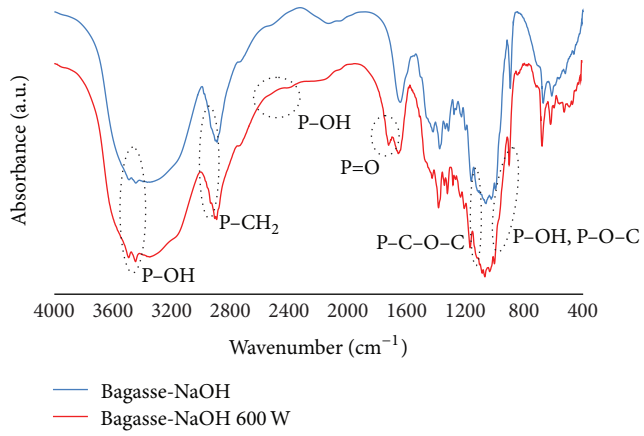


Figure 6: IR spectra of unmodified bagasse after treatment by NaOH solution (Bagasse-NaOH) and modified bagasse (Bagasse-NaOH 600 W).

microwave heating (RS-NaOH-450 W) removed 85% of $Cd^{2+}$ in 60 min, which was faster than Dowax in the first 60 min (Figure 7). It reached the highest % removal of $Cd^{2+}$ at 120 min (88%). On the other hand, unmodified rice straw (RS) adsorbed only 29% of $Cd^{2+}$ in 60 min. It should be noted that the modified rice straw prepared by oil bath reaction (RS-NaOH oil 3 hr), with the highest ion exchange capacity, could remove only 65% of $Cd^{2+}$ after 180 min adsorption. Bagasse-NaOH 600 W reached its highest % removal at 180 min (76%). The unmodified rice straw (RS) and the unmodified bagasse (Bagasse) showed as low as 29.6% and 8.1% removal, respectively.

As seen in Figure 8, all of adsorbents could remove $Pb^{2+}$ better than $Cd^{2+}$. Especially, RS-NaOH 450 W removed $Pb^{2+}$ much faster in the first step and reach 92% removal after 30 min, while Dowax took 90 min to give the same % removal.

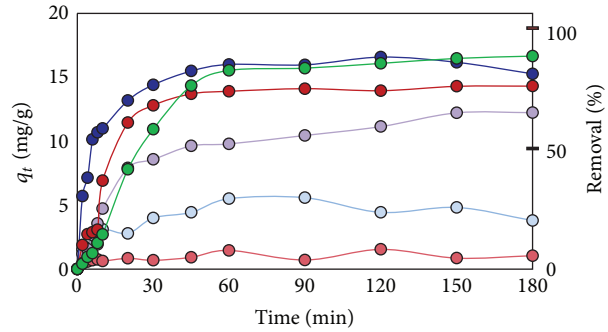


Figure 7: Plot of $Cd^{2+}$ adsorption capacity at time ($q_t$) and % removal versus adsorption time for effect of various sorbents (RS (light blue), RS-oil 3 hr (purple), RS-NaOH 450 W (blue), Bagasse (pink), Bagasse-NaOH 600 W (red), and Dowax (green)).

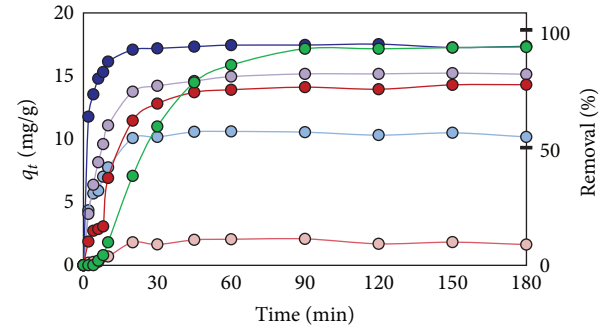


Figure 8: Plot of $Pb^{2+}$ adsorption capacity at time ($q_t$) and % removal versus adsorption time for effect of various sorbents (RS (light blue), RS-oil 3 hr (purple), RS-NaOH 450 W (blue), Bagasse (pink), Bagasse-NaOH 600 W (red), and Dowax (green)).

Apparently, the modified rice straws reached the adsorption equilibrium faster than the commercial resin. On the other hand, Bagasse-NaOH 600 W reached its highest % removal at 90 min (91%). The unmodified rice straw (RS) and the unmodified bagasse (Bagasse) showed as low as 54.59% and 8.83% removal, respectively.

On the sorption test of $Cr^{3+}$ ion, RS-NaOH 450 W removed 78% $Cr^{3+}$ ion in 20 min, and the % removal attained 85% (Figure 9). RS-oil 3 hr decreased $Cr^{3+}$ concentration to 8.5 ppm in 180 min. On the other hand, Dowax could remove 96% of ions after 180 min. On the other hand, Bagasse-NaOH 600 W reached its highest % removal at 180 min (76%). The unmodified rice straw (RS) and the unmodified bagasse (Bagasse) showed 34% and 10.2% removal, respectively.

It was reported that the adsorption kinetics of divalent ions follows pseudo-second-order kinetics [19]. The kinetics rate equation can be rewritten as follows:

$$\frac{dq_t}{d_t} = k(q_e - q_t)^2. \quad (2)$$

Its integrated rate law for a pseudo-second-order reaction has a linear form of

$$\frac{t}{q_t} = \frac{1}{kq_e{}^2} + \frac{t}{q_e}. \quad (3)$$

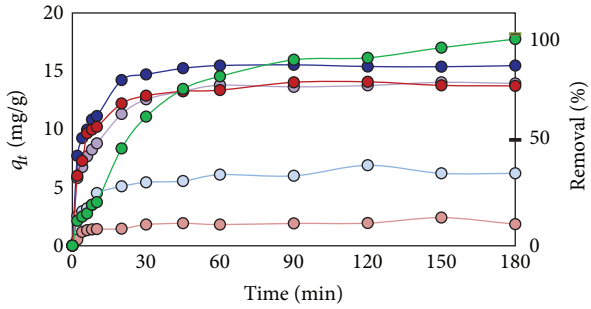


FIGURE 9: Plot of $Cr^{3+}$ adsorption capacity at time ($q_t$) and % removal versus adsorption time for effect of various sorbents (RS (light blue), RS-oil 3 hr (purple), RS-NaOH 450 W (blue), Bagasse (pink), Bagasse-NaOH 600 W (red), and Dowax (green)).

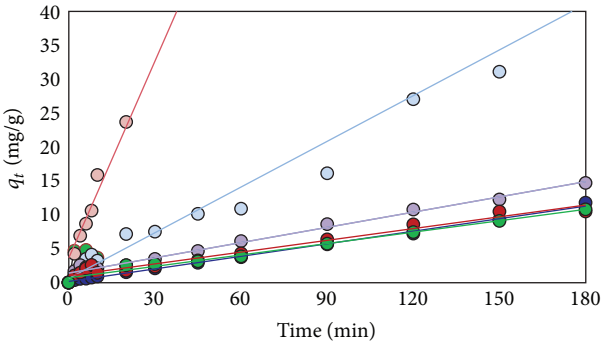


FIGURE 10: Plot of $t/q_t$ of $Cd^{2+}$ versus time for effect of different kinds of various adsorbents (RS (light blue), RS-oil 3 hr (purple), RS-NaOH 450 W (blue), Bagasse (pink), Bagasse-NaOH 600 W (red), and Dowax (green)).

The rate constant and $q_e$ can be determined experimentally by plotting of $t/q_t$ against $t$.

The plots of data obtained from adsorption of $Cd^{2+}$, $Pb^{2+}$, and $Cr^{3+}$ are shown in Figures 10, 11, and 12, respectively. The constants derived from these plots are listed in Table 5.

Adsorption kinetics of the modified rice straws and the modified bagasse showed good fitting with the pseudo-second-order model. It was found that adsorption of the trivalent $Cr^{3+}$ gave the best fitting results for all kinds of sorbents. On the other hand, Dowax showed a large deviation from the theoretical plot at time less than 30 min for adsorption of $Cd^{2+}$ and $Pb^{2+}$, so that it was fit by data of 30~180 min. For every condition, Dowax showed (ion exchange resin) the highest adsorption capacity (17.83–20.16 mg/g), and the next in the series were RS-NaOH 450 W, Bagasse-NaOH 600 W, RS-oil 3 hr, and rice straw for adsorption of $Pb^{2+}$ and $Cr^{3+}$. On the other hand, Bagasse-NaOH 600 W showed the next highest adsorption capacity (17.27 mg/g). Although the modified bagasse (Bagasse-NaOH 600 W, 3.62 meq/g) had higher ion capacity than the modified rice straw (RS-NaOH 450 W, 2.61 meq/g), the adsorption of heavy metal ions of the modified bagasse (Bagasse-NaOH 600 W) was less effective than the modified rice straw.

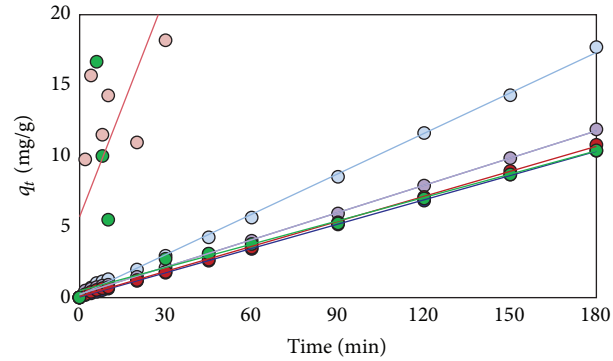


FIGURE 11: Plot of $t/q_t$ of $Pb^{2+}$ versus time for effect of different kinds of various adsorbents (RS (light blue), RS-oil 3 hr (purple), RS-NaOH 450 W (blue), Bagasse (pink), Bagasse-NaOH 600 W (red), and Dowax (green)).

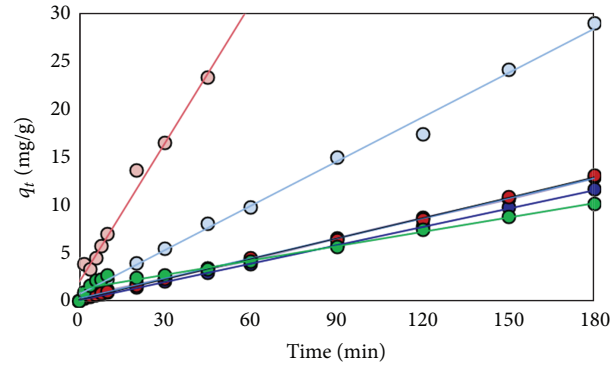


FIGURE 12: Plot of $t/q_t$ of $Cr^{3+}$ versus time for effect of different kinds of various adsorbents (RS (light blue), RS-oil 3 hr (purple), RS-NaOH 450 W (blue), Bagasse (pink), Bagasse-NaOH 600 W (red), and Dowax (green)).

It should be noted that the modified rice straw from microwave reaction (RS-NaOH 450 W) gave the largest initial rate of adsorption, which means the rapid decrease of metal concentration during adsorption. Dowax showed the smallest rate constants so that it took more time for removal of metal ions. Apparently, the modified rice straws attained adsorption equilibrium faster than the commercial resin. This result implied that the ability of adsorption of the modified bagasse was not dependent only on the ion exchange capacity.

Although RS-NaOH 450 W had lower ion exchange capacity than those of RS-oil 3 hr, it could remove more ions with faster speed. It is considered that the microwave reaction takes place at the whole porous structure of cellulose. But the oil bath reaction takes place only on the surface of the particle of cellulose. The reason that the modified rice straw showed better adsorption ability than the modified bagasse might come from its low crystallinity indices of untreated rice straw (37.7%) compared to the untreated sugarcane bagasse (44.4%), which were reported by Sakdaronnarong and Jonglertjunya [11]. So the adsorption ability of the modified rice

Table 5: Parameters form fits to the pseudo-second-order model.

| Ions | Sample | $R^2$ | $q_e$ (mg/g) | $k$ (g/mg min) | Initial rate (mg/g min) |
|---|---|---|---|---|---|
| $Cd^{2+}$ | RS | 0.9618 | 4.45 | $7.92E-02$ | 1.57 |
| | RS-oil 3 hr | 0.9861 | 13.35 | $3.98E-03$ | 0.71 |
| | RS-NaOH 450 W | 0.9972 | 16.18 | $2.13E-02$ | 5.58 |
| | Baggage | 0.9113 | 1.03 | $2.56E-01$ | 0.27 |
| | Baggage-NaOH 600 W | 0.9673 | 17.27 | $3.27E-03$ | 0.98 |
| | Dowax | 0.9876 | 17.83 | $4.45E-03$ | 1.41 |
| $Pb^{2+}$ | RS | 0.9988 | 10.50 | $4.94E-02$ | 5.45 |
| | RS-oil 3 hr | 0.9993 | 15.58 | $1.74E-02$ | 4.22 |
| | RS-NaOH 450 W | 0.9999 | 17.45 | $9.33E-02$ | 28.41 |
| | Baggage | 0.9528 | 1.92 | $4.76E-02$ | 0.17 |
| | Baggage-NaOH 600 W | 0.9996 | 16.98 | $3.87E-02$ | 11.16 |
| | Dowax | 0.992 | 18.21 | $6.21E-03$ | 2.06 |
| $Cr^{3+}$ | RS | 0.9957 | 6.50 | $3.43E-02$ | 1.45 |
| | RS-oil 3 hr | 0.9993 | 14.33 | $1.72E-02$ | 3.54 |
| | RS-NaOH 450 W | 0.9996 | 15.70 | $2.86E-02$ | 7.04 |
| | Baggage | 0.979 | 2.07 | $1.19E-01$ | 0.51 |
| | Baggage-NaOH 600 W | 0.9994 | 14.08 | $2.79E-02$ | 5.52 |
| | Dowax | 0.9709 | 20.16 | $1.89E-03$ | 0.77 |

straw from the microwave reaction may be contributed not only the ion exchange capacity but also the morphology of the material.

## 4. Conclusions

In this research, biosorbents with high ion exchanged capacities were successfully prepared from rice straw and bagasse. The treatment by NaOH solution much improved the degree of substitution and ion exchange capacities of the obtained sorbents.

The rice straw, which was pretreated by NaOH solution, gave the highest phosphorus content when it was phosphorylated by microwave at 450 W (RS-NaOH 450 W, 7.07% P, 2.60 meq/g). The reaction at 150°C for 3 hours in oil bath, gave the modified rice straw with 6.32% phosphorus and the highest ion exchange capacity for rice straw adsorbent (RS-oil 3 hr, 2.99 meq/g). On the other hand, the bagasse treated by NaOH solution gave the highest phosphorus content when it was phosphorylated by microwave at 600 W (Bagasse-NaOH 600 W, 7.76% P, 3.62 meq/g). On the adsorption experiment, both the modified rice straw and the modified bagasse could reach adsorption equilibrium faster than the commercial resin and did not show much difference of % removal from that of the commercially available ion exchange resin (Dowax). Although the modified bagasse in this work had more ion capacity than the modified rice, the modified bagasse presented a good adsorption capacity for $Cd^{2+}$, $Cr^{3+}$, and $Pb^{2+}$ ions with maximum adsorption capacity as modified rice. The result suggested that the modified rice straw is a good candidate for the biodegradable ion exchange resin.

## Conflict of Interests

The author declares that there is no conflict of interests regarding the publication of this paper.

## Acknowledgment

This research received a grant from the Office of the National Research Council of Thailand (NRCT) in the fiscal year of 2008.

## References

[1] R. L. Nelson, P. K. Thor, and C. R. Heaton, "Rice straw buring: alternative policy implications," *California Agriculture*, pp. 4–6, 1980.

[2] I. Gaballah and G. Kilbertus, "Recovery of heavy metal ions through decontamination of synthetic solutions and industrial effluents using modified barks," *Journal of Geochemical Exploration*, vol. 62, no. 1-3, pp. 241–286, 1998.

[3] B. Yu, Y. Zhang, A. Shukla, S. S. Shukla, and K. L. Dorris, "The removal of heavy metal from aqueous solutions by sawdust adsorption—removal of copper," *Journal of Hazardous Materials*, vol. 80, no. 1–3, pp. 33–42, 2000.

[4] Y. Suzuki, T. Kametani, and T. Maruyama, "Removal of heavy metals from aqueous solution by nonliving Ulva seaweed as biosorbent," *Water Research*, vol. 39, no. 9, pp. 1803–1808, 2005.

[5] H. A. Mahvi, D. Naghipour, F. Vaezi, and S. Nazmara, "Tea waste as an adsorbent for heavy metal removal from industrial wastewater," *American Journal of Applied Sciences*, vol. 2, no. 1, pp. 372–375, 2005.

[6] B.-G. Lee and R. M. Rowell, "Removal of heavy metal ions from aqueous solutions using lignocellulosic fibers," *Journal of Natural Fibers*, vol. 1, no. 1, pp. 97–108, 2004.

[7] N. Saito and M. Aoyama, "Adsorption of heavy metal ions by phosphorylated woods," *Journal of the Hokkaido Forest Products Research Institute*, vol. 5, p. 15, 1991.

[8] W. S. Eun and R. M. Rowell, "Cadmium ion sorption onto lignocellulosic biosorbent modified by sulfonation: the origin of sorption capacity improvement," *Chemosphere*, vol. 60, no. 8, pp. 1054–1061, 2005.

[9] R. Gong, Y. Jin, J. Chen, Y. Hu, and S. Sun, "Removal of basic dyes from aqueous solution by sorption on phosphoric acid modified rice straw," *Chemosphere*, vol. 60, no. 8, pp. 1054–1060, 2005.

[10] S. Rungrodnimitchai and J. Dokbua, "Heavy metal ions absorbents from rice straw," in *Proceedings of the International Conference on Green and Sustainable Innovations*, Chaing Mai, Thailand, 2006.

[11] C. Sakdaronnarong and W. Jonglertjunya, "Rice straw and sugarcane bagasse degradation mimicking lignocellulose decay in nature: an alternative approach to biorefinery," *ScienceAsia*, vol. 38, pp. 364–372, 2012.

[12] N. Inagaki, S. Nakamura, H. Asai, and K. Katsuura, "Phosphorylation of cellulose with phosphorous acid and thermal degradation of the product," *Journal of Applied Polymer Science*, vol. 20, no. 10, pp. 2829–2836, 1976.

[13] S. Rungrodnimitchai and U. Subjaroenkul, "Biosorbents from rice straw prepared by microwave heating," in *Proceedings of the Prague Meeting on Macromolecules*, Prague, Republic of Chez, July 2009.

[14] S. Rungrodnimitchai, "Rapid preparation of heavy metal ion adsorbents from rice straw," in *Proceedings of the International Symposium on Engineering, Energy and Environment*, Rayong, Thailand, November 2009.

[15] S. Rungrodnimitchai, "Modification of rice straw for heavy metal ion adsorbents by microwave heating," *Macromolecular Symposia*, vol. 295, no. 1, pp. 100–106, 2010.

[16] U. Subjaroenkul and S. Rungrodnimitchai, "Study on preparation of cellulose phosphate with high ion exchange capacity from bagasse and its adsorption kinetics," in *Proceedings of the 1st EnvironmentalAsia International Conference*, Bangkok, Thailand, March 2011.

[17] A. Pandey, C. R. Soccol, P. Nigam, and V. T. Soccol, "Biotechnological potential of agro-industrial residues. I: sugarcane bagasse," *Bioresource Technology*, vol. 74, no. 1, pp. 69–80, 2000.

[18] X. Zhang and D. O. Hayward, "Applications of microwave dielectric heating in environment-related heterogeneous gas-phase catalytic systems," *Inorganica Chimica Acta*, vol. 359, no. 11, pp. 3421–3433, 2006.

[19] Y. S. Ho and G. McKay, "The kinetics of sorption of divalent metal ions onto sphagnum moss peat," *Water Research*, vol. 34, no. 3, pp. 735–742, 2000.

Hindawi Publishing Corporation
The Scientific World Journal
Volume 2014, Article ID 893203, 11 pages
http://dx.doi.org/10.1155/2014/893203

*Research Article*

# Natural Organic Matter Removal and Fouling in a Low Pressure Hybrid Membrane Systems

**Vedat Uyak,[1] Muge Akdagli,[2] Mehmet Cakmakci,[3] and Ismail Koyuncu[2]**

[1] *Department of Environmental Engineering, Faculty of Engineering, Pamukkale University, Kinikli, 20020 Denizli, Turkey*
[2] *Department of Environmental Engineering, Faculty of Civil, Istanbul Technical University, Maslak, 34469 Istanbul, Turkey*
[3] *Department of Environmental Engineering, Faculty of Civil, Yildiz Technical University, Esenler, 34220 Istanbul, Turkey*

Correspondence should be addressed to Vedat Uyak; vuyak@pau.edu.tr

Received 31 October 2013; Accepted 8 December 2013; Published 8 January 2014

Academic Editors: M. Kumar, K. Kuroda, and G. Singh



The objective of this study was to investigate powdered activated carbon (PAC) contribution to natural organic matter (NOM) removal by a submerged MF and UF hybrid systems. It was found that filtration of surface waters by a bare MF and UF membranes removed negligible TOC; by contrast, significant amounts of TOC were removed when daily added PAC particles were predeposited on the membrane surfaces. These results support the assumption that the membranes surface properties and PAC layer structure might have considerably influential factor on NOM removal. Moreover, it was concluded that the dominant removal mechanism of hybrid membrane system is adsorption of NOM within PAC layer rather than size exclusion of NOM by both of membrane pores. Transmembrane pressure (TMP) increases with PAC membrane systems support the view that PAC adsorption pretreatment will not prevent the development of membrane pressure; on the contrary, PAC particles themselves caused membrane fouling by blocking the entrance of pores of MF and UF membranes. Although all three source waters have similar HPI content, it appears that the PAC interaction with the entrance of membrane pores was responsible for offsetting the NOM fractional effects on membrane fouling for these source waters.

## 1. Introduction

Natural organic matter (NOM) is composed of a heterogeneous mixture of humic substances, carboxylic acids, proteins, amino acids, hydrocarbons, and polysaccharides [1–3]. Because of the complex nature of NOM, surrogate parameters of total organic carbon (TOC), ultraviolet absorbance at 254 nm ($UV_{254}$), and specific $UV_{254}$ ($SUVA_{254}$) are often used to represent its general properties. The physical and chemical nature of NOM varies according to the water source, age, and season [4]. Therefore, effective removal of NOM has been a challenge for water utilities. On the other hand, chlorine can react with NOM to form disinfection by products (DBPs), which are considered carcinogenic and mutagenic [5].

Because of more stringent drinking water quality regulations, pressure driven membrane processes, such as microfiltration (MF) and ultrafiltration (UF), are increasingly popular in drinking water treatment, since conventional treatment processes, including coagulation, sedimentation, and sand filtration, may not meet the criteria. The extensive use of membranes, however, is still limited, mainly due to membrane fouling problems. Previous studies regarding the membrane filtration of surface waters have identified NOM as one of the major foulants in the membrane process [6–8]. Effective removal of NOM by MF and UF process may not be sufficient when they are solely used. To improve the membrane performance level, various hybrid membrane systems have been developed, such as coagulation-UF/MF, powdered activated carbon-UF (PAC-UF), and iron oxide adsorption-UF [8–14].

PAC-UF systems were found to be effective in the removal of organic compounds having both low and high molecular weights. It was reported that approximately 90% of humic acids was removed with operation of an initial concentration of 10 mg/L at a PAC dosage of 100 mg/L [13]. The primary role of PAC particles added to the UF system was to remove low molecular weights of hydrophilic precursor, which cannot be removed by UF alone. It was found that the addition of PAC

into feed water containing humic acids caused a decrease in permeate flux with respect to membrane fouling, even though the organic removal by PAC was enhanced during UF [14–17].

The membrane-adsorption filtration systems are regarded as an alternative way to achieve a high removal efficiency of NOM in a cost-effective manner [13]. The cross-flow microfiltration hybrid system demands higher energy for the operation. However, the submerged membrane hybrid system requires only a low suction pressure, thus requiring lower energy for its operation. In this hybrid system, the entire treatment activity can be carried out in a single unit. In this system, TOC which normally can pass through the MF are pre-adsorbed onto PAC particles. The PAC together with adsorbed organics is then separated by the membrane filtration process. Literature studies showed that the addition of PAC could: (i) provide better physical removal of NOM, (ii) reduce the direct loading of dissolved organic pollutants onto the membrane, and (iii) prevent membrane fouling [18–20]. Kim et al. [21] found that the system could consistently remove more than 95% TOC with a PAC dose of 40 g/L for 40 days from a synthetic wastewater. The aim of this study was to assess the PAC pretreatment method for reducing NOM fouling of pilot scale MF and UF hybrid membranes. The main focus proposed is to assess the relative effects of PAC adsorption.

## 2. Experimental Section

*2.1. Source Waters Quality.* Water quality is an important factor in understanding membrane fouling. Three surface waters used for studying NOM fouling with the two different low pressure membranes were Terkos, Omerli, and Buyukcekmece lake water. These surface water supplies are the major drinking water sources of Istanbul City. Table 1 summarizes the physicochemical characteristics of these source waters. The highest $SUVA_{254}$ value (2.81 L/mg∗m) and bromide ($Br^-$) ion concentration (230 $\mu$g/L) were observed in Buyukcekmece water, while a low to moderate level of TOC and $UV_{254}$ value of 4.52 mg/L and 0.100 $cm^{-1}$, respectively, was measured in Omerli water.

*2.2. Membranes and PAC.* The NOM rejection and membrane fouling were performed on commercial polypropylene hollow fiber MF (Zena Membranes, Czechoslovakia) and ZW-10 model UF membranes (Zenon Environmental Inc., Canada) (Figure 1). The module operated at constant flow in an outside/in type of configuration. The operating vacuum pressure provided by the pump induces a flow of water from outside to the inside of the membrane fibers. Each membrane was anticipated to show different trends of membrane fouling depending on source waters characteristics and membrane properties. Both of MF and UF membranes have surface area of 0.93 $m^2$, respectively. The pore sizes of MF and UF membranes are 0.10 and 0.047 $\mu$m, respectively. Besides, Table 2 lists the relevant properties of these membranes according to their manufacturer and data available in the literature. On the other hand, AquaSorb BP2 PAC was used for adsorption purposes. AquaSorb BP2 PAC has 27 $\mu$m average pore size, 1.56 $cm^3$/g pore volume, and 950 $m^2$/g surface area. The PAC was firstly mixed with water in a beaker, and then its solution was added into the first part of reactor.

Table 1: Characterization of surface water source quality parameters [22].

| Parameters | Unit | Buyukcekmece | Terkos | Omerli |
|---|---|---|---|---|
| pH | — | 8.20 | 7.92 | 7.40 |
| Turbidity | NTU | 18 | 2.39 | 1.52 |
| Color | mg/L Pt-Co | 28 | 20 | 10 |
| Conductivity | $\mu$S/cm | 540 | 344 | 278 |
| Alkalinity | mg/L $CaCO_3$ | 139 | 124 | 113 |
| Hardness | mg/L $CaCO_3$ | 182 | 130 | 114 |
| $Ca^{+2}$ | mg/L | 161 | 46 | 40 |
| TDS | mg/L | 258 | 169 | 136 |
| Bromide ($Br^-$) | $\mu$g/L | 230 | 110 | 50 |
| TOC | mg/L | 6.45 | 6.54 | 4.52 |
| DOC | mg/L | 5.12 | 5.70 | 3.75 |
| $UV_{254}$ | 1/cm | 0.144 | 0.150 | 0.100 |
| $SUVA_{254}$ | L/mg × m | 2.81 | 2.63 | 2.67 |

*2.3. Experimental Hybrid Membrane Filtration Setup.* MF and UF experiments were performed in a submerged hybrid membrane system (Figure 2). Prior to experiment, all membranes were cleaned with deionized (DI) water and compacted at operating conditions. As seen in Figure 2, surface lake waters were taken from the 1,500 liter tank by peristaltic pump and transferred into the membrane reactor. The hybrid submerged membrane reactor is made of Plexiglas. The volume of the reactor was 30 liter and it was separated into two parts with a baffle system. The first compartment serves as an adsorption zone, while the second part was used for submerged membrane filtration. The raw water was transferred into first part of the reactor which the water was firstly contacted with PAC and then passed into the second part containing submerged membrane by a bottom canal. Water level sensor was located at the first part of the reactor to be kept constant water level in the reactor. Permeating and backwashing operations were performed automatically with automatic control system. Pressure gauge was placed in the vacuum line in order to measure transmembrane pressure (TMP). All measured data were monitored online and stored by HACH model SC1000 data logging system. Samples were taken once a day from the permeate line, reactor, and the raw water tank. Permeate flow rate was kept constant and was monitored daily during the experiments. The operating fluxes for MF and UF systems were set as 150 L/$m^2$-h and 18 L/$m^2$-h, respectively. Air was supplied from a porous ceramic plate below the membrane module in order to provide dissolved oxygen to create turbulence along the membrane surface which helps to remove particles that deposit on the outside of the membrane fiber. Experiments continued for one week and both MF and UF membranes were cleaned between each experiment. Different chemicals were used during chemical cleaning procedure of each membrane. These two membrane

MF membrane UF membrane

Figure 1: A general photographic image of MF and UF membranes.

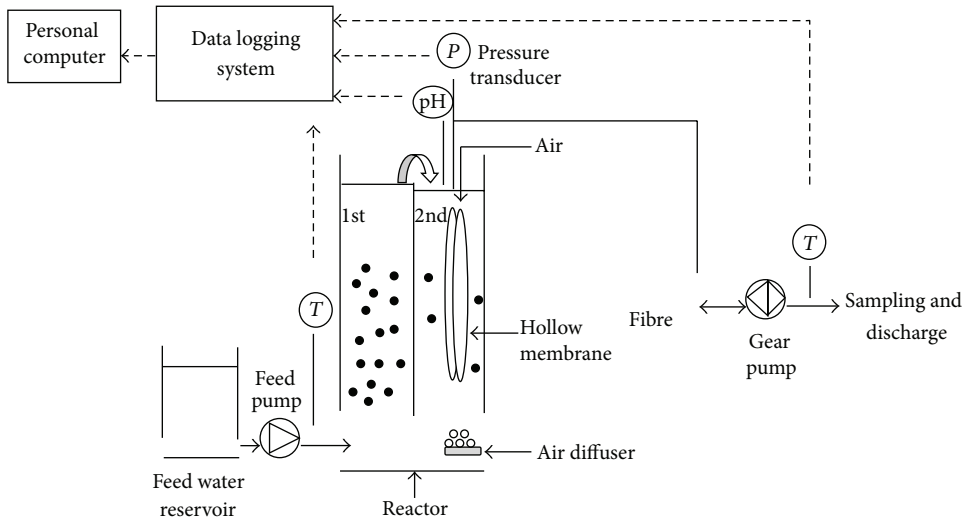


Figure 2: A schematic diagram of pilot plant.

modules were cleaned according to the following steps: (a) surface cleaning with DI water, (b) acidic wash in 2% HCl solution for 2 hours, (c) basic wash with 1 N NaOH solution for overnight, and (d) final cleaning in 0.4% NaOCl for 2 h. Membranes were rinsed with DI water after every step and prior to all experiments [21].

*2.4. Analytical Methods.* TOC analysis was employed by high temperature combustion according to Standard Methods (SM) 5310 B using a Shimadzu TOC-VCPH analyzer equipped with an auto-sampler [23]. The instrument provided reliable, accurate, and reproducible data with a minimum detection limit of 2 $\mu$g/L C. Further, UV absorbance measurements were determined with a Perkin Elmer Lambda 25 UV Visible spectrophotometer at a wavelength of 254 nm. On the other hand, a Superlite DAX-8 (Supelco, USA) and Amberlite XAD-4 (Rohm and Haas, Germany) was used to fractionate NOM into three groups, that is, hydrophobic (DAX-8 adsorbable), transphilic (XAD-4 adsorbable) and hydrophilic (neither DAX-8 nor XAD-4 adsorbable) fractions. The chemical fraction of NOM contained source waters

Table 2: Typical characteristics of membranes used in this study.

| Parameters | MF | UF |
|---|---|---|
| Flux rate | 150 L/m$^2$-h | 18–72 L/m$^2$-h |
| Max. operating temperature | 40°C | 40°C |
| Max. operating pressure | 5.5–3.5 bar | 0.60 bar |
| pH range | 5–10 | 5–9 |
| Effective membrane surface area | — | 0.93 m$^2$ |
| Membrane material | Polypropylene | Polypropylene |
| Molecular weight cut-off | 0.1 $\mu$m | 0.04 $\mu$m |
| Membrane type | Hydrophilic | Hydrophilic |

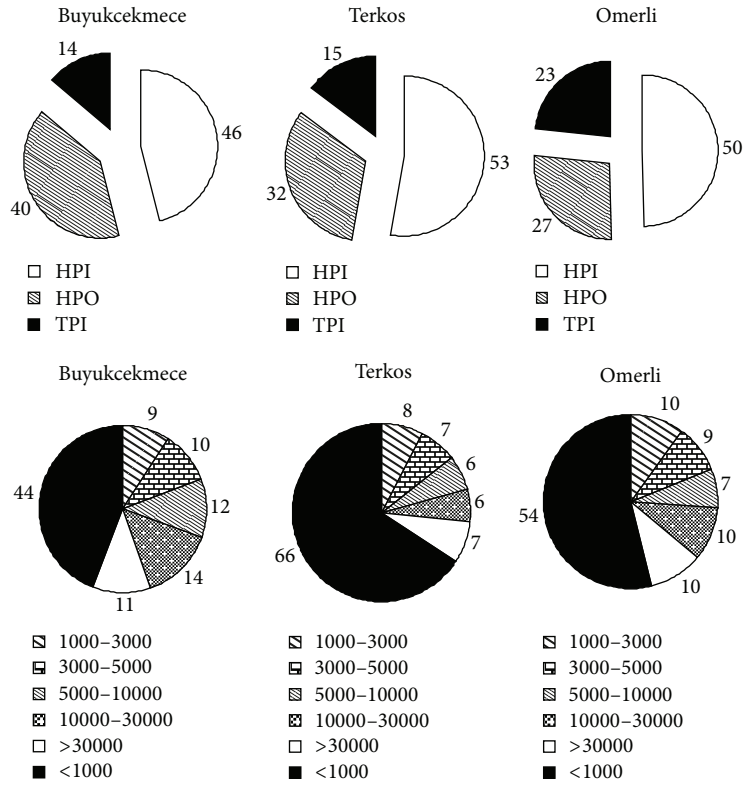


Figure 3: Chemical NOM fractionation and molecular weight distribution of source waters (%).

was displayed in Figure 3. The molecular weight distribution of the source waters was determined using sequential filtration through membranes of decreasing molecular weight cut off (MWCO) [24]. Source waters were fractionated in a 76 mm diameter stirred cell (model 8400, Amicon, Beverly, MA, USA) using a serious of regenerated cellulose acetate UF membranes from Millipore designated YM30, YM10, YM5, YM3 and YM1 with nominal MWCOs of 30, 10, 5, 3 and 1 kDa, respectively. The distribution of molecular weights is shown in Figure 3. Other parameters such as turbidity, pH and conductivity were also determined with online monitoring system (Hach-Lange SC1000).

## 3. Results and Discussion

*3.1. NOM Reduction by PAC Pretreatment.* Removal of organic precursor by membrane process is impacted by many factors such as water chemistry (pH, ionic environment), NOM characteristics (hydrophilic-hydrophobic character, MW distribution), and membrane properties (pore size, hydrophilicity, surface charge) [8, 25–27]. The performances of the MF and UF membrane-adsorption hybrid systems in removing NOM compounds, with respect to TOC and $UV_{254}$ rejection for the 3 water samples analyzed, are summarized in Figures 4–7. The efficiency of the membrane-adsorption hybrid system depends on PAC addition mode and raw water properties [19]. The effects of PAC addition to MF and UF membrane filtration performances were examined with a pilot submerged hybrid membrane system. To learn the effects of the presence of PAC concentration on membranes performance, addition of PAC into MF and UF membrane reactor was performed with different modes. These different PAC methods of UF are classified as No PAC addition, 25 g/L PAC addition once during the study period, and 25 g/L PAC addition every day. On the other hand, a PAC addition mode of MF membrane reactor was defined as No PAC addition, and 25 g/L PAC addition every day. During the pilot plant studies, samples collection from feed and permeate line were conducted once a day for seven days period. The results were evaluated with residual TOC and $UV_{254}$ value of permeated water.

The box plots of the comparison of residual TOC and $UV_{254}$ level of adsorbent/membrane systems with different PAC methods for Terkos water are provided in Figures 4 and 5. The median value of organic precursors was demonstrated with red line located inside of each box. Moreover, the median residual TOC level for two PAC conditions with MF membrane was found to be 4.45 and 0.76 mg/L, respectively (Figure 4) while, PAC/UF hybrid system lowered the median residual TOC concentration for three PAC conditions to 4.61, 2.83, and 2.19 mg/L, respectively (Figure 5). Filtration of Terkos water by a bare MF and UF membranes removed negligible TOC (<18% for MF and 13% for UF); by contrast, significant amounts of TOC (85% for MF and 51% for UF) were removed when 25 g/L-day PAC were predeposited on the both of membrane surfaces (Figure 4). Since the MF membrane pore diameter (0.1 $\mu$m) is too large compared to molecular size of NOM present in three source waters (Table 1), the dominant removal mechanism of PAC/MF hybrid system is adsorption of organic matter within PAC layer rather

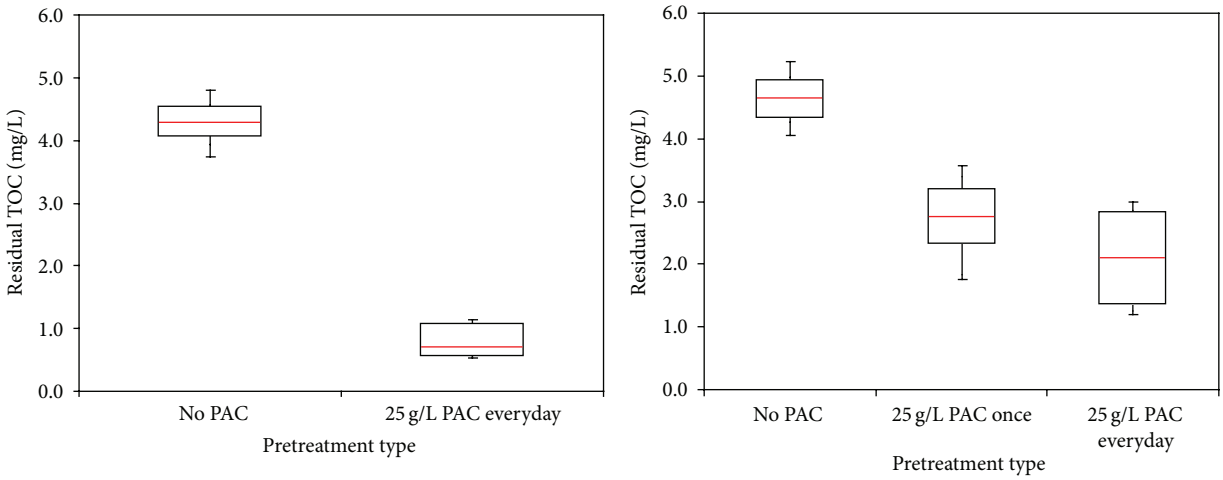


Figure 4: TOC removal with MF and UF in Terkos water.

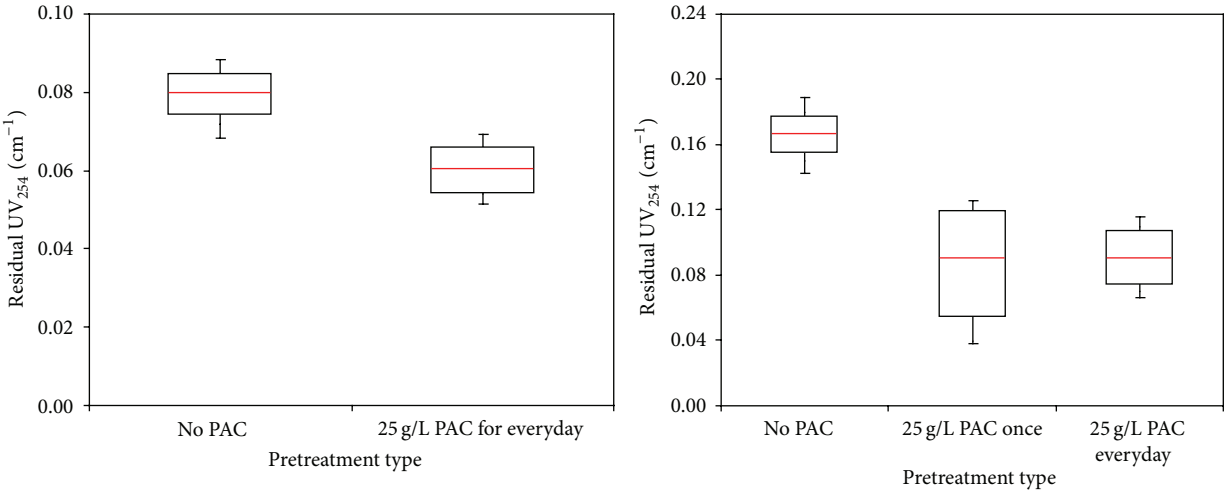


Figure 5: $UV_{254}$ removal with MF and UF in Terkos water.

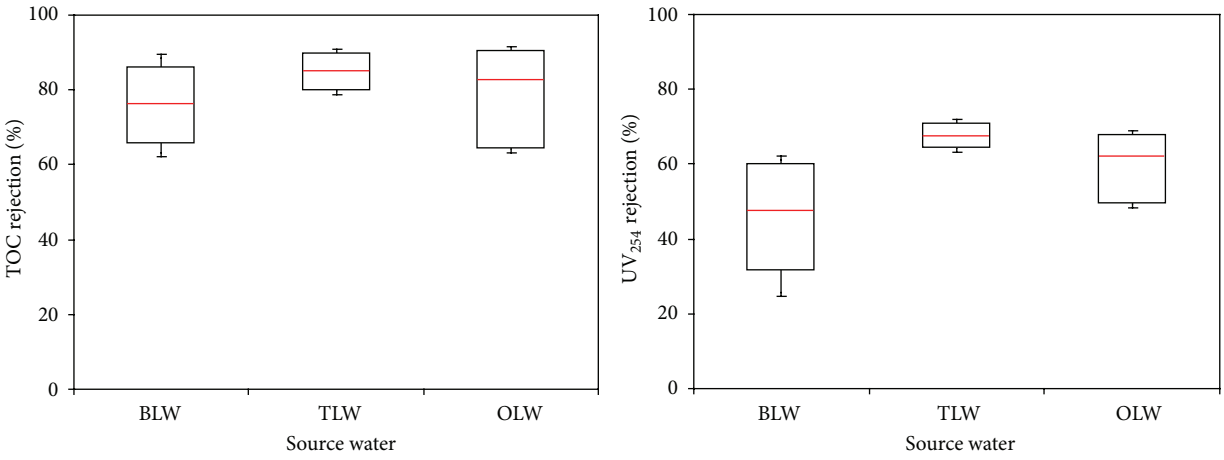


Figure 6: TOC and $UV_{254}$ removal with PAC/MF for Istanbul water sources.

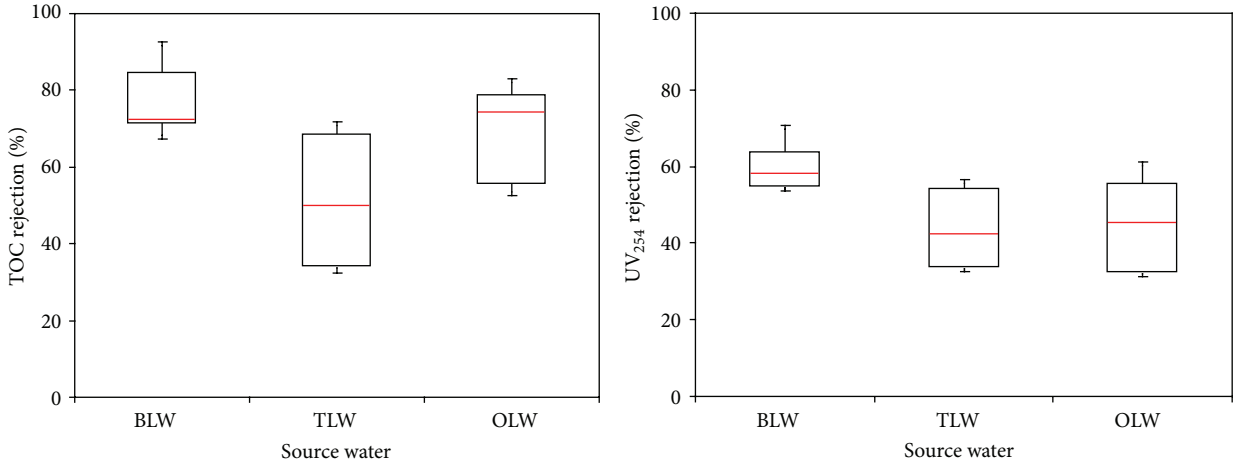


FIGURE 7: TOC and $UV_{254}$ removal with PAC/UF for Istanbul water sources.

than size exclusion/steric hindrance of NOM by membrane pores. On the other hand, raw waters background ionic strength ($Ca^{+2}$ concentrations) attenuates potential electrostatic repulsions between NOM molecules and the membrane. As indicated by Ates et al. [28]; the bare MF membrane rejects relatively large particulate molecules more, showing that the colloidal and dissolved NOM compounds are preferentially transmitted through the membrane pores, as its molecular size is relatively small. In other words, organic substances can easily pass through MF membrane without PAC treatment. However, in the case of PAC/MF hybrid system, the PAC particles was adsorbed onto the surface of membrane pores and prevent the transition of NOM molecules and this resulted in higher level of organic precursor removals compared to the bare MF membrane. Thus, the accumulation of high and low molecular weight organics inside the PAC layer was prompted, while the NOM fouling mode was transformed from pore plugging to cake formation at the entrance of MF pores.

On the other hand, the organic precursors of TOC and $UV_{254}$ removals efficiency of UF membrane were found to be less than MF membrane in the presence of PAC (Figures 4 and 5). These results support the assumption that the surface related properties (surface roughness and surface charge) of membranes and PAC layer structure (surface deposition) might have considerably influential factor on organic precursors removal. In the case of 25 g/L PAC addition for every day, the average TOC removal efficiency of PAC/UF system (Terkos water) was found to be 51% (Figure 4). As can be seen from Figure 5, lower average $UV_{254}$ rejection (68% for MF and 44% for UF) was observed with PAC/MF and PAC/UF systems. Inconsistent with the literature findings, the PAC removed $UV_{254}$ less efficiently than TOC, suggesting that they selectively bind more hydrophilic molecules. Furthermore, these findings indicate that PAC adsorbent preferentially removes aliphatic organics to which $UV_{254}$ is not attributed to [29]. With PAC/MF hybrid system for three Istanbul surface waters, average TOC removals were at or above 80%, while average $UV_{254}$ rejections were at or under 59% indicating different rate of organic precursor removal efficiencies (Figure 6). It was also reasonable to expect that the adsorption of hydrophilic compounds, which are enriched in proteins [30], occurred at the organic amino groups and carboxylic sites of PAC. These findings are in agreement with Henderson et al. [31] and Campinas and Rosa [19]. Moreover, as summarized in Figure 6, the highest and lowest average TOC (85% versus 76%) and $UV_{254}$ (48% versus 68%) removal were observed for Terkos and Buyukcekmece waters, respectively. Furthermore, it is clear from Figure 6 that the overall PAC/MF hybrid system rejection efficiency of TOC and $UV_{254}$ remained in the middle range for Omerli water.

The data of UF system demonstrate that UF alone reject negligible TOC and $UV_{254}$ (Figure 5) as found by Li and Chen [17]. On the other hand, Figure 7 depicted that during the PAC/UF operation, the highest average TOC removal efficiency (76%) was observed for Buyukcekmece water, while the lowest average TOC removal efficiency of Terkos water was found to be 50%. Interestingly, even though Terkos water has the highest TOC and $UV_{254}$ removal with PAC/MF system, the PAC/UF hybrid system resulted in lowest TOC and $UV_{254}$ rejection for same water samples as summarized in Figure 7. These findings indicate that the PAC particles accumulated onto the MF membrane pores at short time and this resulted in more NOM related compounds removal. In fact, most of the rejection of organic precursor occurred inside the PAC layer not at MF membrane surface. On the other hand, NOM structure and organic and inorganic properties of raw water have a significant impact on organic precursor rejection with two different membranes. As summarized in Figure 7, the NOM was removed more efficiently by the PAC/MF system than PAC/UF system. Furthermore, lower organic precursor rejections by PAC/UF hybrid membrane process could be essentially related to the exclusion of PAC particles (27 $\mu$m) by UF membrane pores (0.04 $\mu$m). It was concluded that the UF membranes reject PAC particles more, showing that the low molecular weight (<1 kDa) organics (Terkos; 66%, Buyukcekmece; 44%, and Omerli; 54%) are preferentially transmitted through the UF membrane pores,

as its molecular size is relatively small compared with that of its aromatic counterpart in raw water samples. Furthermore, the enhancement of organic precursor removals with PAC/MF system is probably explained by the pore blocage caused by PAC adsorption to the porous surface and/or by the additional sieving provided by the PAC deposits onto the MF membrane surface, as observed by others [19, 24].

It is important to note that the presence of dissolved $Mg^{+2}$ and $Ca^{+2}$ in the waters of Buyukcekmece, Terkos, and Omerli, has a strong influence on the UF membrane performance. The $Ca^{+2}$ ions can bind with the acidic functional groups of the NOM, elevating the degree of hydrophobicity of the NOM molecules and developing a dense thick fouling layer on the UF membrane surface [32]. The findings of Lohwacharin et al. [16] indicated that the addition of $Ca^{+2}$ into River Obitsu significantly improved the NOM rejection in the presence of carbon black (CB), and they reported that the increased removal of NOM by addition of $Ca^{+2}$ was caused by the intermolecular bridging of hydrophilic compounds and CB induced by $Ca^{+2}$, notably at pH 7.7. As can be seen in Figure 7, the removal efficiency of TOC and $UV_{254}$ precursor compounds shows an increase with $Ca^{+2}$ concentration of source waters (Table 1). However, the MF performance of water with higher $Ca^{+2}$ content was largely or even mostly influenced by the PAC particles accumulation onto the MF membrane pores, rather than by the $Ca^{+2}$ complexation with NOM compounds in source waters.

*3.2. NOM Fouling Potential of Hybrid Membrane System.* This section focused systematically on the effects of membrane type, source waters chemistry, and PAC pretreatment on membrane fouling. In order to compare fouling data obtained with three surface waters containing different concentration of TOC, MF, and UF, membrane fouling profiles are plotted as a function of filtration period (Figures 8 and 9). Figure 8 shows the variation of MF membrane fouling obtained with different sources of NOM. Based on filtration period, Buyukcekmece water resulted in the greatest membrane fouling, while Terkos water and Omerli water followed similar fouling trends after 30 h filtration time. The maximum TMP values of source waters were found to be 100, 200, and 90 mbar for Terkos, Buyukcekmece, and Omerli waters, respectively. Considering the dominant chemical NOM fraction of these source waters (Figure 3), these data suggest that all three surface waters should have had similar fouling trend. However, Buyukcekmece water which has a hydrophilic (HPI) fraction of 46% resulted in the highest fouling potential compared to Terkos and Omerli waters. Furthermore, two source waters of Terkos and Omerli water showed a similar fouling pattern since they have similar HPI fraction percent as shown in Figure 3 (53% versus 50%). I was concluded that since all three source waters have similar HPI content (Figure 3), it appears that the PAC interaction with membrane pores was responsible for offsetting the NOM fractional effects on membrane fouling for all three source waters. Besides, Zhao et al. [18] concluded that hydrophobic/hydrophilic character or the molecular size distribution ratio of NOM plays a quite limited role on PAC cake

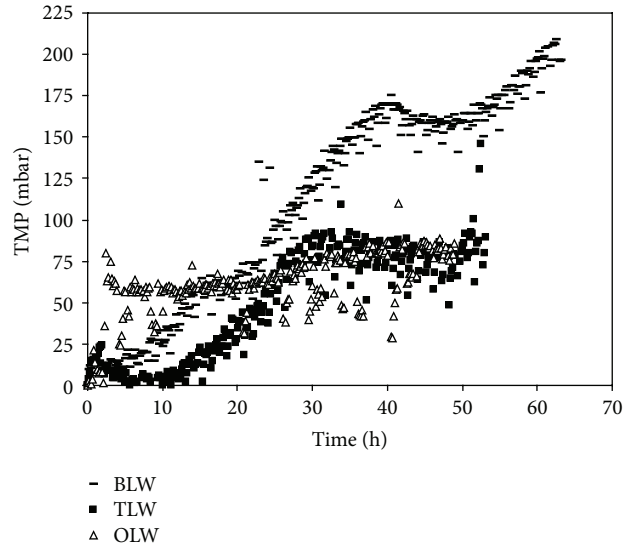


Figure 8: TransMembrane pressure versus time for PAC/MF system.

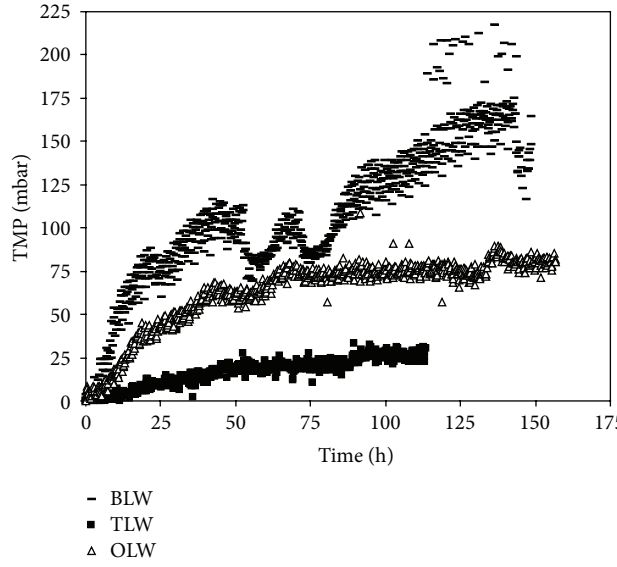


Figure 9: TransMembrane pressure versus time for PAC/UF system.

formation, while a more relevant effect is due to the combination of ionic strength, colloidal movement, PAC pore constriction, and pore blockage mechanisms. Several studies indicated that the fouling caused by gel layer formation and concentration polarization is less severe that caused by the pore adsorption and pore blocking mechanisms [33–35]. It was reported that both pore adsorption and pore blocking mechanisms directly block the narrow passage, that is, the membrane pore, for water, while gel and concentration polarization layers forming on top of membrane surface do not directly block the passage of water. Therefore, the extent of membrane fouling by these mechanisms will be quite different [17].

Solution chemistry has an important effect on the surface charge characteristics of polymeric membranes. Moreover, the higher level of conductivity (540 $\mu$S/cm) and TDS (258 mg/L) parameters (ionic composition) combining effects (Table 1) in Buyukcekmece water is supposed to be responsible for higher NOM fouling compared to other two source waters. As reported in several literature studies, especially the intensity of high ionic strength of this source water prompted the membrane fouling further. It is generally agreed that NOM fouling is more severe in a high ionic environment [24, 36]. The reason for the deleterious effect of solution high ionic strength is that at high ionic strength NOM molecules are smaller and their configuration are more spherical leading to augmented diffusivities. This promotes significant diffusion of NOM molecules into the membrane pores, leading to enhanced membrane fouling due to pore adsorption as was the case with Buyukcekmece water. High ionic strength may also compress the double layer of the NOM molecules, leading to intensified aggregation and cake formation [37]. As a result, the cake formed in a high ionic strength solution is more compact and has higher resistance [38]. Therefore, the membrane fouling increases faster as was the case with Buyukcekmece water at high ionic strength than at those of low ionic strength, such as Terkos and Omerli waters.

In our results, adsorption of NOM onto the MF and UF membrane increased with increased level of $Ca^{+2}$ for Buyukcekmece water (Figures 8 and 9), probably due to reduction of electrostatic repulsion. This is consistent with other studies reporting increased adsorption by electrostatic charge shielding, complexation, and/or bridging effects [39]. Our results also indicate that $Ca^{+2}$ induced a change in the NOM fouling mechanism, which was associated with remarkably more NOM deposited on the membrane. It is believed that $Ca^{+2}$ played a crucial role in the formation of lower level NOM fouling with Terkos and Omerli waters. We suppose that higher level of NOM fouling with Buyukcekmece water ($Ca^{+2}$: 161 mg/L) is caused by calcium complexation, which is reported in literature and known as the egg-box model [40]. This gel probably caused the increase in membrane fouling because it is tighter and less permeable than the cake layer formed with Terkos ($Ca^{+2}$: 46 mg/L) and Omerli ($Ca^{+2}$: 30 mg/L) waters. Furthermore, as the pH increases, the membrane surface and pores become more negatively charged due to the presence of anions. As a result, the pore size of the membrane is reduced because of the repulsion between neighbor negatively charged groups and adopts an extended conformation. As it was stated by many studies, alkaline pH showed higher NOM rejections and membrane fouling.

On the other hand, Figure 9 shows the variation of UF membrane fouling obtained with different source waters contained NOM. PAC is expected to compete with the UF membrane for the adsorption of NOM compounds that otherwise would adsorb on the membrane, causing its fouling. However, some authors have indicated that although PAC itself does not impose significant membrane fouling, when in the presence of NOM it increases the fouling resistance [17, 41]. It is believed that NOM acts as a glue that binds the PAC particles to one another and to the membrane surface, enhancing fouling. For direct comparison purposes, TMP development curves for both hybrid systems are depicted in Figures 8 and 9, respectively. It was found that Buyukcekmece water resulted in the highest NOM fouling as compared to other two water sources. While the TMP value of 200 mbar was obtained for 65 h with PAC/MF system, in the case of PAC/UF hybrid system, the 200 mbar value of TMP was occurred after 150 h filtration period. This findings revealed that NOM fouling of PAC/UF membrane developed for longer filtration times (>150 h) than those of MF membrane (<70 h). Since PAC particles were not be able to diffuse the UF membrane pores effectively, the membrane fouling periods of UF membrane resulted in longer than those of MF membrane. It was assumed that the structure of surface cake layer of UF membrane was more permeable than those of MF module; thus, the NOM fouling period and intensity of MF took place earlier than those of UF system as shown in Figures 8 and 9.

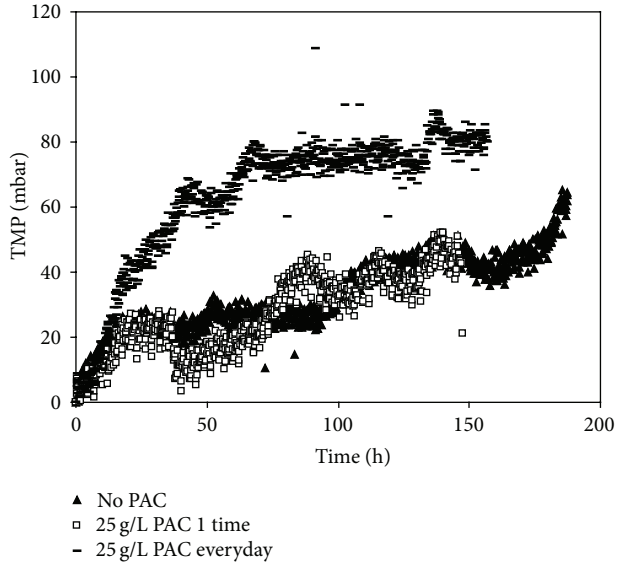


Figure 10: Comparison of transmembrane pressure values in terms of PAC addition modes in PAC/UF system of Omerli water.

In order to investigate the effects of PAC addition modes on UF TMP development, three different PAC addition methods were performed with UF system for Omerli water. Figure 10 shows significant differences at all PAC addition methods, which indicates that 25 g/L PAC addition for every day promoted the membrane fouling more. This same trend has already been obtained by other authors [8, 14, 42]. Moreover, no substantial differences were obtained for No PAC and 25 g/L PAC 1 time addition for Omerli water. This result indicates that the amount of PAC added into UF membrane system plays a crucial role on TMP development. In other words, accumulation of PAC particles on the surface of UF membrane accelerates the higher level of NOM fouling. These findings also indicate that the higher level of organic

precursors rejection with MF membrane is attributed to less permeable cake layer of MF compared to more permeable cake layer of UF module.

It is clear that Buyukcekmece water has the highest membrane fouling for PAC/UF system as was the case with PAC/MF system. On the other hand, Terkos water showed the lowest level fouling trends with maximum TMP value of 33 mbar (Figure 9). As shown in Figure 9, Omerli water does not follow the same fouling trend as that for Terkos water, indicating that the extent of fouling might be quite different for the similar percent of hydrophilic content (Terkos: 53%, and Omerli: 50%) adsorbed within PAC cake layer on UF membrane. These results may be attributed to the shape of the organic molecules with source waters. Some of the hydrophilic compounds have linear shape while others have globular shape molecule. Thus, the shape of the molecules affects the fouling trends of membranes. On the other hand, Buyukcekmece water which contained moderate hydrophilic NOM (47%) appeared to exert higher TOC and $UV_{254}$ rejection with PAC/UF system despite its higher fouling quantity. This implies that the degree of membrane fouling in this particular case does not necessarily depend to the extent of TOC removal and apparently this observation distinctively described that the TOC fractions which are more effectively removed by the PAC/UF membrane are not the same fractions that contribute to membrane fouling [8, 43].

## 4. Conclusions

The conclusions that can be drawn from the results of this investigation are as follows.

(i) Filtration of Istanbul source waters by a bare MF and UF membranes removed negligible TOC (<20% for MF and 5% for UF); by contrast, significant amounts of TOC (>80% for MF and >65% for UF) were removed when 25 g/L-day PAC were predeposited on the both of membrane surfaces. Since the MF membrane pore diameter is too large compared to molecular size of NOM present in three source waters, the dominant removal mechanism of PAC/MF hybrid system is adsorption of organic matter within PAC layer rather than size exclusion/steric hindrance of NOM by membrane pores.

(ii) Inconsistent with the literature findings, the PAC removed $UV_{254}$ less efficiently than TOC, suggesting that they selectively bind more hydrophilic molecules. Furthermore, these findings indicate that PAC adsorbent preferentially removes aliphatic organics to which $UV_{254}$ is not attributed to.

(iii) The results of this study revealed that higher PAC dose did not reduce the TMP development; on the contrary it prompts the membrane fouling more severe than when no adsorbent was used, even though the PAC adsorbed a significant fraction of the influent NOM. One interpretation of these results is that the PAC particles form gel layers at the membrane surface and that, when the membrane system is pressurized, the gels become compressed and distorted and thereby block the pores on the membrane surface. In addition, it was assumed that the cake layer formed by the PAC particles on the surface of UF membrane is more permeable and thinner than those of MF membrane. This could be explained by the fact that the hydrophilic NOM was not effectively retained by the pore size exclusion and electrostatic repulsion mechanisms as it was relatively smaller in molecular weight than the membrane pore size, possessing greater surface area, and has less electron-rich sites than that of the hydrophobic NOM. This phenomenon enhanced further mass accumulation (adsorption) of the hydrophilic NOM onto the pores that caused significant irreversible fouling by constricting and reducing the effective membrane permeability.

(iv) It is important to note that the presence of dissolved $Mg^{+2}$ and $Ca^{+2}$ in the waters of Buyukcekmece, Terkos, and Omerli has a strong influence on the UF membrane performance. The $Ca^{+2}$ ions can bind with the acidic functional groups of the NOM, elevating the degree of hydrophobicity of the NOM molecules and developing a dense thick fouling layer on the UF membrane surface.

(v) It was concluded that since all three source waters have similar HPI content, it appears that the PAC interaction with membrane pores was responsible for offsetting the NOM fractional effects on membrane fouling for all three source waters. Besides, hydrophobic/hydrophilic character or the molecular size distribution ratio of NOM plays a quite limited role on PAC cake formation, while a more relevant effect is due to the combination of ionic strength, colloidal movement and PAC pore blockage mechanisms.

## Conflict of Interests

The authors declare that there is no conflict of interests regarding the publication of this article.

## Acknowledgment

Funding for this research was provided by The Scientific and Technological Research Council of Turkey (TUBITAK) under Grant 106Y171.

## References

[1] G. R. Aiken, D. M. McKnight, K. A. Thorn, and E. M. Thurman, "Isolation of hydrophilic organic acids from water using nonionic macroporous resins," *Organic Geochemistry*, vol. 18, no. 4, pp. 567–573, 1992.

[2] E. M. Thurman, *Organic Geochemistry of Natural Waters*, Martinus Nijhoff/Dr W. Junk Publishers, Boston, Mass, USA, 1985.

[3] A. W. Zularisam, A. F. Ismail, and R. Salim, "Behaviours of natural organic matter in membrane filtration for surface water

treatment—a review," *Desalination*, vol. 194, no. 1–3, pp. 211–231, 2006.

[4] G. R. Aiken, *Humic Substances and Their Role in the Environment*, John Wiley & Sons, New York, NY, USA, 1988.

[5] J. J. Rook, "Formation of haloforms during chlorination of natural waters," *Water Treatment Examination*, vol. 23, pp. 234–243, 1974.

[6] W. Yuan and A. L. Zydney, "Humic acid fouling during microfiltration," *Journal of Membrane Science*, vol. 157, no. 1, pp. 1–12, 1999.

[7] K. J. Howe and M. M. Clark, "Fouling of microfiltration and ultrafiltration membranes by natural waters," *Environmental Science and Technology*, vol. 36, no. 16, pp. 3571–3576, 2002.

[8] A. W. Zularisam, A. F. Ismail, M. R. Salim, M. Sakinah, and H. Ozaki, "The effects of natural organic matter (NOM) fractions on fouling characteristics and flux recovery of ultrafiltration membranes," *Desalination*, vol. 212, no. 1–3, pp. 191–208, 2007.

[9] P. Choksuchart, M. Héran, and A. Grasmick, "Ultrafiltration enhanced by coagulation in an immersed membrane system," *Desalination*, vol. 145, no. 1–3, pp. 265–272, 2002.

[10] Y. Chang and M. M. Benjamin, "Iron oxide adsorption and UF to remove NOM and control fouling: addition of iron oxide particles to a UF system can significantly increase NOM removal efficiency, slowing membrane fouling," *Journal of the American Water Works Association*, vol. 88, no. 12, pp. 74–88, 1996.

[11] J. D. Lee, S. H. Lee, M. H. Jo, P. K. Park, C. H. Lee, and J. W. Kwak, "Effect of coagulation conditions on membrane filtration characteristics in coagulation—microfiltration process for water treatment," *Environmental Science and Technology*, vol. 34, no. 17, pp. 3780–3788, 2000.

[12] S. J. Lee, K. H. Choo, and C. H. Lee, "Conjunctive use of ultrafiltration with powdered activated carbon adsorption for removal of synthetic and natural organic matter," *Journal of Industrial and Engineering Chemistry*, vol. 6, no. 6, pp. 357–364, 2000.

[13] M. Tomaszewska and S. Mozia, "Removal of organic matter from water by PAC/UF system," *Water Research*, vol. 36, no. 16, pp. 4137–4143, 2002.

[14] M. M. Zhang, C. Li, M. M. Benjamin, and Y. J. Chang, "Fouling and natural organic matter removal in adsorbent/membrane systems for drinking water treatment," *Environmental Science and Technology*, vol. 37, no. 8, pp. 1663–1669, 2003.

[15] S. Mozia, M. Tomaszewska, and A. W. Morawski, "Studies on the effect of humic acids and phenol on adsorption-ultrafiltration process performance," *Water Research*, vol. 39, no. 2-3, pp. 501–509, 2005.

[16] J. Lohwacharin, K. Oguma, and S. Takizawa, "Use of carbon black nanoparticles to mitigate membrane fouling in ultrafiltration of river water," *Separation and Purification Technology*, vol. 72, no. 1, pp. 61–69, 2010.

[17] C. W. Li and Y. S. Chen, "Fouling of UF membrane by humic substance: effects of molecular weight and powder-activated carbon (PAC) pre-treatment," *Desalination*, vol. 170, no. 1, pp. 59–67, 2004.

[18] P. Zhao, S. Takizawa, H. Katayama, and S. Ohgaki, "Factors causing PAC cake fouling in PAC-MF (powdered activated carbon-microfiltration) water treatment systems," *Water Science and Technology*, vol. 51, no. 6-7, pp. 231–240, 2005.

[19] M. Campinas and M. J. Rosa, "Assessing PAC contribution to the NOM fouling control in PAC/UF systems," *Water Research*, vol. 44, no. 5, pp. 1636–1644, 2010.

[20] Y. Matsui, H. Hasegawa, K. Ohno et al., "Effects of superpowdered activated carbon pretreatment on coagulation and trans-membrane pressure buildup during microfiltration," *Water Research*, vol. 43, no. 20, pp. 5160–5170, 2009.

[21] H. S. Kim, H. Katayama, S. Takizawa, and S. Ohgaki, "Development of a microfilter separation system coupled with a high dose of powdered activated carbon for advanced water treatment," *Desalination*, vol. 186, no. 1–3, pp. 215–226, 2005.

[22] M. Akdagli, *Pilot scale submerged membrane treatment of lake waters [M.S. thesis]*, Istanbul Technical University, Istanbul, Turkey, 2010.

[23] APHA, AWWA, and WEF, *Standard Methods for the Examination of Water and Wastewater*, APHA, AWWA, WEF, Washington, DC, USA, 20th edition, 1998.

[24] W. Yuan and A. L. Zydney, "Humic acid fouling during ultrafiltration," *Environmental Science and Technology*, vol. 34, no. 23, pp. 5043–5050, 2000.

[25] A. R. Costa, M. N. de Pinho, and M. Elimelech, "Mechanisms of colloidal natural organic matter fouling in ultrafiltration," *Journal of Membrane Science*, vol. 281, no. 1-2, pp. 716–725, 2006.

[26] N. Lee, G. Amy, J. Croué, and H. Buisson, "Identification and understanding of fouling in low-pressure membrane (MF/UF) filtration by natural organic matter (NOM)," *Water Research*, vol. 38, no. 20, pp. 4511–4523, 2004.

[27] C. Jarusutthirak, G. Amy, and J. Croué, "Fouling characteristics of wastewater effluent organic matter (EfOM) isolates on NF and UF membranes," *Desalination*, vol. 145, no. 1–3, pp. 247–255, 2002.

[28] N. Ates, L. Yilmaz, M. Kitis, and U. Yetis, "Removal of disinfection by-product precursors by UF and NF membranes in low-SUVA waters," *Journal of Membrane Science*, vol. 328, no. 1-2, pp. 104–112, 2009.

[29] J. Lohwacharin, K. Oguma, and S. Takizawa, "Ultrafiltration of natural organic matter and black carbon: factors influencing aggregation and membrane fouling," *Water Research*, vol. 43, no. 12, pp. 3076–3085, 2009.

[30] J. P. Croué, M. F. Benedetti, D. Violleau, and J. A. Leenheer, "Characterization and copper binding of humic and nonhumic organic matter isolated from the South Platte River: evidence for the presence of nitrogenous binding site," *Environmental Science and Technology*, vol. 37, no. 2, pp. 328–336, 2003.

[31] R. K. Henderson, A. Baker, S. A. Parsons, and B. Jefferson, "Characterisation of algogenic organic matter extracted from cyanobacteria, green algae and diatoms," *Water Research*, vol. 42, no. 13, pp. 3435–3445, 2008.

[32] M. R. Teixeira and M. J. Rosa, "The impact of the water background inorganic matrix on the natural organic matter removal by nanofiltration," *Journal of Membrane Science*, vol. 279, no. 1-2, pp. 513–520, 2006.

[33] N. Lee, G. Amy, and J. P. Croué, "Low-pressure membrane (MF/UF) fouling associated with allochthonous versus autochthonous natural organic matter," *Water Research*, vol. 40, no. 12, pp. 2357–2368, 2006.

[34] W. Yuan, A. Kocic, and A. L. Zydney, "Analysis of humic acid fouling during microfiltration using a pore blockage-cake filtration model," *Journal of Membrane Science*, vol. 198, no. 1, pp. 51–62, 2002.

[35] Y. Ye, P. Le Clech, V. Chen, A. G. Fane, and B. Jefferson, "Fouling mechanisms of alginate solutions as model extracellular polymeric substances," *Desalination*, vol. 175, no. 1, pp. 7–20, 2005.

[36] K. L. Jones and C. R. O'Melia, "Protein and humic acid adsorption onto hydrophilic membrane surfaces: effects of pH and ionic strength," *Journal of Membrane Science*, vol. 165, no. 1, pp. 31–46, 2000.

[37] A. R. Costa and M. N. de Pinho, "Effect of membrane pore size and solution chemistry on the ultrafiltration of humic substances solutions," *Journal of Membrane Science*, vol. 255, no. 1-2, pp. 49–56, 2005.

[38] S. Shirazi, C. Lin, and D. Chen, "Inorganic fouling of pressure-driven membrane processes—a critical review," *Desalination*, vol. 250, no. 1, pp. 236–248, 2010.

[39] S. Lee and M. Elimelech, "Relating organic fouling of reverse osmosis membranes to intermolecular adhesion forces," *Environmental Science and Technology*, vol. 40, no. 3, pp. 980–987, 2006.

[40] T. A. Davis, B. Volesky, and A. Mucci, "A review of the biochemistry of heavy metal biosorption by brown algae," *Water Research*, vol. 37, no. 18, pp. 4311–4330, 2003.

[41] C. F. Lin, Y. J. Huang, and O. J. Hao, "Ultrafiltration processes for removing humic substances: effect of molecular weight fractions and PAC treatment," *Water Research*, vol. 33, no. 5, pp. 1252–1264, 1999.

[42] J. Kim, Z. Cai, and M. M. Benjamin, "Effects of adsorbents on membrane fouling by natural organic matter," *Journal of Membrane Science*, vol. 310, no. 1-2, pp. 356–364, 2008.

[43] K. Kimura, Y. Hane, Y. Watanabe, G. Amy, and N. Ohkuma, "Irreversible membrane fouling during ultrafiltration of surface water," *Water Research*, vol. 38, no. 14-15, pp. 3431–3441, 2004.

Hindawi Publishing Corporation
The Scientific World Journal
Volume 2013, Article ID 890854, 8 pages
http://dx.doi.org/10.1155/2013/890854

*Research Article*

# Assessment of Trihalomethane Formation in Chlorinated Raw Waters with Differential UV Spectroscopy Approach

**Kadir Özdemir,[1] İsmail Toröz,[2] and Vedat Uyak[3]**

[1] *Department of Environmental Engineering, Bulent Ecevit University, Incivez, 67100 Zonguldak, Turkey*
[2] *Department of Environmental Engineering, Istanbul Technical University, Maslak, 34469 Istanbul, Turkey*
[3] *Department of Environmental Engineering, College of Engineering, Pamukkale University, Kinikli, 20020 Denizli, Turkey*

Correspondence should be addressed to Kadir Özdemir; kadirozdemir73@yahoo.com

Received 26 September 2013; Accepted 27 October 2013

Academic Editors: M. Kumar and K. Kuroda



In this study, the changes in UV absorbance of water samples were characterized using defined differential UV spectroscopy (DUV), a novel spectroscopic technique. Chlorination experiments were conducted with water samples from Terkos Lake (TL) and Büyükçekmece Lake (BL) (Istanbul, Turkey). The maximum loss of UV absorbance for chlorinated TL and BL raw water samples was observed at a wavelength of 272 nm. Interestingly, differential absorbance at 272 nm ($\Delta UV_{272}$) was shown to be a good indicator of UV absorbing chromophores and the formation of trihalomethanes (THMs) resulting from chlorination. Furthermore, differential spectra of chlorinated TL waters were similar for given chlorination conditions, peaking at 272 nm. The correlations between THMs and $\Delta UV_{272}$ were quantified by linear equations with $R^2$ values >0.96. The concentration of THMs formed when natural organic matter is chlorinated increases with increasing time and pH levels. Among all THMs, $CHCl_3$ was the dominant species forming as a result of the chlorination of TL and BL raw water samples. The highest chloroform ($CHCl_3$), dichlorobromomethane ($CHCl_2Br$), and dibromochloromethane ($CHBr_2Cl$) concentration were released per unit loss of absorbance at 272 nm at pH 9 with a maximum reaction time of 168 hours and $Cl_2$/dissolved organic carbon ratio of 3.2.

## 1. Introduction

Disinfection of surface water supplies containing natural organic matter (NOM) with chlorine leads to formation of chlorinated brominated, and in much smaller levels, iodinated by-products defined as disinfection by-products (DBPs) [1–3]. Trihalomethanes (THMs) and halo acetic acids (HAAs) are the main groups of DBPs commonly found in drinking waters [4–7]. Such hazardous compounds have been shown to be related to the occurrence of cancer, growth retardation, spontaneous abortion, and congenital cardiac effects [8–13]. Therefore, strict regulations for water quality have been recently imposed in some European countries [14]. These regulations should ensure the safety of drinking water through the elimination (or reduction to a minimum concentration) of the hazardous substances in water. The maximum contaminant level of THMs was set to 80 $\mu$g/L by United States Environmental Protection Agency (USEPA) [15]. Whereas the European Union (EC) has set the THMs limit to 100 $\mu$g/L [16]. The THMs limit in Turkey is also 100 $\mu$g/L [17].

The relationships among chlorination conditionals such as pH, temperature, reaction time, bromide concentration, chlorine dosage and NOM concentration, and the formation of DBPs are highly nonlinear and complex [18]. Developing formal kinetic or statistical models for DBP formation currently requires substantial cost and effort associated with analysis of DBPs, thus restricting the amount of data that can be obtained from any single laboratory or field study of the chlorination reactions and limiting the availability of information that may be useful in formulating or testing models of the reaction sequence [19]. Several researches have attempted to correlate water quality parameters to DBP formation in an effort to find a useful surrogate parameter to

predict DBP formation or to better understand the chemical nature of DBP formation processes [20–22]. The use of surrogate parameters to monitor formation of chlorinated by-products can be used as an alternative to mechanistic or statistical models for estimating DBPs formation. Many surrogate parameters that have been most widely used to estimate DBP formation potential (DBPFP) include ultraviolet absorbance (UV), specific UV absorbance (SUVA), which is UV absorbance divided by dissolved organic carbon (DOC) concentration and DOC. It was reported that the correlation between UV absorbance at 254 nm ($UV_{254}$) wavelength and the THM formation potential (THMFP) was strong [23].

Since SUVA is strongly correlated with the aromaticity and reactivity of NOM, it has been used extensively as a conventional parameter [24, 25] and can therefore be used to estimate the concentration of NOM moieties in a water sample.

It has been reported that simple and reliable relationships existed between change in UV absorbance of NOM and formation of DBPs during the chlorination processes [21, 26–28]. As the aromatic functional groups are thought to be both dominant chromospheres in NOM and the dominant sites of attack by chlorine on NOM molecules, $UV_{254}$ has frequently been proposed to predict the concentration of DBP precursors. Although the use of UV spectroscopy to estimate DBP formation is problematic, a technique known as differential UV spectroscopy (DUV) has been developed [29]. ΔUV has been shown to be an effective spectrophotometric method for monitoring the amount of DBPs formed by chlorination of NOM. This approach focuses on the change in UV absorbance caused by the chlorination reaction, rather than the overall UV spectrum of water. The differential UV spectrum of chlorinated NOM is defined as shown in

$$\Delta UV_{\lambda} = UV_{\lambda}^{\text{chlorinated}} - UV_{\lambda}^{\text{inital}}, \quad (1)$$

where $UV_{\lambda}^{\text{inital}}$ is the UV absorbance at wavelength $\lambda$ prior to chlorination, $UV_{\lambda}^{\text{chlorinated}}$ is the UV absorbance at wavelength $\lambda$ after chlorination, and $\Delta UV_{\lambda}$ is the differential UV absorbance at wavelength $\lambda$.

As the chlorination reaction with NOM occurs primarily at sites that absorb UV light, DUV could provide a sensitive and highly specific probe for chlorination reactions. Moreover, the magnitude of decrease in UV absorbance at 272 nm ($\Delta UV_{272}$) was found to be an excellent indicator of total organic halogen formation resulting from chlorination, independent of chlorine to DOC ratio, bromide concentration, pH, reaction time, and NOM source [21, 30, 31].

In this study, we investigated the applicability of differential absorbance to quantify the reactivity of NOM from raw waters.

## 2. Materials and Methods

*2.1. Sample Collection.* During this study, water samples were taken from Terkos and Büyükçekmece Lakes in Istanbul, Turkey. Samples were collected during the summer period (June, July, and August) in 2010. Terkos Lake (TL) and Büyükçekmece Lake (BL) are the main surface water sources of Istanbul, providing nearly 1 million $m^3$ raw water to the drinking water treatment plants of Kağıthane and Büyükçekmece. The characteristics of raw water quality parameters are presented in Table 1. Raw water samples were collected as grab samples and stored in a refrigerator at 4°C to retard biological activity.

*2.2. Chlorination Procedure.* Chlorination of raw water samples was conducted in accordance with Standard Methods 5710 B [32]. Before chlorination, sample pH values were adjusted to pH 5, 7, and 9 by addition of HCl or NaOH solution. The chlorinated samples were placed into 125 mL amber glass bottles with polypropylene screw caps and TFE-faced septa. Raw water samples were chlorinated to $Cl_2$/DOC ratios of 0.8, 1.6, and 3.2 before incubation in the dark for either 1, 4, 24, 48, 96, or 168 hours. After the reaction periods, chlorine residual concentrations were determined with DPD ferrous titrimetric method according to Standard Methods 4500 Cl-F [32]. Sodium sulfite solution was used as a quenching agent for all chlorinated samples prior to UV spectrophotometric and THM analyses.

*2.3. Analytical Procedure.* THM measurements were performed by liquid-liquid extraction (LLE) with n-pentane. For THMs, a total of six THM calibration standards were prepared using certificated commercial mix solutions (Accu Standard, Inc., purity >99%). Samples were analyzed by gas chromatography (GC) equipped with a microelectron capture detector ($\mu$ECD) for THM analyses. A capillary column of (DB-1 J&W Science) 30 m × 0.32 mm and 1.0 $\mu$m film thickness was used. Samples were injected in split/splitless mode with helium as a carrier gas and nitrogen gas as a make-up gas. The minimum quantification limits for THM species ranged between 0.5 and 1 $\mu$g/L. DOC concentrations were measured on a Schimadzu 5000 total carbon analyzer equipped with an AS auto sampler according to method 5310 B in Standard Methods [32]. The instrument provided reliable, accurate, and reproducible data with a minimum detection limit of 2 $\mu$g/L. The UV absorbance readings between wavelengths of 250 and 410 nm were determined using a Shimadzu 1608 UV/VIS spectrophotometer.

## 3. Result and Discussion

*3.1. Differential UV Spectra of Chlorinated NOM.* The changes of UV absorbance spectra for TL and BL water samples, including NOM before and after chlorination, are shown in Figure 1. The UV absorbance values of TL and BL water samples at given wavelengths (250–400 nm) are significantly decreased for different reaction times (1, 4, 12, 96, and 168 hours) after chlorination. For instance, the UV absorbance of TL raw water samples at a wavelength of 272 nm was reduced from 0.095 to 0.06 $cm^{-1}$ by 1 h chlorination. Whereas the UV absorbance of BL raw water samples at the same wavelength decreased from 0.064 to 0.032 $cm^{-1}$ by 1 h after chlorination.

The similar trend with corresponding to UV spectra of chlorinated TL and BL raw water samples was determined at the range of 250–400 nm for the desired reaction times. The

Table 1: Raw water quality parameters.

| Parameter | Unit | Terkos Lake | Büyükçekmece Lake |
|---|---|---|---|
| | | Average value | |
| pH | — | 7.97 ± 0.16 | 8.19 ± 0.14 |
| Turbidity | NTU | 3.34 ± 0.46 | 3.24 ± 0.27 |
| Total Hardness | mg $CaCO_3$/L | 116.3 ± 6.7 | 166.4 ± 10.3 |
| Alkalinity | mg $CaCO_3$/L | 103.1 ± 7.53 | 114 ± 7.7 |
| Temperature | °C | 17.2 ± 2.3 | 17.1 ± 2.1 |
| DOC | mg/L | 4.78 ± 0.3 | 4.71 ± 0.45 |
| UV254 | $cm^{-1}$ | 0.13 ± 0.01 | 0.095 ± 0.008 |
| Br | $\mu$g/L | 90 ± 20 | 180 ± 20 |
| DBPFP | $\mu$g/L | 278 ± 30.2 | 230 ± 24.4 |
| Conductivity | $\mu$S/cm | 305 ± 13.5 | 470 ± 16 |
| SUVA | L/mg·m | 3.04 ± 0.14 | 2.02 ± 0.23 |

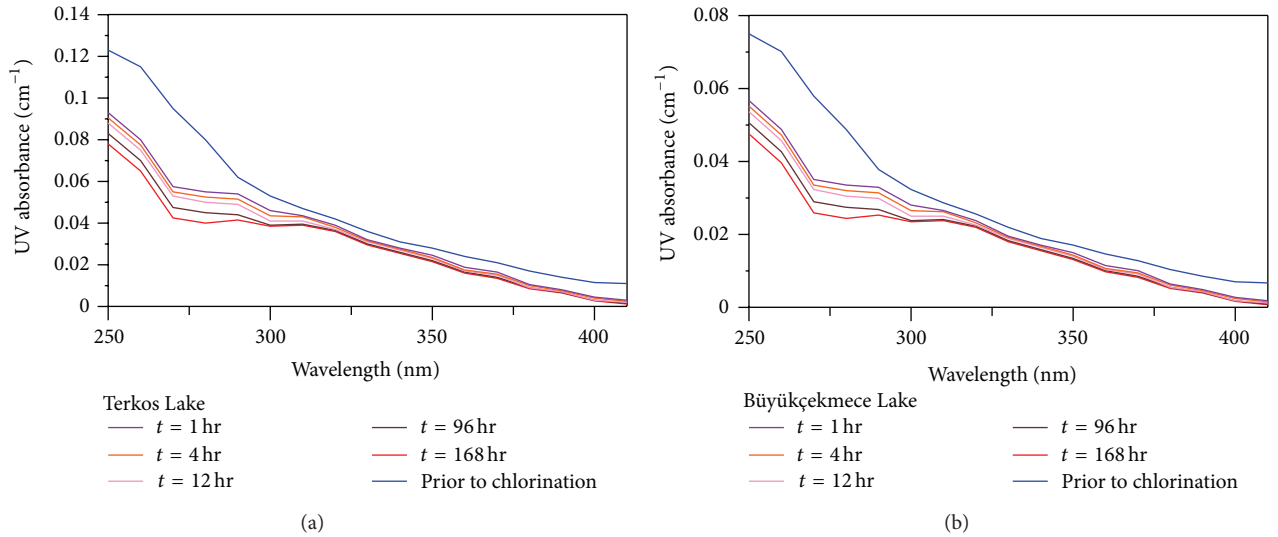


Figure 1: Chlorinated UV absorbance spectra at varying reaction times and at pH 7 for (a) TL water samples and (b) BL water samples.

maximum loss of UV absorbance in TL and BL water samples was recorded at 400 nm and 168 h reaction time, reaching 0.0012 and 0.001 $cm^{-1}$, respectively. The ratio of decreasing UV absorbance of chlorinated water samples containing NOM followed consistent pattern as a function of wavelength and at a given reaction time.

Changes in the UV spectrum of chlorinated NOM-containing TL and BL raw water samples are presented with differential absorbance spectrum between 250 and 400 nm (Figure 2).

The measurement of differential UV spectrum of TL and BL raw water samples was characterized using (1). These findings demonstrate several shared properties of the differential spectra. The sign of differential absorbance was always negative at 250–400 nm wavelengths because the UV absorbance of NOM surface water supplies decreased with chlorination. The differential spectra of chlorinated TL and BL raw water samples consistently peak at 272 nm. In fact, 272 nm was the maximum differential absorbance for all chlorinated TL and BL raw water samples at all reaction times. The TL and BL differential absorbance values of water samples at 272 nm at a reaction time of 4 h were 0.04 and 0.0285 $cm^{-1}$, respectively. The highest $\Delta UV_{272}$ values were observed at a reaction time of 168 h (0.0525 and 0.04 $cm^{-1}$ for TL and BL samples, resp.), demonstrating that the magnitude of the differential spectra developed with increasing chlorination reaction time, and is consistent with the results of other studies [28, 29, 33].

We also found that the differential spectrum of chlorinated TL and BL water including NOM was related to other independence parameters of water quality and chlorination conditions. Furthermore, these spectra exhibited a peak at 272 nm, suggesting that differential absorbance is an effective spectrophotometric parameter providing insight into the

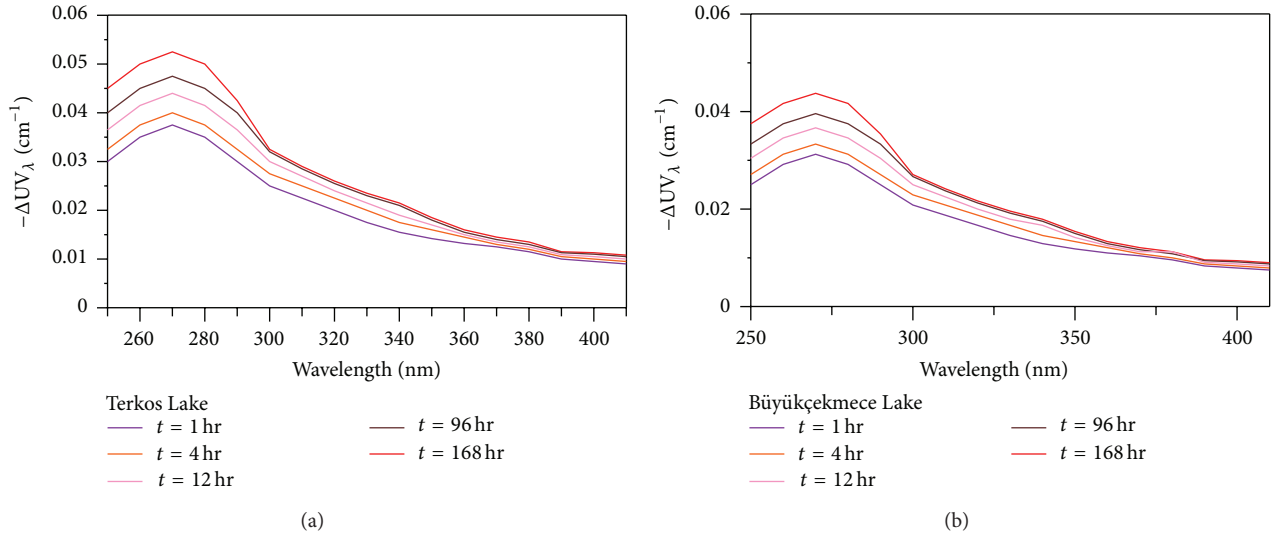


Figure 2: Differential spectra at varying reaction times and at pH 7 for (a) TL water samples and (b) BL water samples.

reactivity of NOM molecules with regard to the formation of DBPs such as THMs. An observation was also made in previous publications [21, 31, 34, 35].

*3.2. Relationship between $\Delta UV_{272}$ and THM Concentrations.* A series of experiments were conducted upon TL and BL water samples to examine THM formation at three $Cl_2$/DOC ratios (0.8, 1.6, and 3.2), for the chlorination pH (pH = 7) and at reaction times from 1 h to 168 h. We identified strong correlations between total THM (TTHM) concentrations and $\Delta UV_{272}$ values obtained by the chlorination of TL raw waters (Figure 3).

These correlations were modeled by linear regression analysis with $R^2$ values >0.98 given by the following.

TL waters

$$\text{TTHM}\,(\mu\text{g/L}) = 4952.2\ \Delta UV_{272} - 25.12. \quad (2)$$

BL raw waters

$$\text{TTHM}\,(\mu\text{g/L}) = 4339.5\ \Delta UV_{272} - 3.08. \quad (3)$$

The highest TTHM content and $\Delta UV_{272}$ value (395.62 $\mu$g/L and 0.079 cm$^{-1}$, resp.) were obtained for the chlorinated TL raw water samples with the SUVA level of 3.04 L/mg·m, at the maximum $Cl_2$/DOC ratio (3.2) and reaction time (168 h). The relationship between hydrophobic SUVA and the formation of TTHM is dependent on the activated aromatic structures which are the major components in NOM. In high SUVA water (e.g., TL raw water), high chlorine reactivity resulted in the formation of more THMs than in low SUVA level waters (e.g., BL raw water that has hydrophilic organic fractions).

*3.3. The Effects of pH, Reaction Time, and Chlorine Dose on THMs Formation.* Solution pH has a significant effect on the speciation and amount of THM forming as a result of chlorination. We found that higher pH resulted in increased THM concentrations for the two surface water sources studied. $CHCl_3$, dichlorobromomethane ($CHCl_2Br$), and dibromochloromethane ($CHBr_2Cl$) are common THM compounds in chlorinated TL and BL raw waters. The concentrations of $CHCl_3$ generated in chlorinated TL and BL raw waters, as estimated by $\Delta UV_{272}$ and at pHs 5, 7, and 9 are shown in Figure 4.

The relationship between $CHCl_3$ concentrations and $\Delta UV_{272}$ could be well fitted by a straight line ($R^2 > 0.98$). As the pH increased for each raw water source, more $CHCl_3$ was formed per unit of UV absorbance destroyed. Furthermore, the highest $CHCl_3$ concentration and $\Delta UV_{272}$ absorbance value (222.55 $\mu$g/L and 0.0865 cm$^{-1}$, resp.) were measured at the highest pH level tested (TL water, pH 9, $Cl_2$/DOC 3.2, and 168 h reaction time). Whereas the lowest $CHCl_3$ concentration and $\Delta UV_{272}$ value (67.16 $\mu$g/L and 0.059 cm$^{-1}$, resp.) were measured at the most acidic pH (BL water, pH 5, $Cl_2$/DOC 3.2, 168 h reaction time). This can be explained using the mechanism of DBPs formation as described by Reckhow and Singer [36]. According to this mechanism, base-catalyzed hydrolysis prevails under alkaline conditions, resulting in more $CHCl_3$ at pH 9, relative to acidic conditions (pH 5). Although $CHCl_3$ formation to $\Delta UV_{272}$ regression lines did not pass through the origin for all pHs studied, this can be explained by some initial reactions between NOM and $Cl_2$. These reactions demolish the aromaticity of activated functional groups and produce chlorinated intermediates before $CHCl_3$ formation [29, 37, 38]. $CHCl_2Br$ and $CHBr_2Cl$ were the other major THMs identified in chlorinated TL and BL raw waters. The concentrations of $CHCl_2Br$ and $CHBr_2Cl$ were also found to increase with increasing pH levels with the highest $CHCl_2Br$ and $CHBr_2Cl$ concentrations (39.72 and 19.77 $\mu$g/L) found at pH 9 at 168 h reaction time and $Cl_2$/DOC ratio of 3.2. Despite relatively low concentrations of $CHCl_2Br$

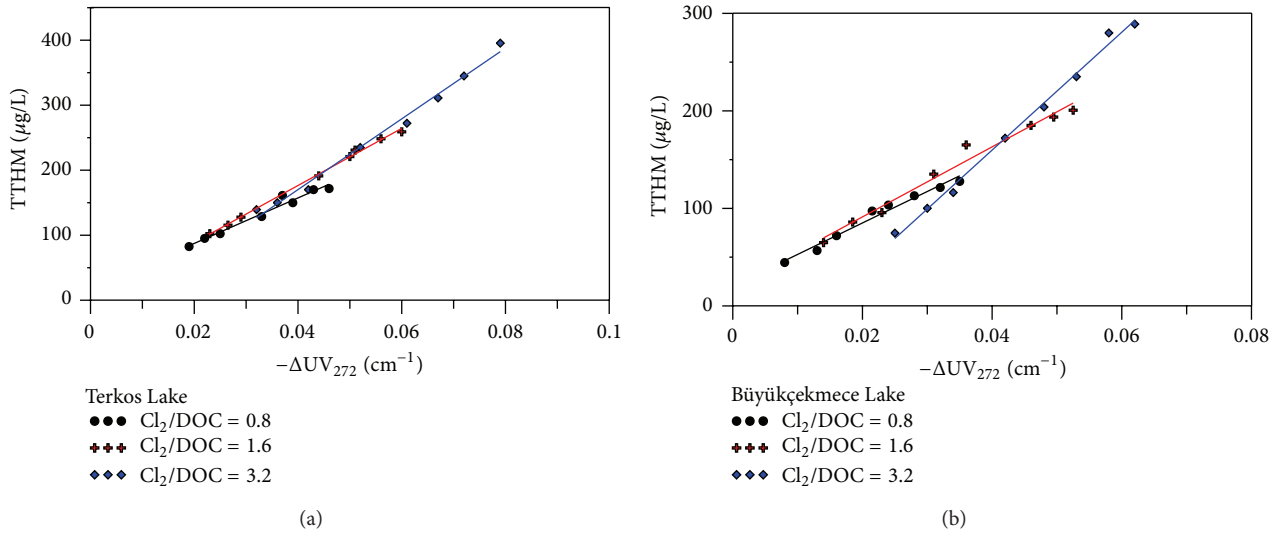


Figure 3: Correlations between $\Delta UV_{272}$ values and TTHM concentrations at different $Cl_2$ to DOC ratios, pH 7, and reaction times from 1 h to seven days for (a) TL water and (b) BL water samples.

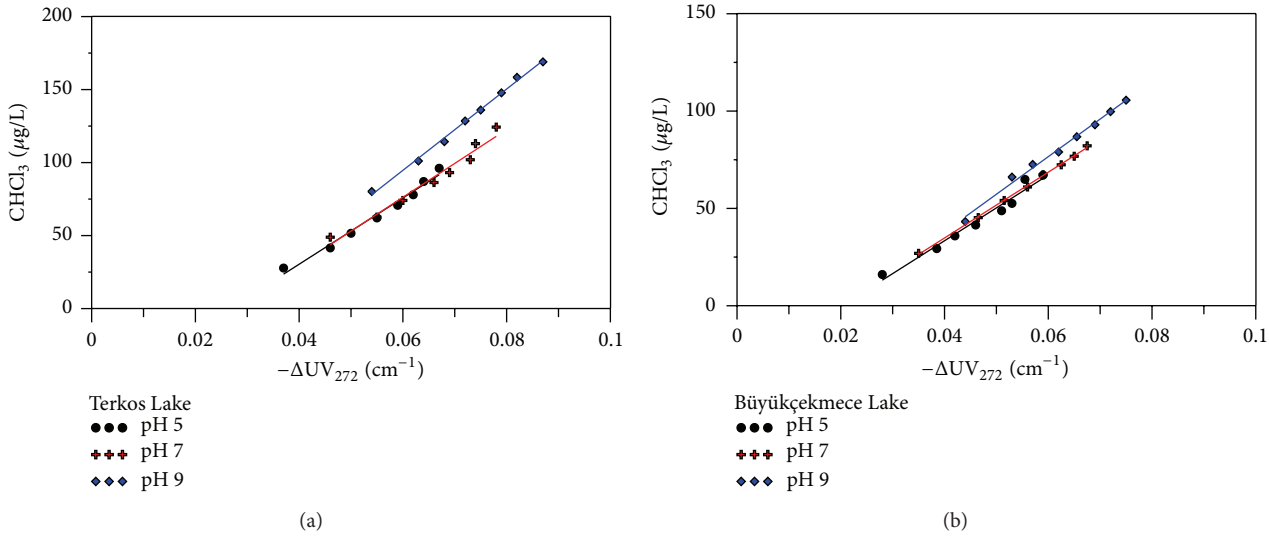


Figure 4: The relationship between $CHCl_3$ and $\Delta UV_{272}$ at different pH (pH 5, pH7, and pH 9) and $Cl_2$ to DOC ratios from 0.8 to 3.2 (a) in chlorinated TL water and (b) for in chlorinated BL water.

and $CHBr_2Cl$ in the chlorinated water samples, there was a strong linear correlation between $CHCl_2Br$ and $CHBr_2Cl$ and $\Delta UV_{272}$ (Figures 5 and 6).

## 4. Conclusion

The chlorination of TL and BL water samples including NOM resulted in decreasing UV absorbance at all wavelengths due to the destruction of UV-absorbing chromospheres and produced characteristic UV spectra. The shape of these differential UV spectra for the chlorinated TL and BL water samples was similar for the given chlorination conditions. In particular, the maximum loss of UV absorbance for the chlorinated raw water samples was observed at 272 nm. This study also examined the relationships between $\Delta UV_{272}$ and the formation of THMs in chlorinated waters from TL and BL water sources for Istanbul, Turkey.

The correlation between $\Delta UV_{272}$ and TTHM was quantified by linear regression analysis, showing $R^2$ values >0.96. The highest TTHM and THM contents of raw water samples were observed at pH 9 (the highest value tested).

Among the THM species formed by chlorination of the TL and BL raw water samples, $CHCl_3$ was predominant. The highest concentrations of THM compounds, as measured

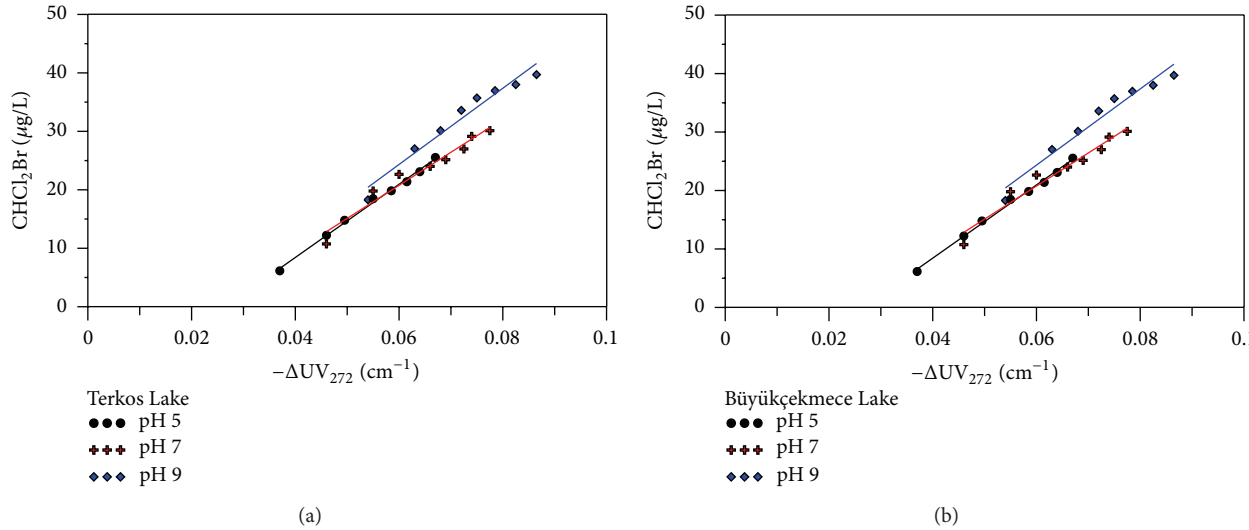


FIGURE 5: The relationship between $CHCl_2Br$ and $\Delta UV_{272}$ at different pH (pH 5, pH7, and pH 9) and $Cl_2$ to DOC ratios from 0.8 to 3.2 (a) for in chlorinated TL water and (b) for in chlorinated BL water.

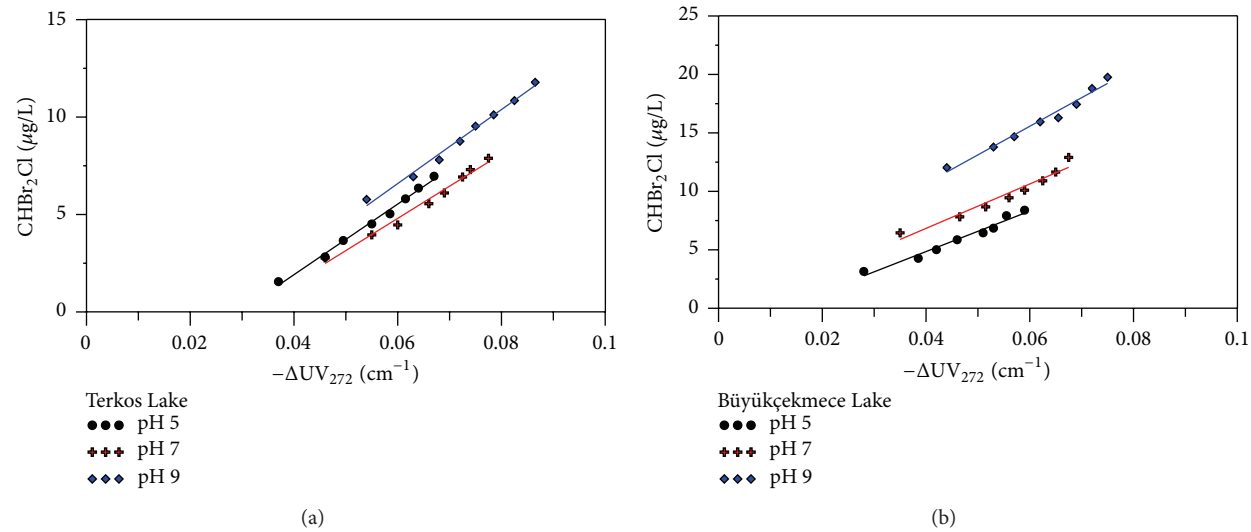


FIGURE 6: The relationship between $CHClBr_2$ and $\Delta UV_{272}$ at different pH and $Cl_2$ to DOC ratios (a) in chlorinated TL water and (b) in chlorinated BL water.

by unit loss of absorbance at 272 nm, were produced at the highest chlorine dosage, maximum reaction time, and pH 9.

These results demonstrate that $\Delta UV_{272}$ is an alternative approach for the continuous and instantaneous monitoring of THM formation under a wide range of chlorination conditions and water qualities.

## Acknowledgment

The authors would like to acknowledge the Scientific and Technological Research Council of Turkey for supporting this study as a part of scientific and technological research project with project no. of 108Y126.

## References

[1] Y. Bichsel and U. Von Gunten, "Formation of iodo-trihalomethanes during disinfection and oxidation of iodide-containing waters," *Environmental Science and Technology*, vol. 34, no. 13, pp. 2784–2791, 2000.

[2] S. D. Richardson, "Drinking water disinfection by-products," in *The Encyclopedia of Environmental Analysis and Remediation*, R. A. Meyers, Ed., vol. 3, pp. 1398–1421, Wiley, New York, NY, USA, 1998.

[3] J. J. Rook, "Formation of haloforms during the chlorination of natural water," *Water Treatment Exam*, vol. 23, pp. 234–243, 1974.

[4] S. K. Golfinopoulos and G. B. Arhonditsis, "Multiple regression models: a methodology for evaluating trihalomethane concentrations in drinking water from raw water characteristics," *Chemosphere*, vol. 47, no. 9, pp. 1007–1018, 2002.

[5] J. W. Miller and P. C. Uden, "Characterization of nonvolatile aqueous chlorination products of humic substances," *Environmental Science and Technology*, vol. 17, no. 3, pp. 150–157, 1983.

[6] M. J. Rodriguez, J.-B. Sérodes, and P. Levallois, "Behavior of trihalomethanes and haloacetic acids in a drinking water distribution system," *Water Research*, vol. 38, no. 20, pp. 4367–4382, 2004.

[7] V. Uyak, K. Ozdemir, and I. Toroz, "Multiple linear regression modeling of disinfection by-products formation in Istanbul drinking water reservoirs," *Science of the Total Environment*, vol. 378, no. 3, pp. 269–280, 2007.

[8] M. I. Cedergren, A. J. Selbing, O. Löfman, and B. A. J. Källen, "Chlorination byproducts and nitrate in drinking water and risk for congenital cardiac defects," *Environmental Research*, vol. 89, no. 2, pp. 124–130, 2002.

[9] L. Dodds, W. King, and C. Woolcott, "Trihalomethanes in public water supplies and adverse birth outcomes," *Epidemiology*, vol. 10, no. 3, pp. 233–237, 1999.

[10] M. Fabbricino and G. V. Korshin, "Modelling disinfection by-products formation in bromide-containing waters," *Journal of Hazardous Materials*, vol. 168, no. 2-3, pp. 782–786, 2009.

[11] I. Ivancev-Tumbas, B. Dalmacija, Z. Tamas, and E. Karlovic, "The effect of different drinking water treatment processes on the rate of chloroform formation in the reactions of natural organic matter with hypochlorite," *Water Research*, vol. 33, no. 18, pp. 3715–3722, 1999.

[12] R. G. Tardiff, M. L. Carson, and M. E. Ginevan, "Updated weight of evidence for an association between adverse reproductive and developmental effects and exposure to disinfection by-products," *Regulatory Toxicology and Pharmacology*, vol. 45, no. 2, pp. 185–205, 2006.

[13] C.-Y. Yang, B.-H. Cheng, S.-S. Tsai, T.-N. Wu, M.-C. Lin, and K.-C. Lin, "Association between chlorination of drinking water and adverse pregnancy outcome in Taiwan," *Environmental Health Perspectives*, vol. 108, no. 8, pp. 765–768, 2000.

[14] P. Roccaro, C. Barone, G. Mancini, and F. G. A. Vagliasindi, "Removal of natural contaminants from water supplies intended for human consumption," in *Proceedings of the 9th International Conference on Environmental Science and Technology*, 2005, Vol A—Oral Presentations, Pts A and B, A1268-A1273.

[15] US EPA, "National primary drinking water regulations: stage 2 disinfectants and disinfection byproducts (D/DBP)," *Final Rule*, vol. 68, p. 159, 2003.

[16] EC, "EEC Council Directive 98/83/EC of 3 November 1998 on the quality of water intended for human consumption," *Official Journal of the European Communities*, vol. L330, no. 32, p. 51298, 1998.

[17] TMH, "Regulation concerning water intended for human consumption," Official News Paper 25730, Turkish Ministry of Health, Ankara, Turkey, 2012.

[18] G. W. Harrington, Z. K. Chowdhury, and D. M. Owen, "Developing a computer model to simulate DBP formation during water treatment," *Journal of the American Water Works Association*, vol. 84, no. 11, pp. 78–87, 1992.

[19] C.-W. Li, G. V. Korshin, and M. M. Benjamin, "Monitoring DBP formation with differential UV spectroscopy: a new application uses differential UV spectroscopy to monitor DBP formation easily, rapidly, and inexpensively," *Journal of the American Water Works Association*, vol. 90, no. 8, pp. 88–100, 1998.

[20] B. D. Black, G. W. Harrington, and P. C. Singer, "Reducing cancer risks by improving organic carbon removal," *Journal of the American Water Works Association*, vol. 88, no. 6, pp. 40–52, 1996.

[21] G. V. Korshin, W. W. Wu, M. M. Benjamin, and O. Hemingway, "Correlations between differential absorbance and the formation of individual DBPs," *Water Research*, vol. 36, no. 13, pp. 3273–3282, 2002.

[22] W. Sung, B. Reilley-Matthews, D. K. O'Day, and K. Korrigan, "Modeling if formation," *Journal of the American Water Works Association*, vol. 92, no. 5, pp. 53–63, 2000.

[23] J. K. Edzwald, W. C. Becker, and K. L. Wattier, "Surrogate parameters for monitoring organic matter and THM precursors," *Journal of the American Water Works Association*, vol. 77, no. 4, pp. 122–131, 1985.

[24] M. Kitis, T. Karanfil, J. E. Kilduff, and A. Wigton, "The reactivity of natural organic matter to disinfection by-products formation and its relation to specific ultraviolet absorbance," *Water Science and Technology*, vol. 43, no. 2, pp. 9–16, 2001.

[25] M. Kitis, T. Karanfil, A. Wigton, and J. E. Kilduff, "Probing reactivity of dissolved organic matter for disinfection by-product formation using XAD-8 resin adsorption and ultrafiltration fractionation," *Water Research*, vol. 36, no. 15, pp. 3834–3848, 2002.

[26] G. V. Korshin, C.-W. Li, and M. M. Benjamin, "The decrease of UV absorbance as an indicator of TOX formation," *Water Research*, vol. 31, no. 4, pp. 946–949, 1997.

[27] C. Li, M. M. Benjamin, and G. V. Korshin, "The relationship between TOX formation and spectral changes accompanying chlorination of pre-concentrated or fractionated NOM," *Water Research*, vol. 36, no. 13, pp. 3265–3272, 2002.

[28] P. Roccaro and F. G. A. Vagliasindi, "Differential vs. absolute UV absorbance approaches in studying NOM reactivity in DBPs formation: comparison and applicability," *Water Research*, vol. 43, no. 3, pp. 744–750, 2009.

[29] G. V. Korshin, C.-W. Li, and M. M. Benjamin, "Use of UV spectroscopy to study chlorination of natural organic matter," *Water Disinfection and Natural Organic Matter*, vol. 649, pp. 182–195, 1996.

[30] G. V. Korshin, C.-W. Li, and M. M. Benjamin, "Monitoring the properties of natural organic matter through UV spectroscopy: a consistent theory," *Water Research*, vol. 31, no. 7, pp. 1787–1795, 1997.

[31] P. Roccaro, H.-S. Chang, F. G. A. Vagliasindi, and G. V. Korshin, "Differential absorbance study of effects of temperature on chlorine consumption and formation of disinfection by-products in chlorinated water," *Water Research*, vol. 42, no. 8-9, pp. 1879–1888, 2008.

[32] APHA, *AWWA, WEF Standard Methods for the Examination of Water and Waste Water*, Washington, DC, USA, 21th edition, 2005.

[33] G. V. Korshin, M. M. Benjamin, and C.-W. Li, "Use of differential spectroscopy to evaluate the structure and reactivity of humics," *Water Science and Technology*, vol. 40, no. 9, pp. 9–16, 1999.

[34] G. V. Korshin and H. S. Chang, "Spectroscopic studies of the roles of distinct chromophores in NOM chlorination and DBP

formation," in *Disinfection By-Products in Drinking Water*, vol. 995 of *ACS Symposium Series*, pp. 158–171, 2008.

[35] P. Roccaro, F. G. A. Vagliasindi, and G. V. Korshin, "Comparison of the performance of spectroscopic indices developed to quantify the halogenation of natural organic matter at varying chlorine concentrations, reaction times and temperatures," in *Disinfection By-Products in Drinking Water Occurrence, Formation, Health Effects, and Control*, vol. 995 of *ACS Symposium Series*, pp. 198–212, 2008.

[36] D. A. Reckhow and P. C. Singer, "Mechanism of organic halid formation during fulvic acid chlorination and implications with respect to preozonation," in *Water Chlorination: Environmental Impact and Health Effect*, vol. 5, pp. 1229–1259, Ann Arbor Science Publishes, Ann Arbor, Mich, USA, 1985.

[37] R. G. Qualls and J. D. Johnson, "Kinetics of the short-term consumption of chlorine by fulvic acid," *Environmental Science and Technology*, vol. 17, no. 11, pp. 692–698, 1983.

[38] N. Y. Tretyakova, A. T. Lebedev, and V. S. Petrosyan, "Degradative pathways for aqueous chlorination of orcinol," *Environmental Science and Technology*, vol. 28, no. 4, pp. 606–613, 1994.

Hindawi Publishing Corporation
The Scientific World Journal
Volume 2013, Article ID 129793, 9 pages
http://dx.doi.org/10.1155/2013/129793

*Research Article*

# Characteristics and Scenarios Projection of Climate Change on the Tibetan Plateau

**Zhenchun Hao,[1] Qin Ju,[1] Weijuan Jiang,[2] and Changjun Zhu[3]**

[1] *State Key Laboratory of Hydrology-Water Resources and Hydraulic Engineering, Hohai University, Nanjing 210098, China*
[2] *NAVECO Ltd., Nanjing 210028, China*
[3] *College of Urban Construction, Hebei University of Engineering, Handan 056038, China*

Correspondence should be addressed to Qin Ju; qinju1980@126.com

Received 12 April 2013; Accepted 13 June 2013

Academic Editors: M. Kumar and K. Kuroda



The Fourth Assessment Report of the Intergovernmental Panel on Climate Change (IPCC AR4) presents twenty-two global climate models (GCMs). In this paper, we evaluate the ability of 22 GCMs to reproduce temperature and precipitation over the Tibetan Plateau by comparing with ground observations for 1961~1900. The results suggest that all the GCMs underestimate surface air temperature and most models overestimate precipitation in most regions on the Tibetan Plateau. Only a few models (each 5 models for precipitation and temperature) appear roughly consistent with the observations in annual temperature and precipitation variations. Comparatively, GFCM21 and CGMR are able to better reproduce the observed annual temperature and precipitation variability over the Tibetan Plateau. Although the scenarios predicted by the GCMs vary greatly, all the models predict consistently increasing trends in temperature and precipitation in most regions in the Tibetan Plateau in the next 90 years. The results suggest that the temperature and precipitation will both increase in all three periods under different scenarios, with scenario A1 increasing the most and scenario A1B increasing the least.

## 1. Introduction

In the context of global warming, climate specialists all over the world show great attention to the projection for future local climate change. Currently, global climate models are considered as an important tool for understanding attributions of past climate change and predicting the future [1–5]. Therefore, it is very important to assess the ability of those models to reproduce the observed climatological features, which will directly affect the "reproduction" of current decadal climate changes, and verify to some extent the credibility for future climate change projections.

IPCC (the Intergovernmental Panel on Climate Change) Data Distribution Center (IPCC-DDC for short) released the Fourth Assessment Report with climate scenarios simulations and projections with 24 climate models. Some climate models predicted climate changes under 9 emission scenarios, among which 3 scenarios are identified as the most important ones for future climate change: high scenario SRES A2 (Special Report on Emission Scenarios A2); middle scenario SRES A1B; and low scenario SRES B1 [1, 2]. It has become a hot research issue to assess global and regional simulation ability and predict climate change tendency for different emission scenarios with a single model or multiple models [3, 4]. Phillips and Gleckr [6] evaluated the ability of the 20 IPCC-AR4 (the Fourth Assessment Report of the Intergovernmental Panel on Climate Change) models to reproduce global land annual mean precipitation; the result shows that new global climate models have better simulations of global land precipitation than the previous version. Based on the atmospheric circulation features of European climate change, AP van Ulden and van Oldenborgh [7] assessed the simulation ability of global climate models over Europe by calculating spatial correlation between observed and simulated values; the result shows that there are 8 models which have well-projected European atmospheric circulation changes. Johnson and Sharma [8] assessed the credibility of global climate models in time and space using the "Variable

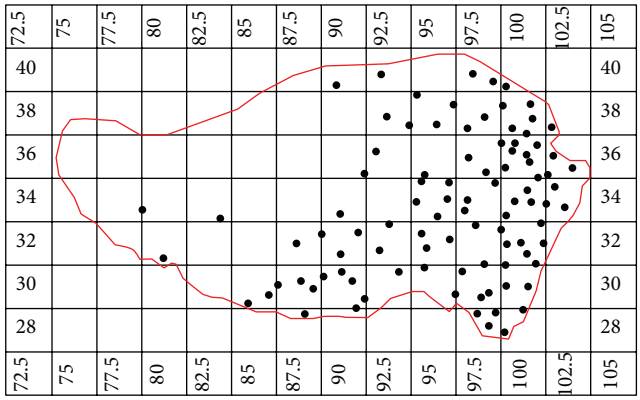


Figure 1: Grid patterns of the GFCM21 climate models on the Tibetan Plateau.

Convergence Score (VCS)" method. Sun et al. [9] evaluated the ability of new global climate models to reproduce frequency, intensity, and other indicators of precipitation, which indicated that precipitation was still too frequent in the latest models. Chinese scientists have been working on future climate change assessment in China. Zhou and Yu [10] assessed the ability of the 19 IPCC AR4 models to reproduce precipitation climatology in China; the result shows that new GCMs simulated much better than the previous with regard to China's climate; most models could represent the average of surface temperature, but the simulation of warming ratio in recent years still needs to be improved. With the 22 IPCC AR4 models, Xu et al. [11] evaluated ability of various models to reproduce China's climate changes in the 20th century; and then pointed out that the temperature simulation of each model was better than precipitation, while that multimodel ensembles mean simulated much better than a single model. Jiang et al. [12, 13] analyzed the ability of the IPCC-AR4 models to reproduce precipitation, temperature, and extreme precipitation index and project future climate changes under different emission scenarios in China. In addition, a lot of research has been done by scholars on climate change assessments and projections of GCMs [14–17].

Messerli and Ives [18] pointed out that mountainous and highland areas were vulnerable and sensitive to climate changes. The climate environments ecosystems in these regions respond most rapidly and significantly to global climate changes [19]. Climate warming on the plateau in past decades has been suggested by meteorological observation and ice core records [20]. The climatic warming trend seems more evident on the plateau than globally during the period from 1950 to 1993 [21]. Therefore, trend analysis of climate changes in high-altitude regions is very important for research on climate changes tendency. Being at an average elevation about 4000 m, the Tibetan Plateau is known as the roof of the world, which covers over 200 million km$^2$ with steep terrain. Besides it has far-reaching effects of global climate changes [22]. Although the Tibetan Plateau has a significant impact on atmospheric circulation and hydrological cycle, researches on the Tibetan Plateau climate changes have been few because of lack of data.

## 2. Data Sets and Methodology

With monthly average temperature and precipitation data of reference period (20 C3 M) of 22 IPCC-AR4 models under contemporary climate condition, this paper compares these data with observed values from 96 meteorological stations on the Tibetan Plateau (Table 2) and assesses generally the ability of GCMs to reproduce precipitation and temperature climatology on the Tibetan Plateau and climate projections under different emission scenarios, in order to make deeper understanding of China's climate changes in the context of sustaining global warming and provide basis for assessing impacts of climate changes on hydrology and water resources. Table 1 lists the basic information about 22 GCMs, as well as the border and number of grids of the Tibetan Plateau. More detailed information about GCMs can be found at http://www-pcmdi.llnl.gov/ipcc/about_ipcc.php. Take GFCM21 pattern from American Geophysical Fluid Dynamics Laboratory, for example. Distribution of grids on the Tibetan Plateau is shown in Figure 1; small black dots indicate 96 meteorological stations.

Currently, the method of multimodel ensembles mean [10, 12, 23] is commonly used for analyzing global climate models data. Compared with a single mode, multi-model ensembles mean reduces errors and reproduces- a more realistic situation. However, with calculating the arithmetic average of multi-model data, characteristics of each model are disappearing in this method, which is not conducive to distinguish simulation features from each model. In order to assess the ability of each model to reproduce temperature and precipitation on the Tibetan Plateau, based on original grid data of monthly temperature and precipitation from GCMs, we have calculated regional monthly average of reference period for each model, analyzed differences between simulated and observed values in time and spatial scales, and taken relative error, absolute error, correlation coefficient, and deterministic coefficient as performance indeices of GCMs [24].

## 3. Model Evaluation: 20th Century Climate of the Tibetan Plateau

*3.1. Temperature.* As seen in Table 2, from comparison between simulations and monthly average observations of 96 stations on the Tibetan Plateau of reference period (1961 ~ 1990), the observation and the simulated values are highly relevant while most correlation coefficients are above 0.96 except INCM3 pattern. So, GCMs have well-simulated temperature on the Tibetan Plateau in a certain degree. The annual mean temperature of the Tibetan Plateau during reference period is 3.3°C. There are great differences between models in simulating multiyear temperatures, while all simulated temperatures are lower than observed values. Compared to observed values, BCM2 pattern has the largest absolute error, that is, 11.6°C below observation; INGSXG pattern has the smallest absolute error, that is, 3.4°C below observation. With regard to deterministic coefficient, only a few patterns have relatively good simulation ability.

Table 1: Information of 22 climate models of IPCC AR4 and boundary configuration on the Tibetan Plateau.

| Model | Abbreviation | Resolution | | Duration | Longitude range/° | Latitude range/° | Grid number |
|---|---|---|---|---|---|---|---|
| | | Longitude° | Latitude/° | | | | |
| BCCR_BCM2.0 | BCM2 | 2.8125 | 2.79 | 1850–2099 | 74.53~105.47 | 25.12~41.86 | 33 |
| CCCMA_CGCM3 T47 (medres) | CGMR | 3.75 | 3.71 | 1850–2300 | 73.13~106.88 | 25.98~40.82 | 22 |
| CNRM_CM3 | CNCM3 | 2.8125 | 2.79 | 1860–2299 | 74.53~105.47 | 25.12~41.86 | 33 |
| CSIRO_Mk3.0 | CSMK3 | 1.875 | 1.8652 | 1871–2200 | 74.06~105.94 | 26.11~41.04 | 32 |
| MIUB_ECHO-G | ECHOG | 3.75 | 3.711 | 1860–2100 | 73.13~106.88 | 25.98~40.82 | 22 |
| LASG_FGOALS-g1.0 | FGOALS | 2.8125 | 2.79 | 1850–2199 | 74.53~105.47 | 25.12~41.86 | 33 |
| GFDL_CM2.0 | GFCM20 | 2.5 | 2 | 1861–2100 | 75~105 | 26~40 | 37 |
| GFDL_CM2.1 | GFCM21 | 2.5 | 2 | 1861–2300 | 75~105 | 26~40 | 37 |
| GISS_AOM | GIAOM | 4 | 3 | 1850–2100 | 72~108 | 24~42 | 27 |
| GISS_E-H | GIEH | 5 | 4 | 1880–2099 | 75~105 | 26~40 | 19 |
| GISS_E-R | GIER | 5 | 4 | 1880–2300 | 75~105 | 26~40 | 19 |
| UKMO_HadCM3 | HADCM3 | 3.75 | 2.5 | 1860–2199 | 73.13~106.88 | 26.25~41.25 | 27 |
| UKMO_HadGEM1 | HADGEM | 1.875 | 1.25 | 1860–2100 | 74.06~105.94 | 25.63~39.38 | 51 |
| INM_CM3.0 | INCM3 | 5 | 4 | 1871–2200 | 72.5~107.5 | 26~42 | 18 |
| INGV_SXG 2005 | INGSXG | 1.125 | 1.1215 | 1870–2100 | 74.81~104.06 | 25.79~39.25 | 74 |
| IPSL_CM4 | IPCM4 | 3.75 | 2.535 | 1860–2230 | 73.12~103.13 | 25.35~38.03 | 29 |
| NIES_MIROC3.2 hires | MIHR | 1.125 | 1.1214 | 1900–2100 | 74.81~104.06 | 25.79~39.25 | 74 |
| NIES_MIROC3.2 medres | MIMR | 2.8125 | 2.79 | 1850–2300 | 74.53~105.47 | 25.12~41.86 | 33 |
| MPI-M_ECHAM5-OM | MPEH5 | 1.88 | 1.87 | 1960–2200 | 74.06~105.94 | 26.11~41.04 | 32 |
| MRI_CGCM2.3.2 | MRCGCM | 2.8125 | 2.79 | 1851–2300 | 74.53~105.47 | 25.12~41.86 | 33 |
| NCAR_CCSM3 | NCCCSM | 1.40625 | 1.400763 | 1890–2099 | 75.23~104.77 | 26.61~39.22 | 53 |
| NCAR_PCM | NCPCM | 2.8125 | 2.79 | 1870–2099 | 74.53~105.47 | 25.12~41.86 | 33 |

With regard to comparison between multiyear monthly mean temperature in reference period of various models and the observed data (Figure 2), it shows that the simulated values of all modes are smaller than the observed; however, the high ones (monthly mean temperature from June to August) are floating around observation. We selected five patterns with the best simulation ability (Figure 3): GGMR, GFCM21, HADCM3, HADGEM, and MRCGCM. Figure 3 shows that climate changes with five models are consistent with the fact, which is also confirmed by Table 1. As seen from Table 1, these five models own a high value of uncertainty coefficient and the best simulation ability in annual mean temperature.

Based on grid output of each model, we have interpolated seasonal mean temperature for each station with Delta-DCSI downscaling method [25]. Traditionally, spring is from March to May; summer is from June to August; fall is from September to November; winter is from December to February of next year. Figure 4 shows the observed values of temperature on the Tibetan Plateau in reference period, which indicates that the average temperature of the Tibetan Plateau is between −5.6 and 14.5°C, with significant seasonal and spatial differences: high temperature in the southeast, decreasing from south to north and from east to west. Take GFCM21 as an example; we have analyzed differences between simulated and observed values of temperature in reference period (shown in Figure 5). Figure 5 shows that simulated temperature of GFCM21 pattern, which has a deviation of −18.1°C ~ 7.2°C from the observed, is much lower than the observed in most part of the region except for edge of the northern and southern areas. Annual mean temperature has a deviation of −14.0°C ~ 5.4°C. The maximum deviation has met −18.1°C which occurred in the western region in fall. The deviation was decreasing from west to east.

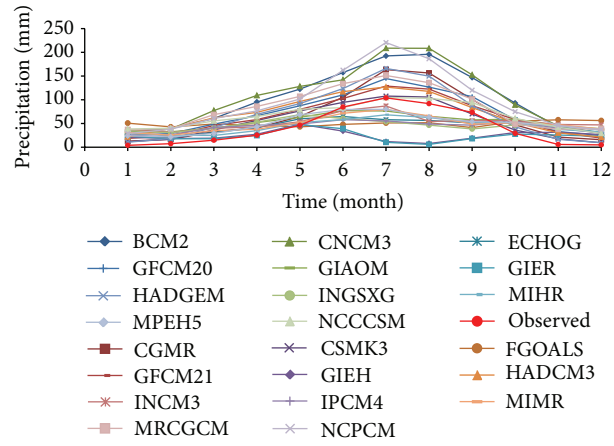


Figure 2: Comparison of annual temperatures (1961 ~ 1990) on the Tibetan Plateau between simulation and observation.

*3.2. Precipitation.* The same method has been applied to assess the ability of each model to reproduce precipitation. Annual mean precipitation on the Tibetan Plateau was

Table 2: Comparison of temperature and precipitation between simulations of climate models and observation.

| Model name for short | Simulated values | | Absolute error of $T$/°C | Relative error of $P$/% | Correlation coefficient | | Deterministic coefficient | |
|---|---|---|---|---|---|---|---|---|
| | $T$/°C | $P$/mm | | | $T$ | $P$ | $T$ | $P$ |
| BCM2 | −8.2 | 1211.3 | −11.6 | 146.0 | 0.984 | 0.938 | 0.353 | 0.389 |
| CGMR | −1.4 | 778.8 | −4.7 | 58.1 | 0.986 | 0.935 | 0.739 | 0.678 |
| CNCM3 | −7.4 | 1259.7 | −10.7 | 155.8 | 0.984 | 0.918 | 0.365 | 0.361 |
| CSMK3 | −6.9 | 639.7 | −10.2 | 29.9 | 0.987 | 0.91 | 0.432 | 0.736 |
| ECHOG | −4.0 | 538.5 | −7.3 | 9.3 | 0.964 | 0.654 | 0.589 | −1.633 |
| FGOAL | −1.8 | 592.2 | −5.2 | 20.2 | 0.966 | −0.084 | 0.649 | 0.559 |
| GFCM20 | −7.7 | 859.4 | −11.1 | 74.5 | 0.982 | 0.923 | 0.365 | 0.623 |
| GFCM21 | −4.0 | 777.3 | −7.3 | 57.8 | 0.985 | 0.922 | 0.570 | −0.705 |
| GIAOM | −3.1 | 636.2 | −6.4 | 29.2 | 0.98 | 0.7 | 0.636 | −3.553 |
| GIEH | −3.1 | 296.9 | −6.4 | −39.7 | 0.975 | −0.211 | 0.584 | −3.069 |
| GIER | −3.8 | 282.5 | −7.1 | −42.6 | 0.97 | −0.141 | 0.572 | 0.490 |
| HADCM3 | −3.9 | 842.3 | −7.3 | 71.0 | 0.984 | 0.881 | 0.541 | 0.644 |
| HADGEM | −4.7 | 828.4 | −8.0 | 68.2 | 0.982 | 0.94 | 0.545 | −0.723 |
| INCM3 | −1.5 | 630.5 | −4.8 | 28.0 | 0.942 | 0.579 | 0.650 | −3.451 |
| INGSXG | −0.1 | 558.4 | −3.4 | 13.4 | 0.965 | 0.313 | 0.700 | −2.949 |
| IPCM4 | −5.5 | 521.9 | −8.9 | 6.0 | 0.97 | 0.508 | 0.526 | −1.273 |
| MIHR | −1.6 | 528.1 | −4.9 | 7.2 | 0.969 | 0.752 | 0.655 | −0.704 |
| MIMR | −2.2 | 585.6 | −5.5 | 18.9 | 0.963 | 0.704 | 0.635 | −0.255 |
| MPEH5 | −2.5 | 596.7 | −5.8 | 21.2 | 0.966 | 0.717 | 0.649 | 0.420 |
| MRCGCM | −1.3 | 986.2 | −4.6 | 100.3 | 0.986 | 0.904 | 0.732 | 0.282 |
| NCCCSM | −4.7 | 796.0 | −8.0 | 61.6 | 0.969 | 0.852 | 0.493 | 0.424 |
| NCPCM | −3.2 | 1153.2 | −6.6 | 134.2 | 0.976 | 0.932 | 0.596 | 0.389 |

($P$: precipitation; $T$: temperature).

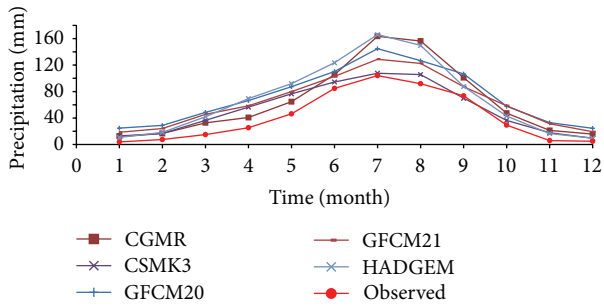


Figure 3: Comparison of five best-performance climate models for temperature.

492.5 mm in reference period which was lower than simulated values of most models (Table 2). Different models had great differences in simulation ability while more than half of models had bad simulation performance. The maximum relative error is up to 155.8% with CNCM3, while the minimum is 6.0% with IPCM4. Some models have good correlation coefficient between simulated and observed values. There are more differences in precipitation simulation ability than in temperature of each model.

With regard to comparison between simulated and observed values of precipitation (Figure 6), most models have not well simulated annual changes of precipitation as the simulated values are higher than the observed. As most precipitation occurred in the period from June to September, only half of the models had higher simulated values than the observed. In general, CGMR, five patterns as CSMK3, GFCM20, GFCM21, and HADGEM, have well simulated annual precipitation trends (Figure 7), especially CSMK3, whose simulated monthly precipitation is very similar to the observation.

Figure 8 shows observed values of precipitation on the Tibetan Plateau in reference period which indicates that precipitation concentrated in spring and summer and there was more precipitation in southeast. Annual mean precipitation was decreasing from south to north and from east to west. As seen from differences of simulated and observed precipitations of GFCM21 shown in Figure 9, the maximum deviation occurred in summer which equaled 13.7 mm/day, followed by spring and summer. With a deviation of −1.4 ~ 2.0 mm/day, the precipitation simulation in winter is the best. For the whole region, deviation of average precipitation varied from −0.8 to 5.7 mm/day with a good simulation in the center of the region.

## 4. Projected Changes in Temperature and Precipitation

Prediction from these climate models of A1B, A2, and B1 scenarios has almost covered all possible climate changes caused

Table 3: Linear trend of temperature and precipitation simulated with models in 2000–2099.

| Model | Scenario | | | | | |
|---|---|---|---|---|---|---|
| | Precipitation/mm·(100a)$^{-1}$ | | | Temperature/°C·(100a)$^{-1}$ | | |
| | A1B | A2 | B1 | A1B | A2 | B1 |
| BCM2 | 85.2 | / | 64.5 | 3.2 | 3.9 | 1.7 |
| CGMR | 105.1 | / | / | 3.3 | / | / |
| CNCM3 | 170.3 | 186.5 | / | 4.5 | 5.5 | 2.1 |
| CSMK3 | 58.6 | 73.5 | 48.9 | 2.8 | 3.9 | 1.7 |
| ECHOG | 83.4 | 66.7 | / | 7.1 | 6.9 | / |
| FGOALS | 51.2 | / | 3.3 | 3.6 | / | 2.7 |
| GFCM20 | 179.8 | 135.6 | 124.3 | 4.9 | 6 | 2.6 |
| GFCM21 | 61 | 111.6 | 68.6 | 4.5 | 5.2 | 2.3 |
| GIAOM | 75.9 | / | 42.9 | 3 | / | 1.4 |
| GIEH | 52.7 | / | / | 3.1 | / | / |
| GIER | / | 32.4 | 5.5 | 2.3 | 4.5 | 1.4 |
| HADCM3 | 118 | 109.1 | 71.6 | 4.6 | 5.5 | 3.2 |
| HADGEM | / | / | / | / | / | / |
| INCM3 | 62.4 | / | 84.5 | 3.9 | / | 2.6 |
| INGSXG | 10.3 | / | / | 4.9 | / | / |
| IPCM4 | 34.6 | 73.6 | 28.3 | 5.8 | 6.3 | 3.5 |
| MIHR | 148.5 | / | 67.8 | 6.1 | / | 4.2 |
| MIMR | 140 | 176.8 | 107.1 | 6.7 | 7.4 | 3.7 |
| MPEH5 | 71.5 | 48.7 | 65 | 6.2 | 6.6 | 4.1 |
| MRCGCM | 127.6 | 132.1 | 76.7 | 3.5 | 4.1 | 2.4 |
| NCCCSM | 68.6 | 127.6 | 62.6 | 3.6 | 5.2 | 1.2 |
| NCPCM | 145.5 | 138.6 | / | 2.7 | 3.5 | / |
| Average | 92.5 | 108.7 | 61.4 | 4.3 | 5.3 | 2.6 |

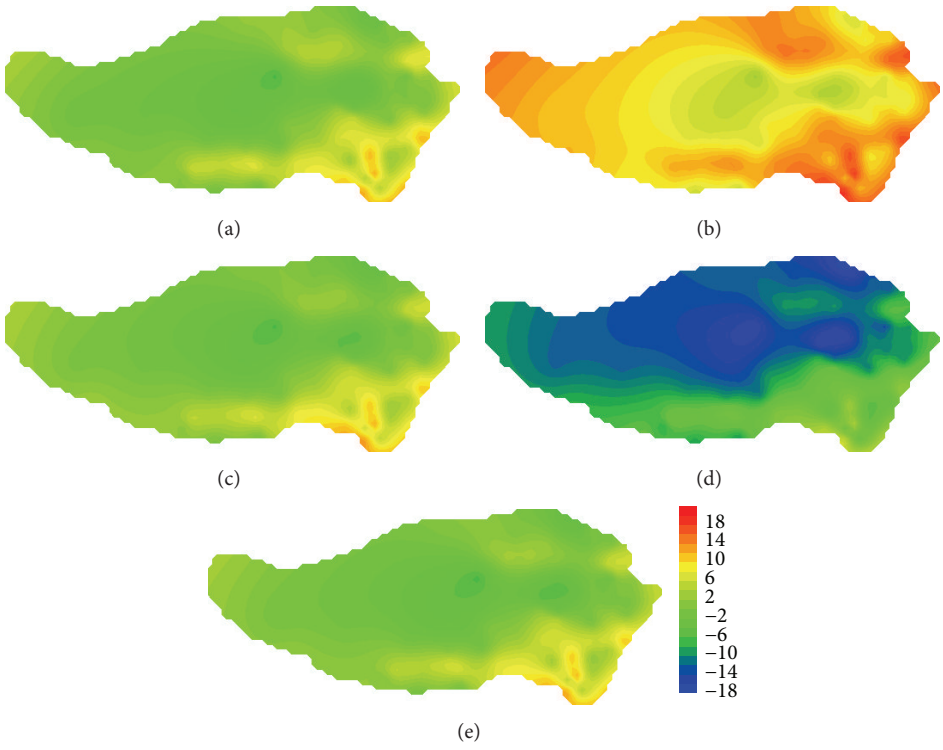


Figure 4: Observed values of temperature on the Tibetan Plateau in reference period: (a) spring; (b) summer; (c) fall; (d) winter; (e) annual.

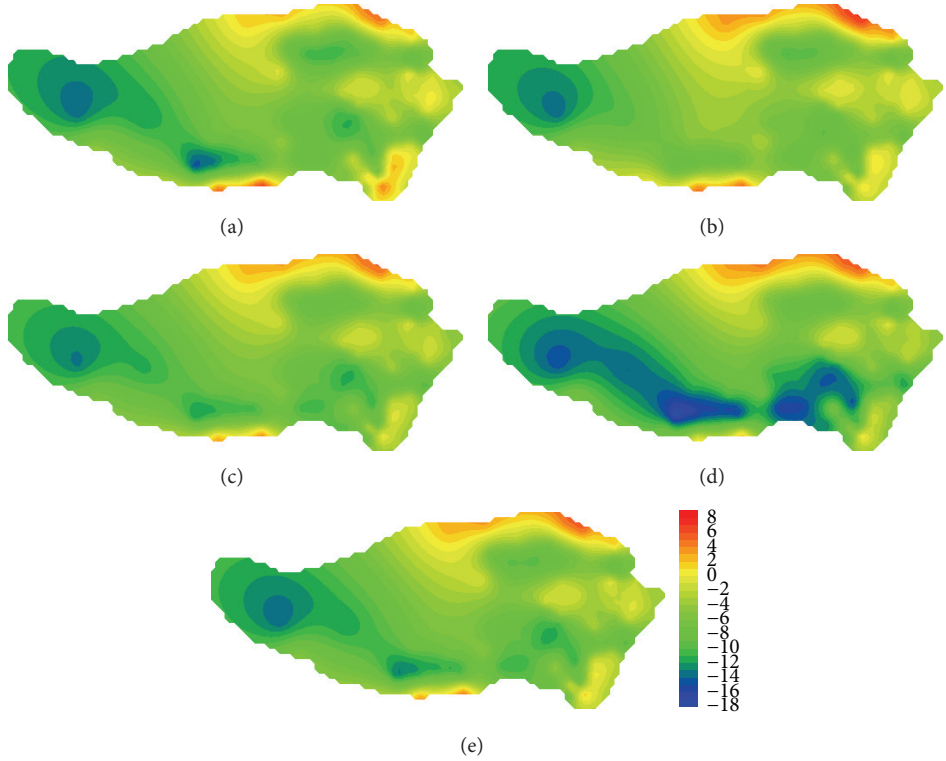


Figure 5: Comparison of the values of temperature on the Tibetan Plateau in reference period between GFCM21's simulation and observation: (a) spring; (b) summer; (c) fall; (d) winter; (e) annual.

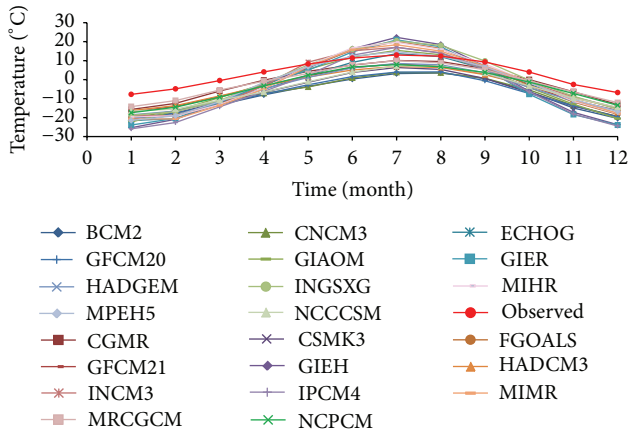


Figure 6: Comparison of precipitation on the Tibetan Plateau between simulation and observation in reference period (1961–1990).

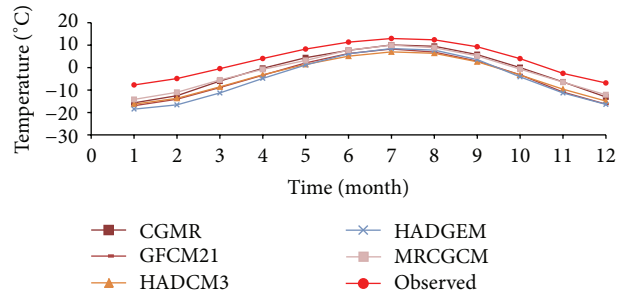


Figure 7: Comparison of precipitation simulated by the six best-performance models.

by growing of greenhouse gas emissions on the Tibetan Plateau. Table 3 presents prediction of linear trends of annual mean precipitation and temperature in the 21st century on the Tibetan Plateau under different emission scenarios. It shows that annual mean precipitation will increase for all the patterns of 3 emission scenarios with greatly various rates. There are 20 models involved under A1B scenario with a variation range of 10.3~179.8 mm/100a and an average of 92.5 mm/100a; there are 13 models involved under A2 scenario with a variation range of 32.4~186.5 mm/100a and an average of 108.7 mm/100a; there are 15 models involved under B1 scenario with a variation range of 0.3~124.3 mm/100a and an average of 61.4 mm/100a. Temperature changes of all the models have the same increasing trend as that of precipitation. Under A1B scenario, all the models except HADGEM are involved to estimate temperature changes with a variation range of 2.3~7.1°C/100a; there are 14 models involved under A2 scenario which shows the highest average increase of 5.3°C/100a and a variation range of 3.5~7.4°C/100a; 15 models are involved under B1 scenario to predict the lowest increase of 2.6°C/100a and a various range of 1.2~4.2°C/100a on the Tibetan Plateau.

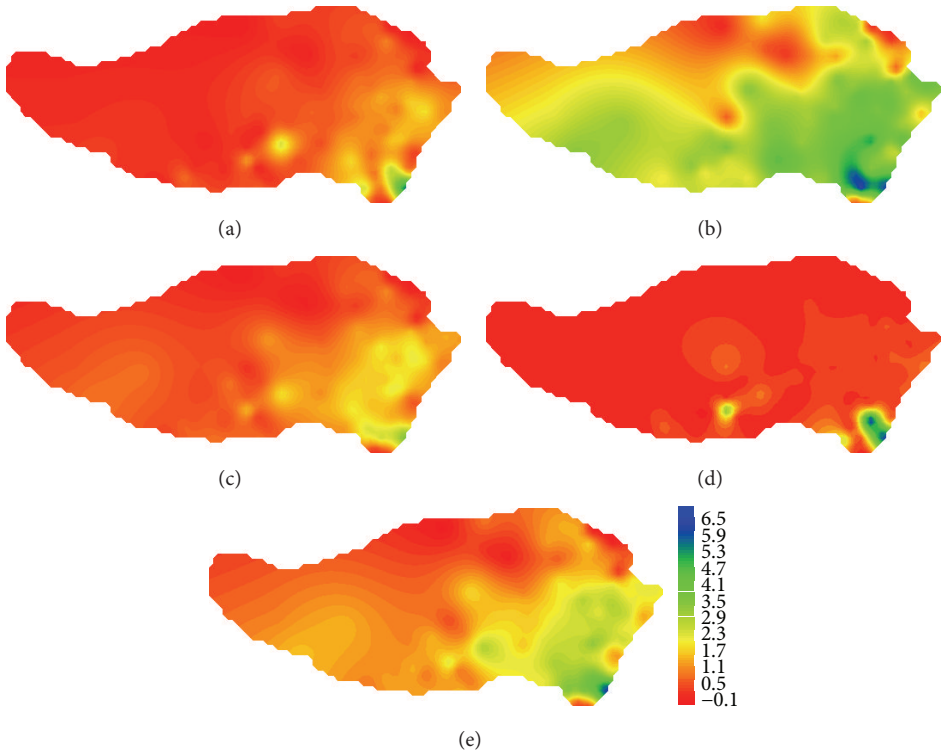


Figure 8: Observed values of precipitation on the Tibetan Plateau in reference period: (a) spring; (b) summer; (c) fall; (d) winter; (e) annual.

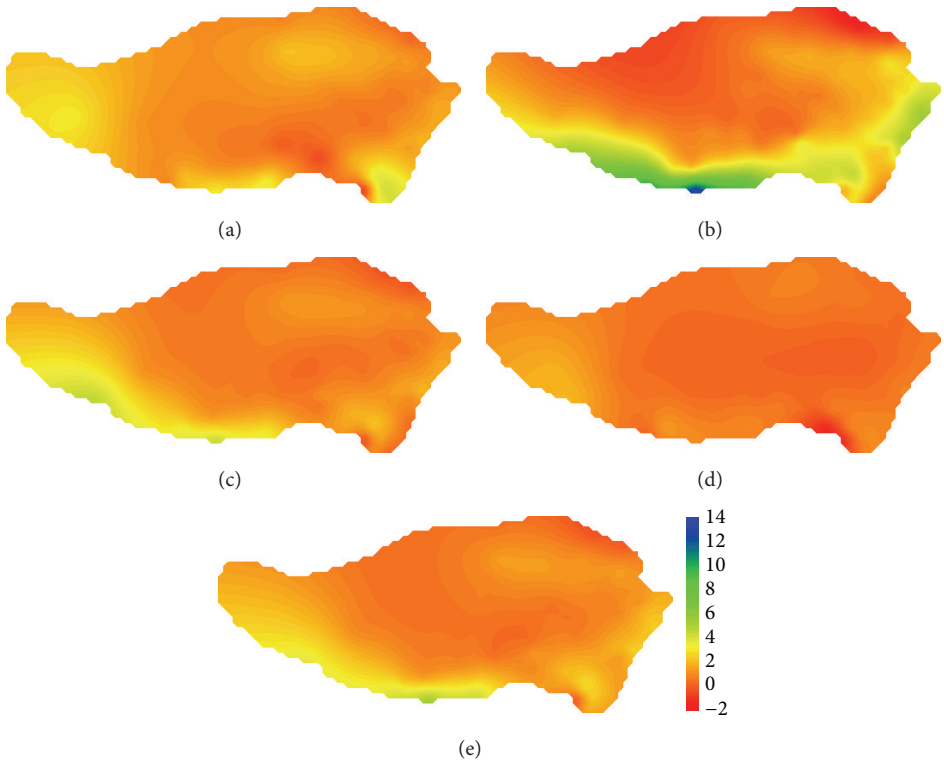


Figure 9: Comparison of the values of precipitation on the Tibetan Plateau in reference period between GFCM21's simulation and observation: (a) spring; (b) summer; (c) fall; (d) winter; (e) annual.

## 5. Conclusions and Discussion

In order to make further climate change projections under A1B, A2, and B1 emission scenarios on the Tibetan Plateau, temperature and precipitation simulation abilities of GCMs have been evaluated which is based on the differences between simulated and observed of reference period with 22 models from IPCC AR4. Some interesting conclusions can be presented and discussed as follows.

(1) 22 climate models have a certain capability to simulation temperature and precipitation on the Tibetan Plateau. The correlation coefficient of temperature of all the models (except INCM3 mode) is above 0.96, but there are still great differences in simulation performance of each model, while only GGMR, GFCM21, HADCM3, HADGEM, and MRCGCM patterns have relatively well simulated climate changes with an annual climate trend similar to the fact. Simulated precipitation of most models is higher than the observed values while the regional simulated values of some models are lower than the observed. However there are more differences between models in precipitation than in temperature. Five models namely, CGMR, CSMK3, GFCM20, GFCM21, and HADGEM have better simulated the precipitation on the Tibetan Plateau which indicates that simulation of most models need to be further improved.

(2) With a general assessment of the simulation ability of temperature and precipitation, it is obvious that GFCM21 and CGMR patterns can basically reproduce climate change on the Tibetan Plateau. Take GFCM21 pattern as an example; simulated temperature in summer is more similar to the observed. At the same time, there are significant spatial differences, while there is less deviation between simulated values of temperature and precipitation and the observed with GFCM21 model in the east part of the Tibetan Plateau.

(3) Under A1B, A2, and B1 emissions scenarios, there is great uncertainty in simulation of temperature and precipitation of the 21st century with climate models on the Tibetan Plateau. Temperature and precipitation of GCMs will all increase with different ratios. Precipitation under A2 scenario will increase most significantly while there is the least increase under A1B scenario. Based on evaluation of simulation performance with 22 climate models from IPCC AR4, there are great differences in the simulated values while only a few models have well simulated temperature and precipitation on the Tibetan Plateau. It is obvious that simulation with GCMs still needs to be further improved. Because of the low resolution of GCMs, parameters of physical process of climate models are also needed to be further improved, so there are great uncertainties in the simulation of temperature and precipitation. In the future, we could think of downscaling methods to predict climate changes in order to find proper method for China and provide more reliable prediction results with multimodel ensembles method. view of many uncertainties of climate models, it is of great importance to investigate climate changes in China with GCMs to reduce those uncertainties.

## Acknowledgments

This work was financially supported by the National Basic Research Program of China (2010CB951101), the National Natural Science Foundation of China (40830639, 41101015), the "Strategic Priority Research Program—Climate Change: Carbon Budget and Relevant Issues" of the Chinese Academy of Sciences (XDA05110102), and the Special Fund of State Key Laboratory of Hydrology-Water Resources and Hydraulic Engineering (1069-50985512).

## References

[1] N. Nakicenovic, J. Alcamo, G. Davis et al., *IPCC Special Report on Emission Scenarios*, Cambridge University Press, Cambridge, UK, 2001.

[2] S. Solomon, D. Qin, M. Manning et al., *Climate Change 2007: The Physical Science Basis. Contribution of Working Group I To the Fourth Assessment Report of the Intergovernmental Panel on Climate Change*, Cambridge University Press, Cambridge, UK, 2007.

[3] T. R. Knutson, T. L. Delworth, K. W. Dixon et al., "Model assessment of regional surface temperature trends (1949–1997)," *Journal of Geophysical Research*, vol. 104, no. D24, pp. 30981–30996, 1999.

[4] G. M. Flato and G. J. Boer, "Warming asymmetry in climate change simulations," *Geophysical Research Letters*, vol. 28, no. 1, pp. 195–198, 2001.

[5] G. A. Meehl, C. Covey, T. Delworth et al., "The WCRP CMIP3 multimodel dataset: a new era in climatic change research," *Bulletin of the American Meteorological Society*, vol. 88, no. 9, pp. 1383–1394, 2007.

[6] T. J. Phillips and P. J. Gleckr, "Evaluation of continental precipitation on 20th century climate simulation: the utility of multimodel statistics," *Water Resources Research*, vol. 42, no. 3, pp. W03201–W03202, 2006.

[7] A. P. van Ulden and G. J. van Oldenborgh, "Large-scale atmospheric circulation biases and changes in global climate model simulations and their importance for climate change in Central Europe," *Atmospheric Chemistry and Physics*, vol. 6, no. 4, pp. 863–881, 2006.

[8] F. M. Johnson and A. Sharma, "GCM simulations of a future climate: how does the skill of GCM precipitation simulations compare to temperature simulations?" in *Proceedings of the 18th World IMACS Congress and International Congress on Modelling and Simulation: Interfacing Modelling and Simulation with Mathematical and Computational Sciences (MODSIM '09)*, pp. 2618–2624, Cairns, Australia, July 2009.

[9] Y. Sun, S. Solomon, A. Dai, and R. W. Portmann, "How often does it rain?" *Journal of Climate*, vol. 19, no. 6, pp. 916–934, 2006.

[10] T. Zhou and R. Yu, "Twentieth-century surface air temperature over China and the globe simulated by coupled climate models," *Journal of Climate*, vol. 19, no. 22, pp. 5843–5858, 2006.

[11] C. Xu, X. Shen, and Y. Xu, "An analysis of climate Change in East Asia by using the IPCC AR4 simulations," *Advances in Climate Change Research*, vol. 3, no. 5, pp. 287–292, 2007.

[12] Z. Jiang, W. Chen, J. Song et al., "Projection and evaluation of the precipitation extremes indices over China based on seven IPCC AR4 coupled climate models," *Chinese Journal of Atmospheric Sciences*, vol. 33, no. 1, pp. 109–120, 2009.

[13] Z. Jiang, X. Zhang, and J. Wang, "Projection of climate change in China in the 21st century by IPCC AR4 Models," *Geographical Research*, vol. 27, no. 4, pp. 787–799, 2008.

[14] Y. Liu, J. Yan, T. Wu, Y. Guo, L. Chen, and J. Wang, "Prediction research of climate change trends over North China in the future 30 years," *Acta Meteorologica Sinica*, vol. 65, no. 1, pp. 45–51, 2007.

[15] J. Tang, X. Chen, M. Zhao, and B. Su, "Numerical simulation of regional climate change under IPCC A2 scenario in China," *Acta Meteorologica Sinica*, vol. 66, no. 1, pp. 13–25, 2008.

[16] L. Zhang, Y. Ding, and Y. Sun, "Evaluation of precipitation simulation in East Asian monsoon areas by coupled ocean atmosphere general circulation models," *Chinese Journal of Atmospheric Sciences*, vol. 32, no. 2, pp. 261–276, 2008.

[17] Y. Sun and Y. Ding, "Validation of IPCC AR4 climate models in simulating interdecadal change of East Asian summer monsoon," *Acta Meteorologica Sinica*, vol. 66, no. 5, pp. 765–780, 2008.

[18] B. Messerli and J. D. Ives, *Mountains of the World: A Global Priority*, Parthenon, New York, NY, USA, 1997.

[19] X. Liu, Z. Cheng, L. Yan, and Z.-Y. Yin, "Elevation dependency of recent and future minimum surface air temperature trends in the Tibetan Plateau and its surroundings," *Global and Planetary Change*, vol. 68, no. 3, pp. 164–174, 2009.

[20] L. G. Thompson, T. Yao, E. Mosley-Thompson, M. E. Davis, K. A. Henderson, and P.-N. Lin, "A high-resolution millennial record of the South Asian Monsoon from Himalayan ice cores," *Science*, vol. 289, no. 5486, pp. 1916–1919, 2000.

[21] M. L. Roderick and G. D. Farquhar, "The cause of decreased pan evaporation over the past 50 years," *Science*, vol. 298, no. 5597, pp. 1410–1411, 2002.

[22] A. Zhisheng, J. E. Kutzbach, W. L. Prell, and S. C. Porter, "Evolution of Asian monsoons and phased uplift of the Himalaya: Tibetan plateau since Late Miocene times," *Nature*, vol. 411, no. 6833, pp. 62–66, 2001.

[23] U. Cubasch, G. A. Meehl, G. J. Boer et al., "Projections of future climate change," in *Climate Change 2001: the Scientific Basis*, J. T. Houghton, Y. Ding, D. J. Griggs et al., Eds., pp. 525–582, Cambridge University Press, 2001.

[24] Q. Ju, *Research of Climate Change and Response of Water Recycling in Yangtze River Basin. Nanjing [Ph.D. thesis]*, Hohai University, 2009.

[25] Z.-C. Hao, L. Li, Y. Xu et al., "Study on Deltu-DCSI downscaling method of GCM output," *Journal of Sichuan University*, vol. 41, no. 5, pp. 1–7, 2009.

Hindawi Publishing Corporation
The Scientific World Journal
Volume 2013, Article ID 838176, 7 pages
http://dx.doi.org/10.1155/2013/838176

*Research Article*

# Occurrence and Distribution of Microcystins in Lake Taihu, China

**Hiroshi Sakai,[1] Aimin Hao,[2] Yasushi Iseri,[3] Song Wang,[4] Takahiro Kuba,[2] Zhenjia Zhang,[4] and Hiroyuki Katayama[1]**

[1] *Department of Urban Engineering, The University of Tokyo, 7-3-1 Hongo, Bunkyo-ku, Tokyo 113-8656, Japan*
[2] *Department of Urban and Environmental Engineering, Kyushu University, 744 Motooka, Nishi-ku, Fukuoka 819-0395, Japan*
[3] *West Japan Engineering Consultants, Inc., 1-1-1 Watanabe-dori, Chuo-ku, Fukuoka 810-0004, Japan*
[4] *School of Environmental Science and Engineering, Shanghai Jiao Tong University, 800 Dongchuan Road, Shanghai 200240, China*

Correspondence should be addressed to Hiroshi Sakai; h_sakai@env.t.u-tokyo.ac.jp

Received 11 April 2013; Accepted 4 June 2013

Academic Editors: M. Kumar and K. Kuroda



The occurrence and distribution of microcystins were investigated in Lake Taihu, the third largest lake in China. An extensive survey, larger and broader in scale than previous studies, was conducted in summer 2010. The highest microcystin concentration was found at southern part of Taihu, which was newly included in this survey. In northern coastal areas, total cellular concentrations of 20 to 44 $\mu$g/L were observed. In northern offshore waters, levels were up to 4.8 $\mu$g/L. Microcystin occurrence was highly correlated with chemical oxygen demand, turbidity, and chlorophyll-a. Extracellular/total cellular microcystin (E/T) ratios were calculated and compared to other water quality parameters. A higher correlation was found using E/T ratios than original microcystin values. These results show that algal blooms are having a severe impact on Lake Taihu, and further and extensive monitoring and research are required to suppress blooms effectively.

## 1. Introduction

The presence of microcystins in water systems is a major threat to human health. Microcystins are contained in *Microcystis* cells and are released when these cells die. The toxicity of microcystin-LR is severe, with an $LD_{50}$ value of about 50 $\mu$g/kg for mice, which is lower than that of potassium cyanide [1]. *Microcystis* blooms occur in lakes and reservoirs, causing problems for both drinking water supplies and recreational water use. The World Health Organization recommends that microcystin values not exceed 1 $\mu$g/L in drinking water [2] and 20 $\mu$g/L in recreational water [3]. The largest microcystin outbreak occurred in 1996 in Brazil, where microcystin-contaminated tap water was supplied to a hemodialysis center, resulting in the deaths of 88 patients [4, 5]. Many other outbreaks of microcystins and other cyanobacterial toxins have occurred; these outbreaks did not result in human deaths, but cases of diarrhea, nausea, and vomiting were reported [6–14]. One study indicated that microcystins may promote liver tumors [15].

Lake Taihu is the third largest freshwater lake in China and recently has been suffering from severe algal blooms [16]. The lake has a surface area of 2,428 $km^2$ [17], and its waters have been utilized for drinking water, sewage disposal, fisheries, and aquaculture [18]. Before 1980, the lake experienced fewer algal blooms, and its water quality met standards for drinking water. However, due to the rapid development of the economy and the intensive use of the lake, water pollution has become increasingly serious in Lake Taihu since the 1980s [17]. In 2006, 93% of the lake was in a state of mid-level eutrophication, versus only 6.1% in 1997. Therefore, eutrophication, cyanobacterial blooms, and the occurrence of cyanotoxins are serious problems in the region.

To examine the eutrophication problem, a three-dimensional model was established to simulate the occurrence of algae in Lake Taihu [19]. This model incorporated the effects of weather, especially wind speed and direction, and succeeded, to a certain extent, in simulating the eutrophication conditions in the lake. At Lake Taihu, southeast trade winds prevail, and this wind could be a primary factor

driving circulation in the lake [19]. Various studies have confirmed the presence of microcystins in Lake Taihu [18, 20–25]. Previous studies recorded levels of around 20 $\mu$g/L total cellular microcystin in Meiliang Bay in 2001 [22] and 30 $\mu$g/L in Gonghu Bay in 2008 [25]. These bays experienced a peak microcystin concentration in August [18, 20, 21] or October [20, 22, 25]. The aforementioned studies also determined algal species [21, 24] and relationships with other water quality parameters [23, 25]. However, the only previous studies on microcystin occurrence focused only on Meiliang or Gonghu bay. Moreover, only a couple of sampling points was surveyed in those areas, particularly in coastal areas. As already revealed by previous research [17, 19], eutrophication occurs all over Lake Taihu not only in Meiliang and Gonghu bays. Therefore, microcystin occurrence should be investigated over the whole area of Lake Taihu, as well as in those two bays.

Although growth information is important for the formulation of countermeasures, algal growth stage has not been examined carefully in previous studies. The growth stage of a bloom will affect remediation strategies; in the early growth phase, nutrient elimination is useful for suppressing further blooming, while in the death phase physical removal of the bloom is recommended. In the present study, to help offset the lack of information on growth stage from the existing parameters, the extracellular/total cellular microcystin (E/T) ratio was used. Microcystins are always contained in algal cells and are released into the environment only when those cells die [26, 27]. There are fewer dead cells in the growth phase, leading to lower extracellular microcystin concentrations and a lower E/T ratio. In contrast, there are more dead cells in the death phase, leading to higher extracellular microcystin concentrations and greater E/T ratios. The viability of the E/T ratio was investigated as another objective of this research. Based on our extensive survey results, we suggest further research directions for managing algal blooms in Lake Taihu.

## 2. Materials and Methods

*2.1. Study Area and Sampling Locations.* Lake Taihu is located in Jiangsu and Zhejiang Provinces, China. It is shallow (mean depth 1.9 m) and has a large surface area (2,428 km$^2$). It serves as an important resource for drinking water, irrigation, aquaculture, and industrial water, in addition to being a popular recreational and tourist attraction [25]. Samples were collected from July 30 to August 2, 2010, from 33 locations across the lake, ranging from Meiliang Bay and Gonghu Bay to the south and eastern parts of the lake (Figure 1). Among the 33 locations, 10 sites (G01–G10) were located in Gonghu Bay, 17 (M01–M17) were located around Meiliang Bay and in the center of the lake, and the remaining 6 sites (S01–S06) were located in eastern and southern parts of the lake. Sampling was conducted in offshore as well as coastal areas.

*2.2. Analysis.* Water temperature, dissolved oxygen (DO), turbidity, chlorophyll, pH, oxidation-reduction potential (ORP), and electrical conductivity were measured at the time of sampling using a multiprobe (Datasonde 5X, HACH).

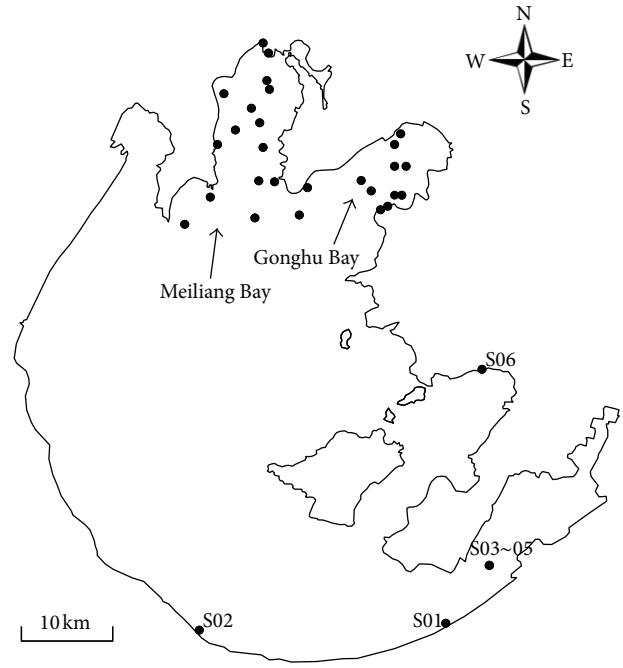


Figure 1: Map showing sampling locations on Lake Taihu.

Chemical oxygen demand (COD Cr) was measured using an HACH DR2800 colorimeter. Dissolved organic carbon (DOC), nitrate, and phosphate were also measured after 0.45 $\mu$m filtration. DOC was measured using a TOC-V (Shimadzu), and nitrate and phosphate were measured using an HACH DR2800 colorimeter. Intracellular and extracellular microcystins were measured using ELISA, as described in previous reports [26, 28]. The detection limit of this method is 50 ng/L as a microcystin-LR equivalent.

## 3. Results

*3.1. Overall Occurrence of Microcystins.* Microcystins were detected in 25 of 34 samples measured, showing a broad occurrence across Lake Taihu. Microcystin concentrations were expressed as total cellular microcystin and extracellular microcystin; the frequency distributions are shown in Figures 2(a) and 2(b). Detailed data are shown in the Supporting Material (See Table S1 available online at http://dx.doi.org/10.1155/2013/838176).

The highest recorded extracellular microcystin concentration was close to 1 $\mu$g/L, the drinking water guideline value suggested by the WHO. The highest concentration was 0.96 $\mu$g/L at M01 (Meiliang Bay) on July 30, followed by 0.88 $\mu$g/L at M06 (also Meiliang Bay) on August 2 and 0.79 $\mu$g/L at S02 (southern Taihu) on July 29. For other samples, the highest recorded extracellular microcystin concentration was 0.22 $\mu$g/L. There were three samples in the range of 0.15–0.2 $\mu$g/L, six samples between 0.1 and 0.15 $\mu$g/L and four samples between 0.05 and 0.1 $\mu$g/L.

Total cellular microcystin concentration was higher than 1 $\mu$g/L for 15 of the 34 samples, with 4 samples exceeding the WHO recommended 20 $\mu$g/L limit for water for recreational

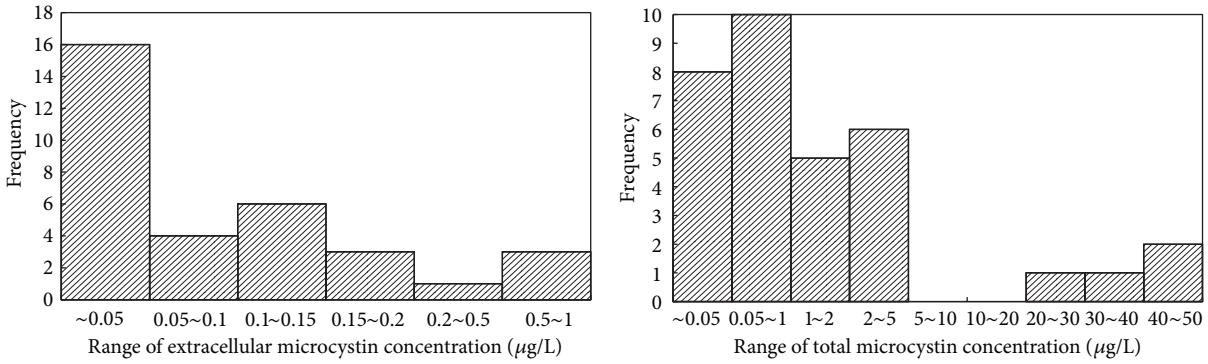


Figure 2: Frequency distributions of total cellular and extracellular microcystins.

use. The highest concentration was 50 $\mu$g/L in sample S02 from Huzhou city, in the southern part of the lake. Levels were also high in the samples from most north shores of Meiliang Bay, at 44 $\mu$g/L at M01 on July 30 and 35 $\mu$g/L at M06 on August 2. A concentration of 20 $\mu$g/L was observed on July 31 at sampling point M02 on the west shore of Meiliang Bay. Another 11 samples from Gonghu Bay and Meiliang Bay also exceeded 1 $\mu$g/L. As this is the concentration of total cellular microcystin in samples, it is not an immediate threat to human health. However, serious impacts on human health would occur if these microcystins were to be released into waters.

*3.2. Spatial Distribution of Microcystins in Gonghu Bay.* In Gonghu Bay, 10 samples were taken and analyzed for various water quality parameters including microcystins. Total cellular microcystin concentrations and sampling point locations are shown in Figure 3. Two sampling series were conducted, on July 30 and August 1, in a north-south direction. Three samples (G01–G03) were taken on July 30, and five samples (G04–G08) were taken on August 1. The two other samples (G09 and G10) were taken on August 2, from the west part of Gonghu Bay. Results from the west and central parts of Gonghu Bay were compared. On July 30, the total cellular microcystin concentration was 0.2 $\mu$g/L at sampling point G02 and was under the detection limit of 0.05 $\mu$g/L at the other two points. The weather on July 30 was cloudy and stormy.

On August 1, microcystin concentrations were under 0.05 $\mu$g/L at the shore (G04) and ranged from 1.4 to 3.6 $\mu$g/L offshore (G05–G08). Although the locations of some sampling points were close to each other, some differences were observed between concentrations on July 30 and August 1. Total cellular microcystin concentration ranged from 0.2 $\mu$g/L on July 30 to more than 1.4 $\mu$g/L on August 1 offshore. This difference could be attributed to changing weather conditions. On July 30, it was cloudy, and a rainstorm began during sampling. This disturbed the surface of the lake and dispersed algae, which would have led to lower recorded concentrations of microcystin on July 30. Conversely, the weather was calm and sunny on August 1. Samples were taken on

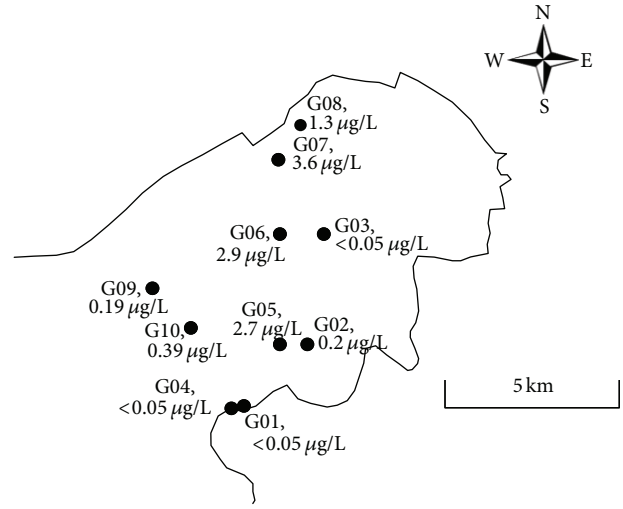


Figure 3: Microcystin distributions in Gonghu Bay.

August 2 in the west part of Gonghu Bay. Concentrations were 0.39 $\mu$g/L at sampling point G10 and 0.19 $\mu$g/L at sampling point G09. Clear differences were found among sampling locations and dates, possibly due to weather conditions.

*3.3. Spatial Distribution of Microcystins in Meiliang Bay.* In Meiliang Bay, 17 samples were taken, and total cellular microcystin concentrations were compared as shown in Figure 4. Higher concentrations were observed on the north and west shores of the bay. Concentrations were 44 $\mu$g/L at sampling point M01 and 35 $\mu$g/L at M06 on the north shore and 20 $\mu$g/L at M02 on the west shore. Among the other 14 samples taken from offshore waters, 3 had concentrations higher than 2 $\mu$g/L, with the highest being 4.8 $\mu$g/L at M10 in the middle of the mouth of Meiliang Bay. The second highest concentration was 2.9 $\mu$g/L at M16 in the western section of the mouth of the bay, and the third highest one was 2.5 $\mu$g/L at M09, north of the M10 sampling point. These three points seem to form a belt that crosses Meiliang Bay from the northeast to the southwest. Four samples (M07, M08, M11, and M16) had concentrations ranging between

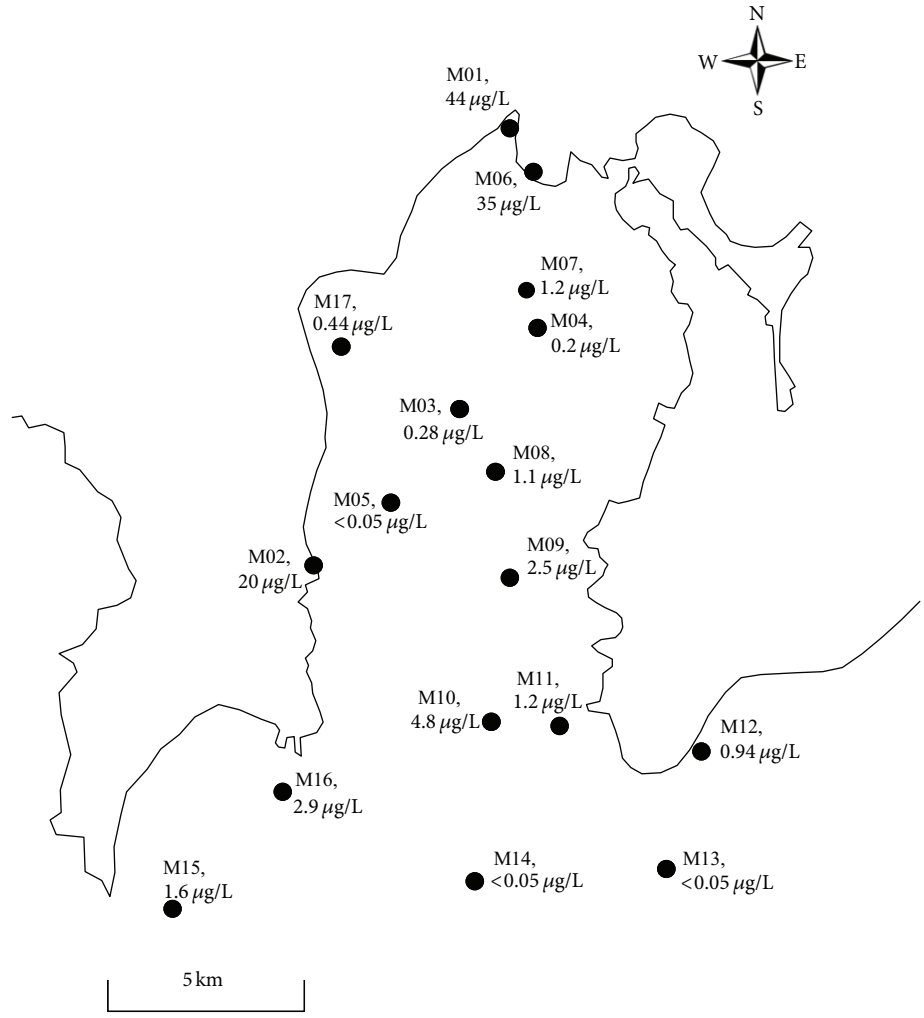


Figure 4: Microcystin distributions in Meiliang Bay.

1 $\mu$g/L and 2 $\mu$g/L. Sampling points located around the belt area included M09, M10, and M16. In other areas, microcystin concentrations were lower than 1 $\mu$g/l. At M13 and M14, which were closer to the center of the lake, concentrations were under the detection limit of 50 ng/L.

Great variation in the concentration was found even within Meiliang Bay, with 20–44 $\mu$g/L observed in coastal areas and 1~5 $\mu$g/L observed around the mouth of the bay, forming a belt from a northeast to a southwest direction. This direction is perpendicular to the prevailing wind direction at Lake Taihu [19]. In other areas, total cellular microcystin concentrations were lower than 1 $\mu$g/L.

*3.4. Microcystin Occurrence in South and East Taihu.* In the southern and eastern regions of Lake Taihu, one sample was taken at Suzhou city, three samples were taken in eastern Taihu, and one sample was taken at Huzhou city; total cellular microcystin concentrations were 0.40 $\mu$g/L, 0.05–0.30 $\mu$g/L, and 50 $\mu$g/L, respectively. Extracellular microcystin concentrations were 0.79 $\mu$g/L at Huzhou city and less than 0.05 $\mu$g/L in other samples. Although there was only one microcystin "hot-spot," this location, at Huzhou city was the most severe in all samples. Therefore, broader investigations should be conducted to better understand the overall occurrence of microcystins in Lake Taihu.

*3.5. Relationships between Microcystins and Other Water Quality Parameters.* Relationships between total cellular and intracellular microcystins and other water quality parameters are summarized in Table 1. The relationships between microcystins and physical parameters (pH, ORP, and EC) were relatively weak, their correlation coefficients ranging from −0.20 to 0.18. Higher correlation coefficients were found between both extracellular and total cellular microcystins and turbidity, chlorophyll-a, and COD: 0.96 and 0.98 for turbidity, 0.71 and 0.61 for chlorophyll-a, and 0.75 and 0.73 for COD, respectively. The correlations between DO and microcystins were not so high at 0.28 and 0.18 for extracellular and total cellular microcystin, respectively. The higher correlations with COD and chlorophyll-a could be attributed to algal biomass, as reported in previous research [23, 25]. The higher correlation with chlorophyll-a and lower correlation with

Table 1: Correlation coefficients for each parameter.

| | COD | DOC | $NO_3$-N | $PO_4$-P | Temp. | DO | Turbidity | Chlorophyll-a | pH | ORP | EC |
|---|---|---|---|---|---|---|---|---|---|---|---|
| Extra cellular | 0.75 | 0.37 | 0.01 | 0.24 | −0.38 | 0.28 | 0.96 | 0.71 | 0.18 | −0.20 | −0.04 |
| Total cellular | 0.73 | 0.32 | 0.15 | 0.17 | −0.31 | 0.18 | 0.98 | 0.61 | 0.13 | −0.08 | 0.02 |

Table 2: Calculated E/T ratios.

| Sample | Area | Date | Weather | Total MCs $\mu$g/L | Extra MCs $\mu$g/L | E/T ratio — |
|---|---|---|---|---|---|---|
| S02 | Huzhou | 29-Jul-10 | Sunny | 50 | 0.79 | 1.6% |
| M01 | Meiliang Bay | 30-Jul-10 | Sunny | 44 | 0.96 | 2.2% |
| M06 | Meiliang Bay | 2-Aug-10 | Sunny | 35 | 0.88 | 2.5% |
| M10 | Meiliang Bay | 2-Aug-10 | Sunny | 4.8 | 0.12 | 2.5% |
| G06 | Gonghu Bay | 1-Aug-10 | Sunny | 2.9 | 0.09 | 3.1% |
| G07 | Gonghu Bay | 1-Aug-10 | Sunny | 3.6 | 0.14 | 4.0% |
| M15 | Meiliang Bay | 2-Aug-10 | Sunny | 1.6 | 0.07 | 4.5% |
| G05 | Gonghu Bay | 1-Aug-10 | Sunny | 2.7 | 0.13 | 4.8% |
| M12 | Meiliang Bay | 2-Aug-10 | Sunny | 0.94 | 0.06 | 6.0% |
| M09 | Meiliang Bay | 2-Aug-10 | Sunny | 2.5 | 0.17 | 6.8% |
| G08 | Gonghu Bay | 1-Aug-10 | Sunny | 1.3 | 0.12 | 9.0% |
| M08 | Meiliang Bay | 2-Aug-10 | Sunny | 1.1 | 0.15 | 14.2% |
| M11 | Meiliang Bay | 2-Aug-10 | Sunny | 1.2 | 0.17 | 14.3% |
| M07 | Meiliang Bay | 2-Aug-10 | Sunny | 1.2 | 0.18 | 14.6% |
| M17 | Meiliang Bay | 2-Aug-10 | Sunny | 0.44 | 0.08 | 19.0% |
| G02 | Gonghu Bay | 30-Jul-10 | Stormy | 0.20 | 0.22 | 107% |

DO suggest that live algal species and dead algal scum coexisted in the samples, which otherwise would have shown high coefficients with DO as well as with chlorophyll-a. Correlation coefficients with DOC, $NO_3$-N, and $PO_4$-P were also low, at 0.37 and 0.32 for DOC, 0.01 and 0.15 for $NO_3$-N, and 0.24 and 0.17 for $PO_4$-P for extracellular and total cellular microcystins, respectively. As algae photosynthesize by utilizing atmospheric carbon dioxide, it could be expected that DOC and microcystins would be independent. The correlation coefficients of $NO_3$-N and $PO_4$-P with microcystins were lower than that with DOC. This suggests that there was no relationship between nutrients and extracellular or total cellular microcystins. Moreover, it can be speculated that other factors, such as meteorological factors (e.g., wind), contributed to the occurrence and distribution of microcystins in Lake Taihu.

*3.6. Extracellular/Total Cellular Microcystin Ratios.* E/T ratios, which characterize an algal bloom by its growth phase, were calculated (Table 2). Our previous study showed E/T ratios of 8.3~15.0% during the exponential growth phase of a pure culture of *M. aeruginosa* PCC 7806 [28]. Thus, this ratio was employed to characterize the algal bloom.

In the present study, G02 had an E/T ratio of 107%, while other samples had smaller E/T ratios. The high ratio at G02 may have been due to the death phase of the bloom. G02 was sampled during stormy weather, and algal cells may have been killed off by the storm, thus releasing intracellular microcystins. In contrast, the other samples may have been in the growth phase. In reference to the E/T ratios of pure culture [28], samples G8 to M17 could be considered to be in the normal growth phase. Samples with values lower than 8.3% might have been affected by external factors.

The correlations of E/T ratios with other water quality parameters were investigated (Table 3). E/T ratios were correlated with chlorophyll-a, pH, DO, $NO_3$-N, and $PO_4$-P, with correlation coefficients of 0.27, 0.31, 0.30, −0.40, and 0.27, respectively. The relatively high correlations with DO, pH, and nutrient parameters should be noted, as they are higher than their correlation coefficients with microcystins, as shown in Table 1. Therefore, E/T ratios, rather than conventional parameters, could be used to express bloom growth conditions. The positive correlation coefficients with chlorophyll-a, DO, pH, and $PO_4$-P mean that higher E/T ratios were correlated with more algal growth in Lake Taihu. The negative correlation coefficient with $NO_3$-N suggests that phosphate concentration could be a limiting factor for algal growth in Lake Taihu. These results indicate that E/T ratios would be more suitable than microcystin concentrations for evaluating bloom growth conditions.

## 4. Discussion

*4.1. Occurrence and Distribution of Microcystins in Lake Taihu.* In this study, we investigated the occurrence and distribution of microcystins in Lake Taihu. First, we investigated various locations of the lake and revealed the occurrence of microcystins across a broad area. Previous studies only

Table 3: Correlation coefficients for each parameter with E/T ratios.

| | COD | DOC | $NO_3$-N | $PO_4$-P | Temp. | DO | Turbidity | Chlorophyll-a | pH | ORP | EC |
|---|---|---|---|---|---|---|---|---|---|---|---|
| E/T ratio | −0.23 | −0.02 | −0.40 | 0.27 | 0.01 | 0.30 | −0.33 | 0.27 | 0.31 | −0.18 | 0.06 |

considered microcystin occurrence in Meiliang and Gonghu bays and showed total cellular microcystin concentrations of around 20 $\mu$g/L in Meiliang Bay in 2001 [22] and 30 $\mu$g/L in Gonghu Bay in 2008 [25]. Peak concentrations occurred in August [18, 20, 21] or October [20, 22, 25]. In this study, we observed a concentration of 44 $\mu$g/L in Meiliang Bay, the highest among existing reports. We also found a high concentration (50 $\mu$g/L) at Huzhou city on the south shore of Lake Taihu. There are two possible reasons why higher concentrations were observed in this study than in previous studies: microcystin concentrations may be increasing, possibly due to climate change, or concentrations at these locations have always been high and simply have not been documented until now. In either case, future surveys should be conducted more frequently and across a broader area to elucidate the overall condition of the lake. Long-term surveys should also be conducted to understand changes over time and to reveal the possible effects of climate change.

*4.2. Use of E/T Ratios to Characterize Algal Blooms.* The characterization of algal blooms by their growth stage, using E/T ratios, is important for the formulation of remediation strategies. If a bloom is in the early stages of growth, nutrient control can suppress further growth and microcystin release. Conversely, if a bloom is in a later stage of growth, physical removal of algae from the lake is recommended. If a bloom is affected by other external factors, the control of these factors will be a means of bloom suppression.

In the present study, one sample showed a high E/T ratio of 107%. This indicates that all microcystins were in the water rather than in algal cells. Therefore, the physical removal of algal cells and microcystin degradation treatment would be an effective measure against this bloom. Other samples showed lower E/T ratios, from 1.6% to 19%. These samples could be in the growth phase, and therefore nutrient control might be better countermeasure against these blooms. As there was a negative correlation between E/T ratio and $NO_3$-N concentration and a positive correlation between E/T ratio and $PO_4$-P, the suppression of phosphate concentration may also be an effective countermeasure in Lake Taihu.

For a few lower E/T ratio samples (S02, M01, and M06), values ranged from 1.6% to 2.5%, although very large total cellular microcystin concentrations (35–50 $\mu$g/L) were observed. If E/T ratio is related to growth condition, samples with lower E/T ratios would be expected to show relatively less growth and lower total cellular microcystin concentration. However, there seems to exist an apparent contradiction, which could be accounted for by the migration of algal cells. E/T ratio is primarily affected by growth conditions but can also be affected by external factors such as dilution or exchange with fresh media. In water, the wind-driven migration of an algal bloom could be the cause. This is because only algal cells would be moved by wind, while the surrounding water would not. Therefore, it is possible that samples with a high total cellular microcystin concentration and low E/T ratio were impacted by the migration of algal cells. In such situations, the removal of algal cells from windward areas would be useful for preventing further leeward hazards.

*4.3. Factors Affecting the Distribution of Microcystins.* We investigated the relationships between the distribution of microcystins and other water quality parameters. Microcystins were correlated with chlorophyll-a and COD but showed only a weak correlation with DO and nutrients. Therefore, the observed algal bloom contained both live and dead cells, depending on sampling location and timing. E/T ratios were more strongly correlated with DO and nutrients than were microcystin concentrations. They also showed that one sample was in the death phase while the other samples were in the growth phase. Three samples showed disproportionately large total cellular microcystin concentrations with low E/T ratios. This could be attributed to the migration of algal cells, as described above, possibly driven by the southeast wind prevailing at Lake Taihu [19]. As shown in Figure 4, the belt of high-concentration sampling sites that cross the mouth of Meiliang Bay is perpendicular to wind direction, which supports the idea of southeast winds contributing to microcystin distribution.

## 5. Conclusions

In this study, we investigated the occurrence and distribution of microcystins in Lake Taihu and reached the following conclusions.

(i) Microcystins occurred over large areas of Lake Taihu. There was spatial variation in the distribution of microcystins, and the highest concentrations were observed in southern parts of the lake.

(ii) Microcystin concentration was well correlated with COD, chlorophyll-a, and turbidity. E/T ratios were better correlated with $NO_3$-N, $PO_4$-P, and DO than was microcystin concentration.

(iii) The use of E/T ratio helped clarify the growth stage of algal blooms and highlighted the possibility of algal cell migration caused by prevailing southeast winds at Lake Taihu.

(iv) Extensive monitoring is required to confirm the advantages of E/T ratios and to better understand the state of algal blooms across Lake Taihu.

## Acknowledgments

This research was partially supported by Japan Society for the Promotion of Science and Japan Science and Technology Agency.

## References

[1] R. M. Dawson, "The toxicology of microcystins," *Toxicon*, vol. 36, no. 7, pp. 953–962, 1998.

[2] World Health Organization, "Cyanobacterial toxins: microcystin-LR," in *Guidelines for Drinking Water Quality*, pp. 95–110, WHO, Geneva, Switzerland, 1998.

[3] World Health Organization, "Algae and cyanobacteria in fresh water," in *Guidelines for Safe Recreational Water Environments*, pp. 136–158, WHO, Geneva, Switzerland, 2003.

[4] E. M. Jochimsen, W. W. Carmichael, J. An et al., "Liver failure and death after exposure to microcystins at a hemodialysis center in Brazil," *The New England Journal of Medicine*, vol. 338, no. 13, pp. 873–878, 1998.

[5] S. Pouria, A. De Andrade, J. Barbosa et al., "Fatal microcystin intoxication in haemodialysis unit in Caruaru, Brazil," *The Lancet*, vol. 352, no. 9121, pp. 21–26, 1998.

[6] R. Berlin, "Haff disease in Sweden," *Acta Medica Scandinavica*, vol. 129, pp. 560–572, 1948.

[7] H. O. Dillenberg and M. K. Dehnel, "Toxic waterbloom in Saskatchewan, 1959," *Canadian Medical Association Journal*, vol. 83, pp. 1151–1154, 1960.

[8] S. Byth, "Palm Island mystery disease," *Medical Journal of Australia*, vol. 2, no. 1, pp. 40–42, 1980.

[9] G. Keleti, J. L. Sykora, L. A. Maiolie, D. L. Doerfler, and I. M. Campbell, "Isolation and characterization of endotoxin from cyanobacteria (blue-green algae)," in *The Water Environment Algal Toxins and Health*, pp. 447–464, Plenum Press, New York, NY, USA, 1981.

[10] A. T. C. Bourke, R. B. Hawes, A. Neilson, and N. D. Stallman, "An outbreak of hepato-enteritis (the Palm Island mystery disease) possibly caused by algal intoxication," *Toxicon*, vol. 21, no. 3, pp. 45–48, 1983.

[11] I. R. Falconer, "Effects on human health of some toxic cyanobacteria (blue-green algae) in reservoirs, lakes, and rivers," *Toxicity Assessment*, vol. 4, no. 2, pp. 175–184, 1989.

[12] E. G. Long, A. Ebrahimzadeh, E. H. White, B. Swisher, and C. S. Callaway, "Alga associated with diarrhea in patients with acquired immunodeficiency syndrome and in travelers," *Journal of Clinical Microbiology*, vol. 28, no. 6, pp. 1101–1104, 1990.

[13] P. C. Turner, A. J. Gammie, K. Hollinrake, and G. A. Codd, "Pneumonia associated with contact with cyanobacteria," *British Medical Journal*, vol. 300, no. 6737, pp. 1440–1441, 1990.

[14] M. G. Teixeira, M. C. Costa, V. L. de Carvalho, M. D. S. Pereira, and E. Hage, "Gastroenteritis epidemic in the area of the Itaparica Dam, Bahia, Brazil," *Bulletin of the Pan American Health Organization*, vol. 27, no. 3, pp. 244–253, 1993.

[15] R. Nishiwaki-Matsushima, T. Ohta, S. Nishiwaki et al., "Liver tumor promotion by the cyanobacterial cyclic peptide toxin microcystin-LR," *Journal of Cancer Research and Clinical Oncology*, vol. 118, no. 6, pp. 420–424, 1992.

[16] L. Guo, "Ecology: doing battle with the green monster of Taihu Lake," *Science*, vol. 317, no. 5842, p. 1166, 2007.

[17] X. W. Mao, F. Xu, B. Xu, and Y. Gao, "Changes of water quality and eutrophication in Taihu Lake, Water Resour," *Protection*, vol. 25, no. 1, pp. 48–51, 2009 (Chinese).

[18] P. P. Shen, Q. Shi, Z. C. Hua et al., "Analysis of microcystins in cyanobacteria blooms and surface water samples from Meiliang Bay, Taihu Lake, China," *Environment International*, vol. 29, no. 5, pp. 641–647, 2003.

[19] J. Mao, Q. Chen, and Y. Chen, "Three-dimensional eutrophication model and application to Taihu Lake, China," *Journal of Environmental Sciences*, vol. 20, no. 3, pp. 278–284, 2008.

[20] J.-Y. Wu, Q.-J. Xu, G. Gao, and J.-H. Shen, "Evaluating genotoxicity associated with microcystin-LR and its risk to source water safety in Meiliang Bay, Taihu Lake," *Environmental Toxicology*, vol. 21, no. 3, pp. 250–255, 2006.

[21] L. Song, W. Chen, L. Peng, N. Wan, N. Gan, and X. Zhang, "Distribution and bioaccumulation of microcystins in water columns: a systematic investigation into the environmental fate and the risks associated with microcystins in Meiliang Bay, Lake Taihu," *Water Research*, vol. 41, no. 13, pp. 2853–2864, 2007.

[22] Q. Xu, W. Chen, and G. Gao, "Seasonal variations in microcystin concentrations in Lake Taihu, China," *Environmental Monitoring and Assessment*, vol. 145, no. 1–3, pp. 75–79, 2008.

[23] W. Chen, L. Peng, N. Wan, and L. Song, "Mechanism study on the frequent variations of cell-bound microcystins in cyanobacterial blooms in Lake Taihu: implications for water quality monitoring and assessments," *Chemosphere*, vol. 77, no. 11, pp. 1585–1593, 2009.

[24] W. Ye, X. Liu, J. Tan, D. Li, and H. Yang, "Diversity and dynamics of microcystin-Producing cyanobacteria in China's third largest lake, Lake Taihu," *Harmful Algae*, vol. 8, no. 5, pp. 637–644, 2009.

[25] Q. Wang, Y. Niu, P. Xie et al., "Factors affecting temporal and spatial variations of microcystins in Gonghu Bay of Lake Taihu, with potential risk of microcystin contamination to human health," *The Scientific World Journal*, vol. 10, pp. 1795–1809, 2010.

[26] H. Sakai, H. Katayama, K. Oguma, and S. Ohgaki, "Kinetics of microcystis aeruginosa growth and intracellular microcystins release after UV irradiation," *Environmental Science and Technology*, vol. 43, no. 3, pp. 896–901, 2009.

[27] L. A. Pearson, M. Hisbergues, T. Borner, E. Dittman, and B. A. Neilan, "Inactivation of an ABC transporter gene, mcyH, results in loss of microcystin production in the cyanobacterium microcystis aeruginosa PCC 7806," *Applied and Environmental Microbiology*, vol. 70, no. 11, pp. 6370–6378, 2004.

[28] H. Sakai, K. Oguma, H. Katayama, and S. Ohgaki, "Effects of low or medium-pressure UV irradiation on the release of intracellular microcystin," *Water Research*, vol. 41, no. 15, pp. 3458–3464, 2007.

Hindawi Publishing Corporation
The Scientific World Journal
Volume 2013, Article ID 854261, 5 pages
http://dx.doi.org/10.1155/2013/854261

*Research Article*

# Quality of Source Water and Drinking Water in Urban Areas of Myanmar

**Hiroshi Sakai,[1] Yatsuka Kataoka,[2] and Kensuke Fukushi[3]**

[1] *Department of Urban Engineering, The University of Tokyo, 7-3-1 Hongo, Bunkyo-ku, Tokyo 113-8656, Japan*
[2] *Institute for Global Environmental Strategies, 2108-11 Kamiyamaguchi, Hayama, Kanagawa 240-0115, Japan*
[3] *Todai Institute for Advanced Study, Integrated Research System for Sustainability Science, The University of Tokyo, 7-3-1 Hongo, Bunkyo-ku, Tokyo 113-8654, Japan*

Correspondence should be addressed to Hiroshi Sakai; h_sakai@env.t.u-tokyo.ac.jp

Received 16 April 2013; Accepted 27 May 2013

Academic Editors: M. Kumar and K. Kuroda



Myanmar is one of the least developed countries in the world, and very little information is available regarding the nation's water quality. This report gives an overview of the current situation in the country, presenting the results of various water-quality assessments in urban areas of Myanmar. River, dam, lake, and well water sources were examined and found to be of generally good quality. Both As and $F^-$ were present in relatively high concentrations and must be removed before deep wells are used. Heterotrophic plate counts in drinking water were highest in public pots, followed by nonpiped tap water, piped tap water, and bottled water. Measures need to be taken to improve low-quality water in pots and nonpiped tap waters.

## 1. Introduction

Access to safe water is a significant issue in developing countries. According to a WHO report, around 780 million people globally do not have access to adequate water supply sources [1]. Additionally, 2.5 billion people do not have access to suitable sanitation facilities. Furthermore, about 2 million people die every year due to diarrheal diseases. Therefore, access to safe water is a crucial requirement in developing countries, where infrastructure is not always provided and often needs to be expanded. Due to the mismatches of urban planning and actual residential area, some areas must rely on inadequate private water supplies. This is a distinct issue in slum area and periurban areas.

Myanmar is a developing country in Southeast Asia. Even among the developing countries, Myanmar falls into the category of least developed countries by United Nations criteria [2]. The water infrastructure needs to be developed for the country's further economic development. However, very few water-quality data are currently available. To the best of our knowledge, only a single water-quality survey has been conducted [3]. That study reported water quality in Lake Inle in the northeastern part of the country. Some water-quality data for dams are provided on the webpage of the Water Environment Partnership in Asia [4] but only for limited quality parameters. To our knowledge, no other information has been reported, and the current water-quality and sanitation situations in Myanmar therefore remain unclear. We visited the country to perform a water-quality survey and assess the current situation with respect to water infrastructure. The survey was conducted in two urban areas, Yangon and Nay Pyi Taw, the former and current capital, respectively. This article reveals the water-quality and sanitation situations in Myanmar for the first time.

## 2. Materials and Methods

*2.1. Study Area.* We surveyed two urban areas, Nay Pyi Taw and Yangon. The city of Nay Pyi Taw became the capital in 2008; the city of Yangon was the previous capital. A survey of drinking-water sources and quality was undertaken. The details of the location of source waters are shown in Figure 1. In Nay Pyi Taw, source waters from a deep well and two dams were examined. In the Yangon area, environmental waters in lakes and rivers were examined.

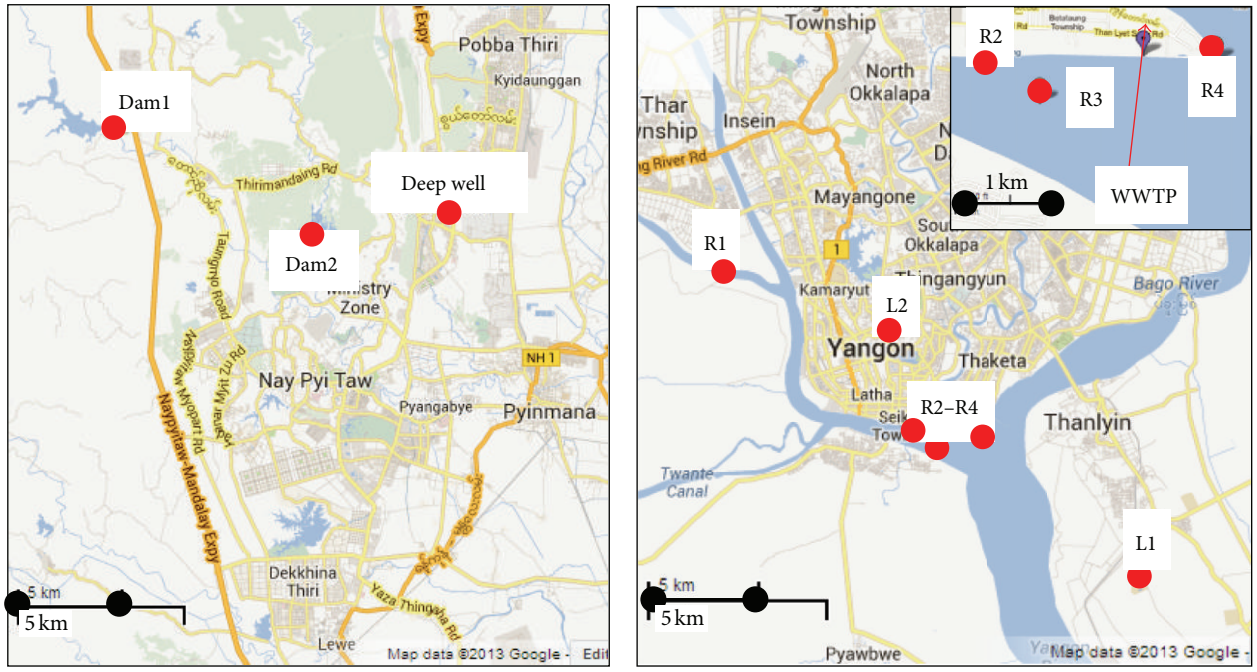


(a) (b)

Figure 1: Maps of sampling locations in (a) Nay Pyi Taw and (b) Yangon.

Table 1: Summary of drinking-water samples.

| Type | Description | Location |
|---|---|---|
| Pot | Pot A | Yangon |
| | Pot B | Suburban Yangon |
| Nonpiped | Pagoda A | Yangon |
| | Building D | Suburban Yangon |
| | After treatment | |
| | Before treatment | |
| Piped | Building A | Yangon |
| | Building B | Nay Pyi Taw |
| | Building C | Nay Pyi Taw |
| Bottle | Manufacturer A | — |
| | Manufacturer B | — |
| | Manufacturer C | — |

Figure 2: Roadside pots containing water for drinking.

Drinking water was collected from various sources including public pots, nonpiped taps, piped taps, and bottled waters, as shown in Table 1. Three bottled waters (500 mL) from different companies were obtained commercially. Piped tap water was collected from three taps in Yangon and Nay Pyi Taw. Nonpiped tap water was collected at a pagoda and at another building (building D). In Myanmar, a pagoda is a meeting place for Buddhists, and complementary drinking water is provided. The tap water at the pagoda was provided by a nonpiped supply source. It was treated by a point-of-use (POU) facility and then stored. Building D was situated outside Yangon city in an area that is not served by the Yangon City Development Committee (YCDC) tap-water service. The water supply system to the building was privately operated by a POU facility that used a combination of a reverse osmosis (RO) membrane treatment and an ultraviolet (UV) disinfection system.

Drinking water was also collected from public pots located on the roadside (Figure 2). In the Yangon area, pots are filled with water, covered, and placed along the roadside for public drinking purposes. We collected samples from various pots and examined the water quality, with a focus on bacterial analysis.

### 2.2. Measured Parameters

*2.2.1. Bacteria.* The numbers of *E. coli* and total coliform bacteria and the heterotrophic plate counts (HPC) were

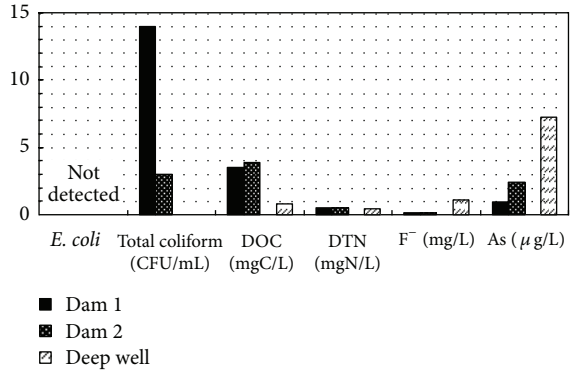


Figure 3: Comparison of water quality in dams and a deep well water at Nay Pyi Taw.

determined using a commercial kit (Petrifilm, 3M, USA) at each site. *E. coli* and total coliform bacteria were incubated at 37°C for 24 hours, and HPC was incubated at 37°C for 48 hours. The validity of this kit has been confirmed [5, 6], and it showed high correlations for *E. coli* and total coliform. High correlations were also reported for HPC, although small differences can arise with different incubation conditions [7].

*2.2.2. Chemical Parameters.* Dissolved organic carbon (DOC), dissolved total nitrogen (DTN), and anions were measured with a TOC analyzer (TOC-L, Shimadzu). Anion concentrations ($F^-$, $Cl^-$, $Br^-$, $NO_2^-$, $NO_3^-$, $PO_4^-$, and $SO_4^-$) were determined by ion chromatography (IC-861, Metrohm) after filtration through a 0.45 $\mu$m polytetrafluoroethylene (PTFE) membrane.

*2.2.3. Heavy Metals.* Dissolved metals were analyzed by ICP-MS (7500 Series, Agilent) after filtration through a 0.45 $\mu$m PTFE membrane.

## 3. Results and Discussions

*3.1. Source Water Quality in Nay Pyi Taw.* Water quality parameters in two dams and a deep well in Nay Pyi Taw were examined and compared. A summary of the results, shown in Figure 3, indicates generally good water quality. No *E. coli* was detected in 1 mL samples at all locations, indicating good bacterial water quality. Total coliform levels were 14 and 3 CFU/mL at the two dams. These values are close to 10 CFU/mL, which is the "class A" Japanese environmental standard for lake water [8]. The DOC was 3.5 mg/L at Dam 1 and 3.0 mg/L at Dam 2, and it was 0.8 mg/L in the deep well. Values of DOC at the two dams were acceptable for water sources, considering that 3 mg/L of TOC in finished water has been adopted as a drinking-water standard in Japan [9]. A previous study had reported about 30–50 mg C/L of TOC in Lake Inle [3]. Compared with the results for Lake Inle, these two dams have a much better water quality.

Two important observations were made with regard to the deep well water quality. Fluoride ion levels were 1 mg/L, which is close to the 1.5 mg/L WHO guideline value [10]. The As level was 7.9 $\mu$g/L, which is also close to the WHO guideline value of 10 $\mu$g/L. Therefore, adequate water treatment must be provided before the well can be used as a drinking-water source. Overall, the water quality in the two dams and the deep well could be considered fair, and the water could be used for drinking with appropriate treatment.

Table 2: Bacterial water quality in Yangon.

| Location | R1 | R2 | R3 | R4 | L1 | L2 |
|---|---|---|---|---|---|---|
| Total coliform (CFU/mL) | 52 | 820 | 32 | 38 | 10 | 110 |
| *E. coli* (CFU/mL) | 20 | 510 | 15 | 16 | <1 | 2 |

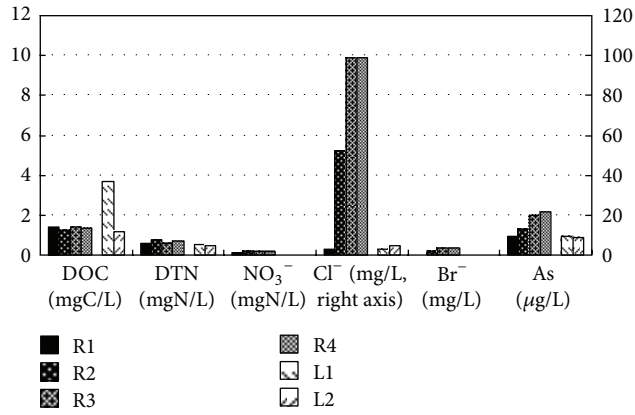


Figure 4: Comparison of water quality in rivers and lakes at Yangon.

*3.2. Environmental Water Quality in Yangon.* Environmental water quality was also surveyed in the Yangon region. The results of bacterial parameters are shown in Table 2. The Japanese standard for total coliform levels in river water is 0.5 CFU/mL for class AA, 10 CFU/mL for class A, and 50 CFU/mL for class B [8]. River waters in Yangon were found to be close to the class B standard, indicating that they can be used for drinking after advanced treatment. Among the sampling points on the Yangon River, R2 was located on the left riverbank, whereas R3 and R4 were located in the center of the river. The total coliform value was highest at R2 on the left riverbank, which was closest to urban activity. There was also a discharge from a wastewater treatment plant on the left riverbank, which would have contributed to the larger number of total coliform recorded at R2.

L1 and L2 are recreational lakes in the Yangon region. At L1, *E. coli* was not detected in 1 mL samples, whereas the level was 2 CFU/mL at L2. Total coliform was also high, with 110 CFU/mL at L2. A previous report indicated total coliform levels of 18–137 CFU/mL in Lake Inle [3]. Considering these numbers, L2 was not suitable as a drinking-water source.

The chemical water-quality parameters are summarized in Figure 4. In river water samples, the DOC was less than 3 mg C/L, which satisfies the Japanese drinking-water-quality standard [9]. Levels of the $Cl^-$ ion tended to increase downstream. The levels of Br ion and As displayed a similar trend, although the decrease was not as marked. In contrast to

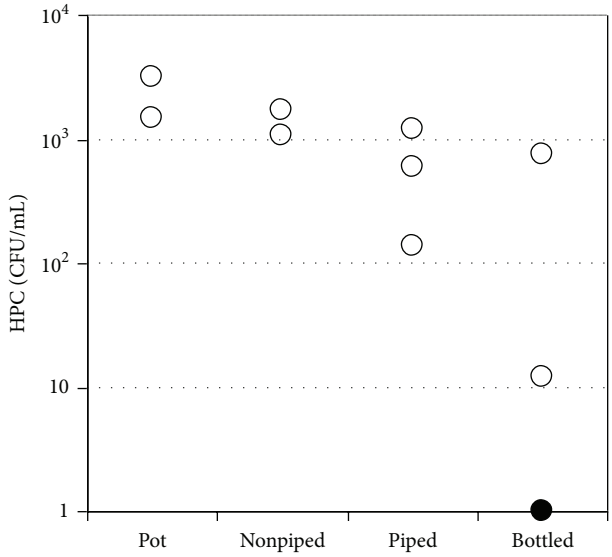


Figure 5: Heterotrophic plate count for potable water.

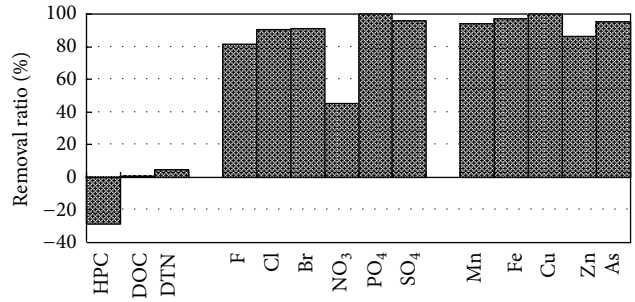


Figure 6: Removal ratio for a point-of-use (POU) facility.

the elemental measurements, DOC, DTN, and nitrate were stable along the river flow. It was therefore assumed that the sources of $Cl^-$, $Br^-$, and As were different from those of carbon and nitrogen.

Samples from L1 and L2 had good water quality with regard to chemical parameters, except for high DOC in L1. Overall, lake and river waters were good in terms of their chemical parameters, but the levels of bacterial contamination needed improvement.

*3.3. Drinking-Water Quality.* Potable drinking-water quality was surveyed for various water sources in Myanmar including (i) public pots, (ii) piped water supply in Yangon and Nay Pyi Taw, (iii) nonpiped water supply, and (iv) bottled water.

For bacterial water quality, *E. coli* was not detected in 1 mL water samples from any water source. However, there was a clear trend in the HPC, as shown in Figure 5. Pot water had HPC levels of 3200 and 1500 CFU/mL. In nonpiped tap water, the HPC level was 1700 and 1170 CFU/mL, and, in piped tap waters, the HPC was 140, 600, and 1200 CFU/mL. Of the three bottled waters examined, HPC was detected in two bottles at 760 and 12 CFU/mL, but HPC was not detected in the other bottled water sample. HPCs have various incubation conditions [11], and different incubation conditions produce different values. The Japanese government has adopted a value of 2000 CFU/mL as a water-quality standard for HPC by incubation at 20°C for 7 days [9]. This is equal to about 740 CFU/mL by incubation at 37°C for 2 days in Petrifilm, which we used in our preliminary investigation (unpublished data). From these results, we concluded that water from all pots, all nonpiped taps, one piped tap, and one bottled water exceeded the converted value of the Japanese drinking-water-quality standard and may not be suitable for drinking.

As shown in Figure 5, HPC was highest in the pots, followed by nonpiped taps, piped taps, and bottled waters. Nonpiped water was surveyed at two taps, at a pagoda and at a building outside the YCDC tap water service area. At those taps, water was supplied after treatment by POU facilities.

Piped water was surveyed at two buildings in Nay Pyi Taw and at one building in Yangon. Piped water supplies contained some residual chlorine: 0.01 mg/L at two taps in Nay Pyi Taw and 0.03 mg/L at a tap in Yangon. At a tap in Yangon, chlorine was present entirely as free chlorine. This residual chlorine may have contributed to the upkeep of water quality in the piped water supply.

It is interesting to note the water-quality distribution in bottled waters, with one bottled water supply having worse water quality than two piped taps. This probably results from the source water quality and the treatment efficiency of different bottled water companies. Other water-quality parameters were also monitored, including As and $F^-$. All measured items satisfied the Japanese drinking-water-quality standards [9].

*3.4. Treatment Efficiency of a POU Facility.* We investigated the performance of a POU facility at a building in Yangon, which was situated outside the YCDC piped water supply area. The water source was ground water, which was treated by an RO membrane followed by UV disinfection. The removal ratios of bacteria (HPC), carbon and nitrogen, anions, and metals are shown in Figure 6. The listed heavy metals were removed with high efficiency. Anions were also removed with high efficiency except for nitrate, for which only a 45% removal was achieved. Because UV treatment does not remove anions and metals, these elements were removed by the RO membrane.

In contrast, DOC and DTN removal was very low: 1% DOC and 5% DTN. The DOC and DTN contents of raw water were 0.55 mg C/L and 0.23 mg N/L, respectively. Considering the removal of anions and metals, the RO membrane would have worked well. A possible explanation is that most organic matter and nitrogen in raw water have a very small molecular weight and can pass through the RO membrane. Further investigation of the molecular weight distribution would confirm this assumption.

It is noteworthy that the bacterial removal ratio was negative. Considering the removal of anions and metals, bacteria could be removed by the RO membrane treatment. UV treatment also contributes to the suppression of bacterial activity, but UV treatment has no residual effect. Therefore, bacterial regrowth may occur in a storage tank after

UV treatment. UV treatment has a high potential to be installed in POU facilities because of its ease of handling and maintenance. Maintaining bacterial water quality after UV treatment is an important issue outside the piped water supply area.

## 4. Conclusion

This study investigated the water quality in urban areas of Myanmar and produced an overview of the current situation. River, dam, lake, and well water samples were examined and found to be of generally good quality. As and $F^-$ were present at relatively high concentrations and must be removed before deep wells can be used. Heterotrophic plate counts in drinking water were highest in pots, followed by nonpiped tap water, piped tap water, and bottled water samples. Measures need to be taken to improve the poor water quality in pots and nonpiped taps.

## Acknowledgments

The authors would like to express appreciations to Dr. Mu Mu Than and Dr. Kyi Kyi Lwin for their kind supports for water sampling. This paper was prepared with a partial support by MEXT through Green Network of Excellence (Eco-Health Project).

## References

[1] WHO, *Progress on Drinking Water and Sanitation*, World Health Organization, Geneva, Switzerland, 2012.

[2] United Nations, "Least developed countries," 2012, http://www.unohrlls.org/en/ldc/25/.

[3] F. Akaishi, M. Satake, M. Otaki, and N. Tominaga, "Surface water quality and information about the environment surrounding Inle Lake in Myanmar," *Limnology*, vol. 7, no. 1, pp. 57–62, 2006.

[4] Water Environment Partnership in Asia, "State of water environmental issues, Myanmar," 2003, http://www.wepa-db.net/policies/state/myanmar/myanmar.htm.

[5] V. Beloti, J. A. de Souza, M. D. A. F. Barros et al., "Evaluation of Petrifilm EC and HS for total coliforms and *Escherichia coli* enumeration in water," *Brazilian Journal of Microbiology*, vol. 34, no. 4, pp. 301–304, 2003.

[6] H. Schraft and L. A. Watterworth, "Enumeration of heterotrophs, fecal coliforms and *Escherichia coli* in water: comparison of 3M Petrifilm plates with standard plating procedures," *Journal of Microbiological Methods*, vol. 60, no. 3, pp. 335–342, 2005.

[7] S. A. Mueller, J. E. Anderson, B. R. Kim, and J. C. Ball, "Comparison of plate counts, Petrifilm, dipslides, and adenosine triphosphate bioluminescence for monitoring bacteria in cooling-tower waters," *Water Environment Research*, vol. 81, no. 4, pp. 401–406, 2009.

[8] Ministry of Environment, "Environmental quality standards for water pollution," 2013, http://www.env.go.jp/en/water/wq/wp.pdf.

[9] Ministry of Health, Labour, and Welfare, "Water quality standards," 2013, http://www.mhlw.go.jp/english/policy/health/water_supply/4.html.

[10] WHO, *Guidelines for Drinking-Water Quality*, World Health Organization, Geneva, Switzerland, 4th edition, 2011.

[11] J. Bartram, J. Cotruvo, M. Exner, C. Fricker, and A. Glasmacher, *Heterotrophic Plate Counts and Drinking-Water Safety*, International Water Association, London, UK, 2003.